

TIDAL HEATING

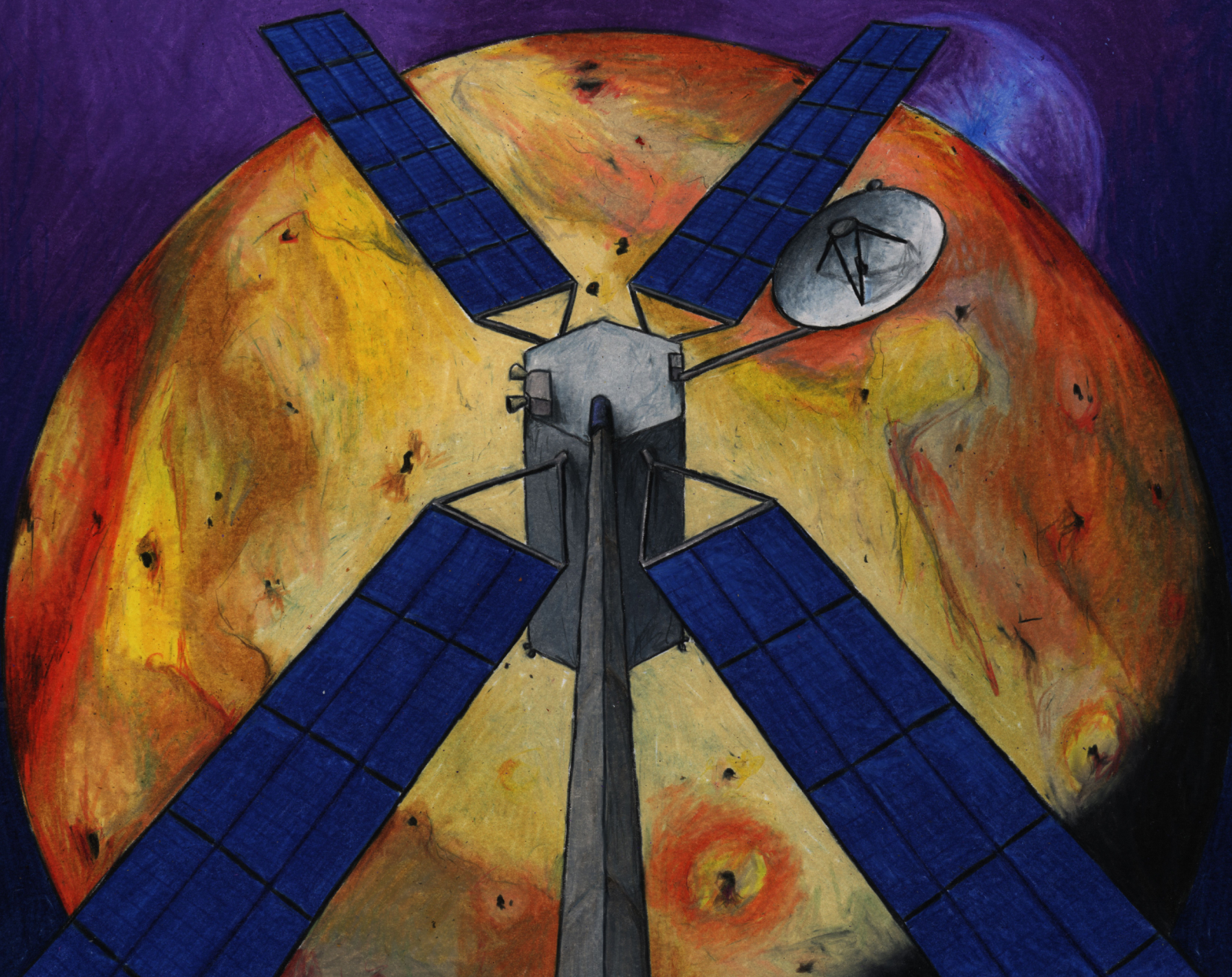
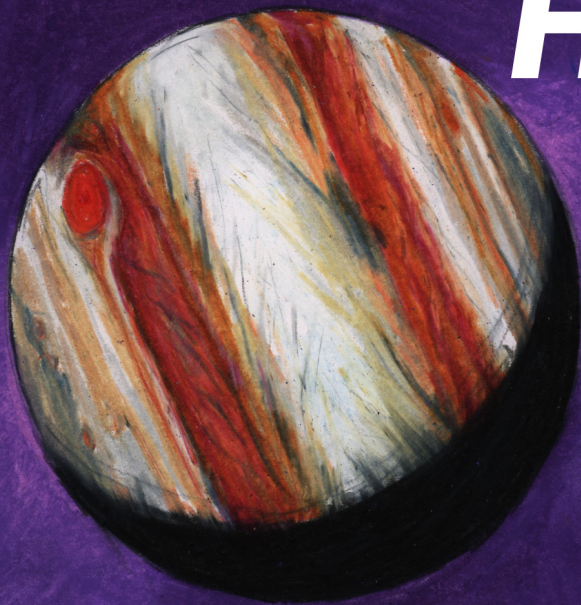
Lessons from
Io and the
Jovian System

co-leads:

Katherine de Kleer (Caltech)

Ryan Park (JPL)

Alfred McEwen (U. Arizona)



Tidal Heating: Lessons from Io and the Jovian System

Study dates: October 15–19 and December 3, 2018

Team Leads: Katherine de Kleer,¹ Alfred S. McEwen,² Ryan S. Park³

Other participants: Carver J. Bierson,⁴ Ashley G. Davies,³ Daniella N. DellaGiustina,² Anton I. Ermakov,³ Jim Fuller,¹ Christopher W. Hamilton,² Camilla D. K. Harris,⁵ Hamish C. F. C. Hay,² Robert A. Jacobson,³ James T. Keane,¹ Laszlo P. Kestay,⁶ Krishan K. Khurana,⁷ Karen W. Kirby,⁸ Valery J. Lainey,³ Isamu Matsuyama,² Christine McCarthy,⁹ Francis Nimmo,⁴ Mark P. Panning,³ Anne Pommier,¹⁰ Julie A. Rathbun,¹¹ Gregor Steinbrügge,¹² David J. Stevenson,¹ Victor C. Tsai,¹ Elizabeth P. Turtle,⁸ John M. Eiler,¹ Edward D. Young,⁷ Kevin J. Zahnle,¹³ Jess F. Adkins,¹ Kathy E. Mandt,⁸ Melissa A. McGrath,¹⁴ Arielle Moullet,¹⁵ J. Hunter Waite,¹⁶ Nicolas M. Schneider¹⁷

¹California Institute of Technology ²University of Arizona ³Jet Propulsion Laboratory, California Institute of Technology ⁴University of California, Santa Cruz ⁵University of Michigan ⁶United States Geological Survey ⁷University of California, Los Angeles ⁸Johns Hopkins Applied Physics Laboratory ⁹Columbia University ¹⁰University of California, San Diego ¹¹Planetary Science Institute ¹²University of Texas at Austin ¹³NASA Ames ¹⁴Search for Extraterrestrial Intelligence (SETI) ¹⁵National Radio Astronomy Observatory (NRAO) ¹⁶Southwest Research Institute (SWRI) ¹⁷LASP, University of Colorado

Keck Institute for Space Studies (KISS) Executive Director: Michele A. Judd

Acknowledgements: We especially thank Michele Judd and others at the Keck Institute for Space Studies for supporting this effort. This research was in part carried out at the Jet Propulsion Laboratory, California Institute of Technology, under a contract with the National Aeronautics and Space Administration.

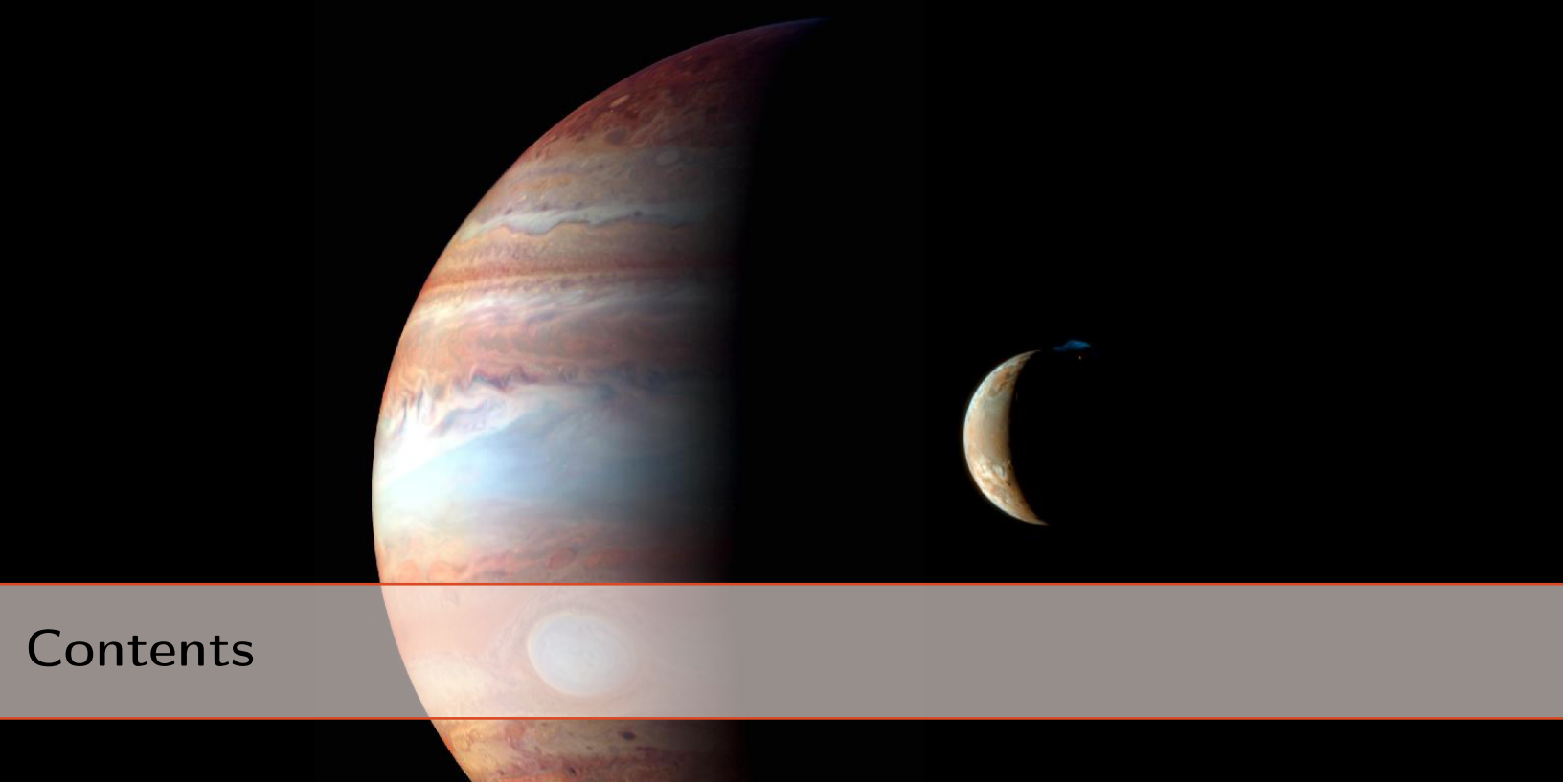
Editing and formatting: Meg Rosenberg

Cover image: James Tuttle Keane; Artwork showing the periodic alignment of Io (foreground), Jupiter, Europa, and Ganymede in the Laplace resonance, and a solar-powered spacecraft encountering Io.

Header image credits: NASA/Johns Hopkins University Applied Physics Laboratory/Southwest Research Institute/Goddard Space Flight Center (Contents); NASA/JPL/University of Arizona (List of Figures, Chapters 2, 3, 4, Bibliography); NASA, ESA, and the Hubble Heritage Team, STScI/AURA (Abstract); NASA/JPL/Malin Space Science Systems (Chapter 1)

Recommended citation: de Kleer, et al. *Tidal Heating: Lessons from Io and the Jovian System*, Final Report for the Keck Institute for Space Studies, 2019.

© June 2019. All rights reserved.

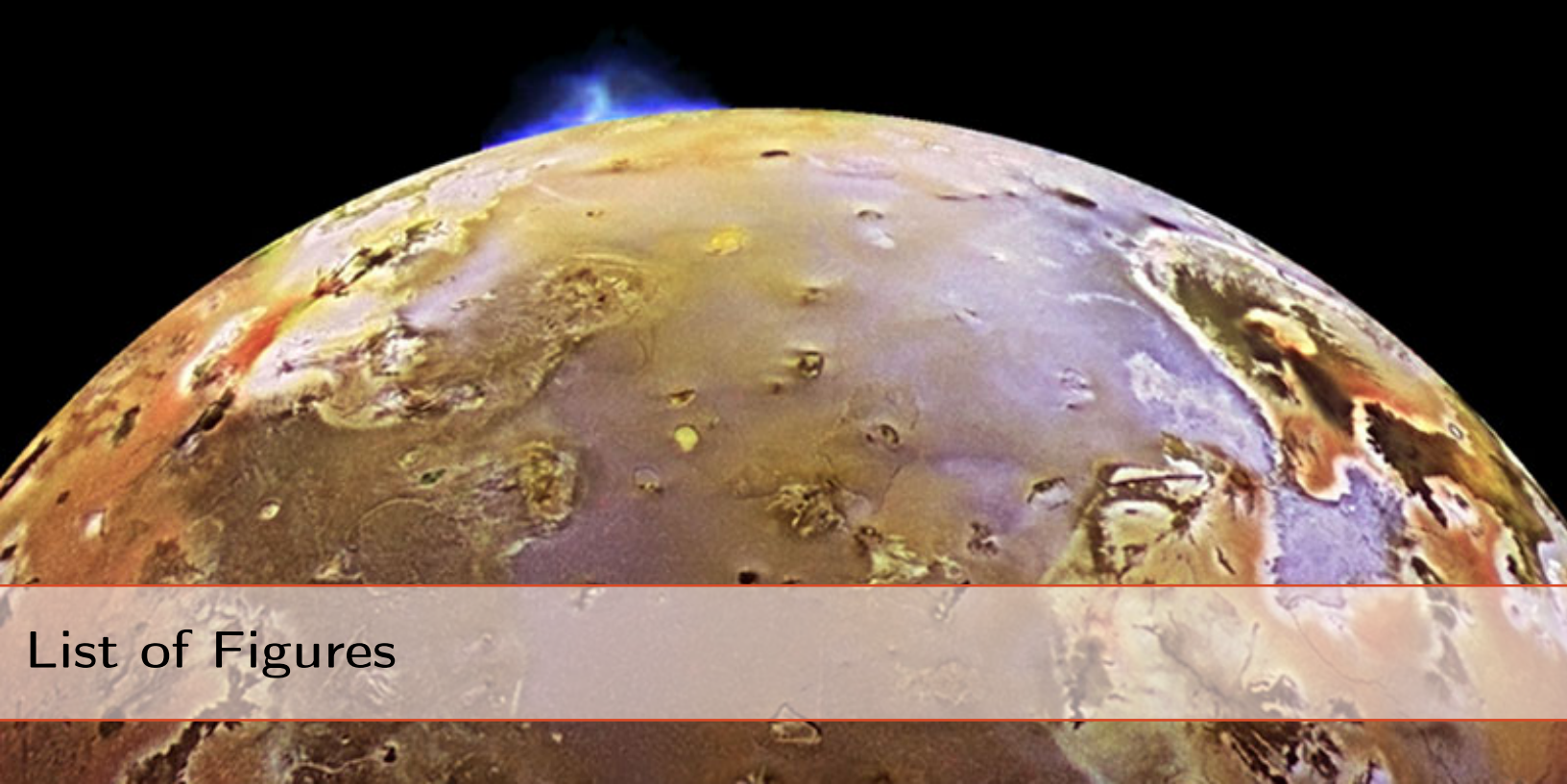


Contents

- List of Figures 5
- Abstract 6
- 1 Introduction and Background 9**
 - 1.1 Introduction 9**
 - 1.2 Science Background 10**
 - 1.2.1 Basics of Tidal Heating and Orbital Evolution 10
 - 1.2.2 Jovian System 11
 - 1.2.3 Saturnian System 13
 - 1.2.4 Exoplanets 15
 - 1.3 Io: Proposed Tidal Heating Processes and Hypothesis Tests 16**
 - 1.4 Europa and Enceladus 21**
 - 1.4.1 Europa 21
 - 1.4.2 Enceladus 22

2	Key Science Questions and Measurements	23
2.1	Question 1: What do volcanic eruptions tell us about the interior?	23
2.1.1	Introduction to Question 1	23
2.1.2	Eruption Temperatures	24
2.1.3	Eruption Styles	26
2.1.4	Spatial Distributions of Volcanoes	27
2.1.5	Temporal Variability	28
2.1.6	Global Average Heat Flow	29
2.1.7	Differentiation and Crustal Recycling	32
2.2	Question 2: How is tidal dissipation partitioned?	32
2.2.1	Introduction to Question 2	32
2.2.2	Constraints from Laboratory Experiments	33
2.2.3	Dissipation in Solid Regions	34
2.2.4	Dissipation in Fluid Regions	35
2.2.5	Need for Advanced Theory	37
2.3	Question 3: Does Io have a melt-rich layer, or “magma ocean”?	38
2.3.1	Introduction to Question 3	38
2.3.2	What Do We Mean by a Magma Ocean?	38
2.3.3	Magnetic Induction	40
2.3.4	Tidal Love Numbers k_2 and h_2	43
2.3.5	Combining Gravity and Topography	44
2.3.6	Seismology	45
2.3.7	Libration Amplitude	45
2.3.8	Experimental Work Needed: Dissipation in High Melt Fraction Environments	47
2.3.9	Petrology	50
2.3.10	Plasma Interaction and Magnetic Fields	51
2.3.11	Relevance to Ocean Worlds	52
2.4	Question 4: Is the Jupiter/Laplace system in equilibrium?	52
2.4.1	Introduction to Question 4	52
2.4.2	Definition of Equilibrium	53
2.4.3	Astrometry in the Jovian System	54
2.4.4	Heat Flow Measurements	55
2.4.5	Stability of Laplace Resonance	55
2.4.6	Summary	57

2.5	Question 5: Can stable isotopes inform long-term evolution of tidally heated bodies?	58
2.5.1	Introduction to Question 5	58
2.5.2	Measurement Potential for Tidally-Heated Satellites	60
2.5.3	Theoretical Advancements Needed	62
3	Technical Development Possibilities	64
3.1	Improvements in Design for Jupiter’s Radiation Environment	64
3.1.1	Impact of the Radiation Environment on Future Missions	64
3.1.2	Updates to Jupiter Radiation Environment Models	64
3.1.3	Transport Analysis Tool Updates	65
3.1.4	Design Improvements for Radiation Environment	65
3.2	New Measurements and Technologies that Address Key Scientific Questions	67
3.2.1	Need for More Efficient Power Sources in Outer Solar System	67
3.2.2	InSAR	68
3.2.3	Small Satellite Constellations	68
3.2.4	Radar Sounding	69
3.2.5	High Dynamic Range Thermal Imagers	69
3.2.6	Advanced Pointing Imaging Camera	70
3.2.7	Orbital Seismology Through Laser Vibrometry	70
3.2.8	Landers and Penetrators	71
4	Conclusions and Future Directions	73
4.1	Spacecraft Mission Opportunities	73
4.1.1	Europa Clipper and JUICE	73
4.1.2	Discovery and New Frontiers	75
4.1.3	Europa or Enceladus Landers	75
4.1.4	Satellite Orbiters	75
4.1.5	Ice Giants Flagship	75
4.2	Telescopic Observations	76
4.3	Programs for Lab experiments	76
4.4	Summary Recommendation: Spacecraft Mission to Io	77
	Bibliography	77



List of Figures

1.1	Schematic diagram of tidal deformation for a tidally-locked satellite	12
1.2	Schematic diagram of the Jovian and Saturnian systems	14
1.3	Resonance locking scenario for a satellite of Saturn	15
1.4	Expected patterns of surface heat flux on Io for three dissipation scenarios	17
1.5	Schematic illustration of Io's interior structure without and with a magma ocean . .	19
1.6	End-member tidal dissipation scenarios in Io for different interior structure models .	20
1.7	Schematic illustration of the solar system's ocean worlds	21
2.1	Plumes detected on Io, Enceladus, and Europa	24
2.2	Thermal emission of a blackbody for ultramafic and mafic eruption temperatures .	25
2.3	Thermal emission from Io's volcanoes	30
2.4	Distribution of hot spots on Io	31
2.5	Schematic illustration of possible physical configurations of melt within Io and other partially molten silicate worlds	38
2.6	The principle behind electromagnetic sounding of Io's interior	41
2.7	Amplitude of libration for Io as a function of core radius and core density	47
2.8	Amplitude of libration of Io given a solid crust over a liquid magma ocean as a function of crustal rigidity	48
2.9	Schematic illustration of two scenarios for satellites in resonance: equilibrium and oscillation	53
2.10	Schematic illustration of the sources, sinks, and transport processes controlling the chemical and isotopic species in/on/around Io	62
4.1	Planned and candidate missions to explore the Galilean satellites	74



Abstract

Tidal heating is key to the evolution and habitability of many worlds across our solar system and beyond. However, there remain fundamental gaps in our understanding of tidal heating and coupled orbital evolution, which motivated a Keck Institute for Space Studies (KISS) workshop on this topic. The Cassini mission has led to many recent results about ocean worlds and what may become a new paradigm for understanding orbital evolution with tidal heating, the model of resonance locking in the parent planet (Fuller et al., 2016). Resonance locking explains how subsurface oceans may persist over much of geologic time, even in tiny Enceladus. The discovery of the Laplace resonance of Io, Europa, and Ganymede orbiting Jupiter led to the prediction of intense tidal heating of Io (Peale et al., 1979); this system provides the greatest potential for advances in the next few decades. Europa Clipper and JUpiter ICy moons Explorer (JUICE) will provide in-depth studies of Europa and Ganymede in the 2030s. The easily observed heat flow of Io, from hundreds of continually erupting volcanoes, makes it an ideal target for further investigation, and the missing link—along with missions in development—to understand the Laplace system.

We identified five key questions to drive future research and exploration: (Q1) What do volcanic eruptions tell us about the interiors of tidally heated bodies (e.g., Io, Enceladus, and perhaps Europa and Triton)? (Q2) How is tidal dissipation partitioned between solid and liquid materials? (Q3) Does Io have a melt-rich layer, or “magma ocean”, that mechanically decouples the lithosphere from the deeper interior? (Q4) Is the Jupiter/Laplace system in equilibrium (i.e., does the satellite’s heat output equal the rate at which energy is generated)? (Q5) Can stable isotope measurements inform long-term evolution of tidally heated bodies?

The most promising avenues to address these questions include a new spacecraft mission making close flybys of Io, missions orbiting and landing on key worlds such as Europa and Enceladus, technology developments to enable advanced techniques, closer coupling between laboratory experiments and tidal heating theory, and advances in Earth-based telescopic observations of solar system and extrasolar planets and moons. All of these avenues would benefit from technological developments. An Io mission should: characterize volcanic processes (Q1); test interior models via a set of geophysical measurements coupled with laboratory experiments and theory (Q2 and Q3); measure the rate of Io's orbital migration (to complement similar measurements expected at Europa and Ganymede) to determine if the Laplace resonance is in equilibrium (Q4); and determine neutral compositions and measure stable isotopes in Io's atmosphere and plumes (Q5). No new technologies are required for such an Io mission following advances in radiation design and solar power realized for Europa Clipper and JUICE. Seismology is a promising avenue for future exploration, either from landers or remote laser reflectometry, and interferometric synthetic aperture radar (InSAR) could be revolutionary on these active worlds, but advanced power systems plus lower mass and power-active instruments are needed for operation in the outer solar system.



1. Introduction and Background

1.1 Introduction

The evolution of planets and satellites, as well as their potential habitability, are central questions in planetary science (National Research Council, 2012). Recent discoveries from spacecraft missions and telescopic programs have illuminated the central role that tidal heating plays in the evolution of worlds across our solar system and beyond. This fundamental process drives the orbital evolution of star–planet or planet–satellite systems as a whole, and shapes the interior structure and geological activity of planetary bodies, impacting the habitability of ocean worlds such as Europa and Enceladus. However, despite its broad-ranging importance, there remain fundamental gaps in our understanding of tidal heating. For example: Where and how is tidal heat actually dissipated? How do we link laboratory experiments of rheology to planetary-scale observations of deformation and heat flow? How are subsurface oceans created and maintained?

While there are well-tested tools in place to study a variety of individual planetary processes, there is no established path forward for unraveling the interconnected roles of tidal heating and orbital evolution. Such investigations will require innovative approaches and new technologies that can pin down the orbital evolution and deformation of these worlds by integrating laboratory work, spacecraft and ground-based observations, and numerical models. Our study brought together some of the brightest minds in planetary sciences, mission design, and instrumentation to generate new, original ideas for revolutionizing our understanding of tidal heating. Our central objective was to integrate the numerous recent advances across the relevant fields, including laboratory studies, telescopic/spacecraft data, and instrumentation under development, to construct a coherent path forward for understanding tidal heating and its influence on the evolution of planetary systems. The combination of recent scientific advances as well as the forthcoming Europa Clipper and

Jupiter ICy moons Explorer (JUICE) missions, the formation of the NASA Ocean Worlds program, potential New Frontiers-class missions to tidally heated worlds (e.g., Io, Enceladus, and Titan) and potential ocean world landers and penetrators make it clear that now is a critical time for integrating what we know, identifying what we do not know, and creating a clear roadmap for the future scientific investigations and technologies that will be needed to optimize efforts in the coming decades.

Among the several tidally heated worlds in our solar system, the effects of tidal heating are most prominent within the Laplace resonance between Jupiter's moons Io, Europa, and Ganymede. Io is the most tidally deformed and heated world in the solar system—as evidenced by the hundreds of continually erupting volcanoes across its surface—and is thus the ideal target for investigating these questions. Furthermore, while several missions are planned to explore the Jovian system in the coming decades (e.g., Europa Clipper and JUICE), joining Juno, which is already orbiting Jupiter, our understanding of orbital dynamics and tidal heating within this system will be limited by a dearth of measurements of Io. Our study therefore emphasized the Jovian system, and Io in particular, as the best laboratory for understanding the fundamental processes of tidal heating and the world most neglected by planned missions.

We planned the Keck Institute for Space Studies (KISS) workshop with a three-pronged approach. First, we reviewed and integrated recent scientific advances and the relevant new or in-development technologies and instrumentation. Second, we identified the key gaps or questions in our current framework for understanding tides and tidal heating. Lastly, we discussed the specific requirements for bridging these gaps, including: the measurements to be acquired, the instrument technologies to be developed or matured, and the new theoretical modeling capabilities and/or data techniques to be developed.

This report is organized as follows. In this chapter, we provide the introduction and background on recent results relevant to tidal heating, especially for Io. Chapter 2, the largest portion of this report, describes the five key questions identified in the workshop, as well as the measurements or theoretical progress needed to address each of them. Chapter 3 describes new technologies needed to make these key measurements. Chapter 4 discusses future directions and how to achieve major progress over the next few decades.

1.2 Science Background

1.2.1 Basics of Tidal Heating and Orbital Evolution

Tidal dissipation within a planet causes its satellites to migrate outward, frequently driving them into mean-motion resonances with each other (Murray and Dermott, 1999). Simultaneously, tidal dissipation within the moons damps the eccentricity excited by the mean-motion resonances

(moving orbits inward), and drives tidal heating, tectonism, and potential volcanic activity. Over long timescales, tides can alter the structure of a moon, changing its tidal response and driving feedbacks between the rotational, orbital, and thermal evolution of the moon. The global loss of energy by tides can be measured by precise astrometric observations of a moon's orbit over time (e.g., Lainey et al., 2009).

A moon in a non-circular orbit experiences a changing gravitational attraction with its parent planet, causing the moon's shape to change over each orbit (Figure 1.1). The magnitude and phase of tidal deformation depends on a body's interior structure, and controls how much heating occurs. Tidal deformation is thus central to understanding a moon's energy budget and probing its internal structure. The same considerations apply to a planet around its host star. Tidal deformation can be measured directly by detecting periodic changes in the shape and gravity field of a moon, and indirectly by measuring the tidal heat produced. Moons with a continuous liquid region in the subsurface, such as a subsurface water or magma ocean, are expected to show a larger tidal response and perhaps rotational parameters such as libration (Van Hoolst et al., 2013). In addition, laboratory studies show that temperature and forcing frequency both have a strong effect on deformation (Faul and Jackson, 2015).

See Sections 2.2–2.4 for much more detailed background on tidal-heating processes.

1.2.2 Jovian System

In 1771, Pierre Simon Laplace described the 4:2:1 resonance of the orbital periods of Io, Europa, and Ganymede. The resonance is characterized by the relation: $L_1 - 3 L_2 + 2 L_3$ is π on average, where L_1 , L_2 , and L_3 denote the mean longitudes of Io, Europa, and Ganymede, respectively. The significance of this relation was realized over 200 years later by Peale et al. (1979), who pointed out that the Laplace resonance creates significant forced eccentricity in the orbits of Io and Europa, such that they are periodically deformed by massive Jupiter, generating internal heating. They predicted runaway melting of the interior of Io, thinning the lithosphere so that it could conduct away the heat, and that the Voyager spacecraft might observe widespread active volcanism. That prediction was dramatically confirmed a few months later by Voyager 1, which captured erupting volcanic plumes and hot spots on Io, and Voyager 2, which revealed Europa's young surface (Smith et al., 1979a,b). The first high-temperature hotspot detection on Io (Witteborn et al., 1979) was actually published prior to the Peale et al. (1979) paper, but they did not favor the volcanic interpretation because it implied an eruption rate higher than ever observed on Earth.

Although Peale et al. (1979) predicted a thin lithosphere, Voyager 1 revealed mountains >10 km high, suggesting that Io must have a thick, cold lithosphere, built up by rapid volcanic resurfacing and subsidence of crustal layers (O'Reilly and Davies, 1981). While supported by petrologic arguments (Keszthelyi et al., 1999), the idea of a magma ocean inside Io generally lost

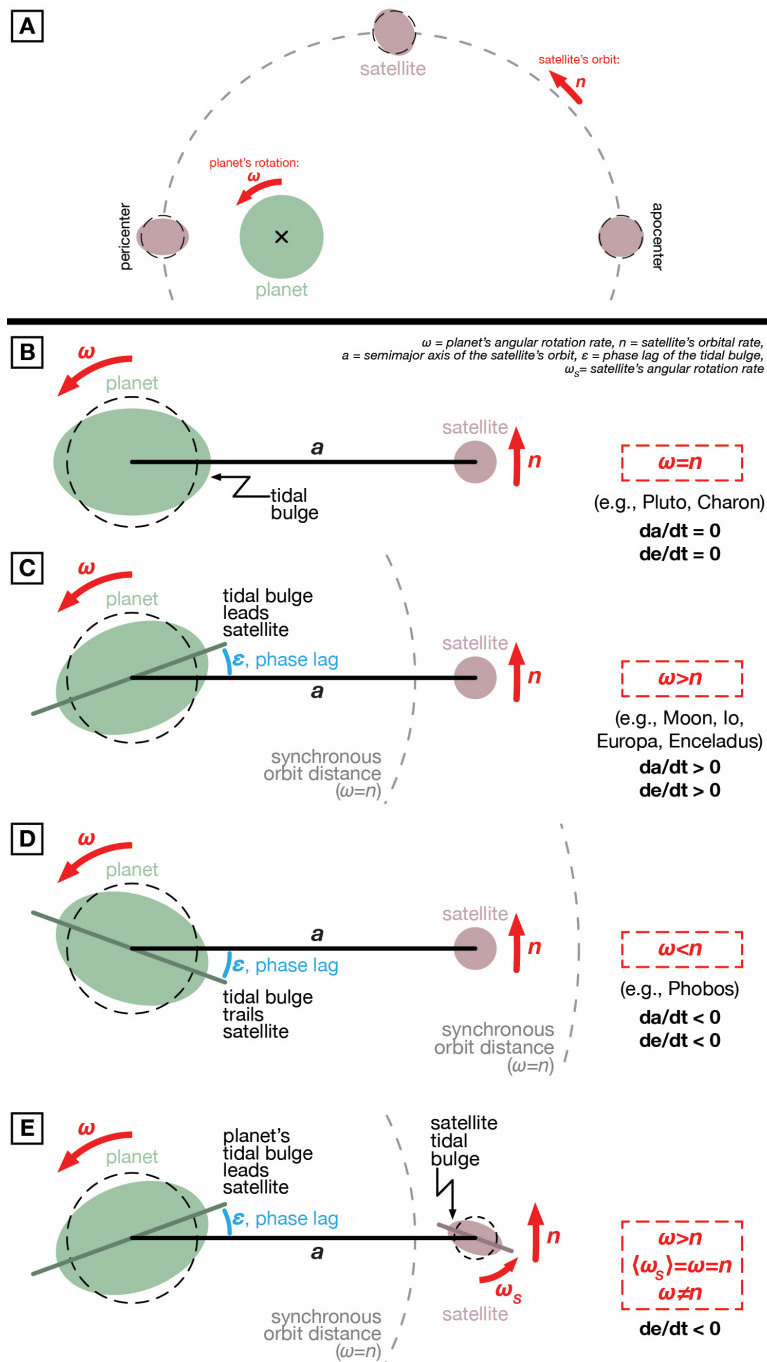


Figure 1.1: A schematic diagram of tidal deformation for a tidally-locked satellite orbiting a planet. Tides deform the satellite at all distances, although deformation is strongest when the satellite is closest to the planet (pericenter) and weakest when the satellite is furthest from the planet (apocenter). B–E, Schematic diagrams of how tides affect the orbit of a tidally-locked satellite (based on Burns and Matthews, 1986).

favor (Moore et al., 2007) because mantle melt easily migrates (Kohlstedt and Holtzman, 2009; Stevenson, 1989). The question was raised again, however, when evidence was presented for a strong induced magnetic signature within Io (Khurana et al., 2011). Induced signatures in Europa, Ganymede, and Callisto had previously been interpreted as being due to salty oceans (Khurana et al., 1998; Kivelson et al., 2002, 2000). Considerable debate persists about whether or not Io has a magma-rich layer of some sort (e.g., Bierson and Nimmo, 2016; Tyler et al., 2015).

Astrometric observations of the positions of the Galilean satellites over an extended period of time were used to constrain the orbital migration rate of Io (Lainey et al., 2009), predicting a present-day heat generation in the system close to the estimated heat flow of Io. This study did not utilize data from the Galileo mission because failure of the high-gain antenna precluded precision ranging, so it lacks the precision of Cassini measurements for the Saturnian moons. Furthermore, this study was based on common assumptions now disproven in the Saturnian system (Lainey et al., 2017). Figure 1.2 provides a schematic of the Jovian and Saturnian systems.

1.2.3 Saturnian System

Results from the Cassini mission include the discovery of Enceladus' venting of water vapor (Hansen et al., 2006; Porco et al., 2006), south polar hot spots (Spencer et al., 2006), and the presence of global subsurface oceans in Enceladus (Thomas et al., 2016) and Titan (Iess et al., 2012). Less recognized, but of key importance to understanding tidal heating, are new results in astrometry and orbital evolution of this system, summarized below.

In the Jovian and Saturnian systems, the planet spins faster than the moons orbit, such that tidal dissipation imparts angular momentum to the moons and they migrate outwards, frequently driving them into mean-motion resonances (MMRs) with each other (Dermott et al., 1988; Murray and Dermott, 1999). There are currently two such resonances in the Saturnian system: the 4:2 resonance of Mimas and Tethys and the 2:1 resonance of Enceladus and Dione. The tidal energy dissipation is often parametrized by a tidal quality factor Q (Goldreich and Soter, 1966). Smaller values of Q in the primary correspond to larger energy dissipation rates and faster migration. Very small values of Q seem implausible because, if constant over time, they would imply the satellites formed inside Saturn's Roche radii. Very large values of Q , again if constant, are unlikely because they would not allow for capture into MMRs within the lifetime of the solar system. Thus the current orbital architectures suggest that outward migration timescales are within an order of magnitude of the age of the solar system (Fuller et al., 2016).

Astrometry of the Saturnian moons, largely based on Cassini radio tracking during close encounters (Lainey et al., 2012, 2017), has revealed outward migration rates much faster than predicted. For a constant tidal Q , these rates indicate that the moons would have migrated far beyond their current positions over the lifetime of the solar system. The measurements also indicate that the effective tidal Q must be different for each moon.

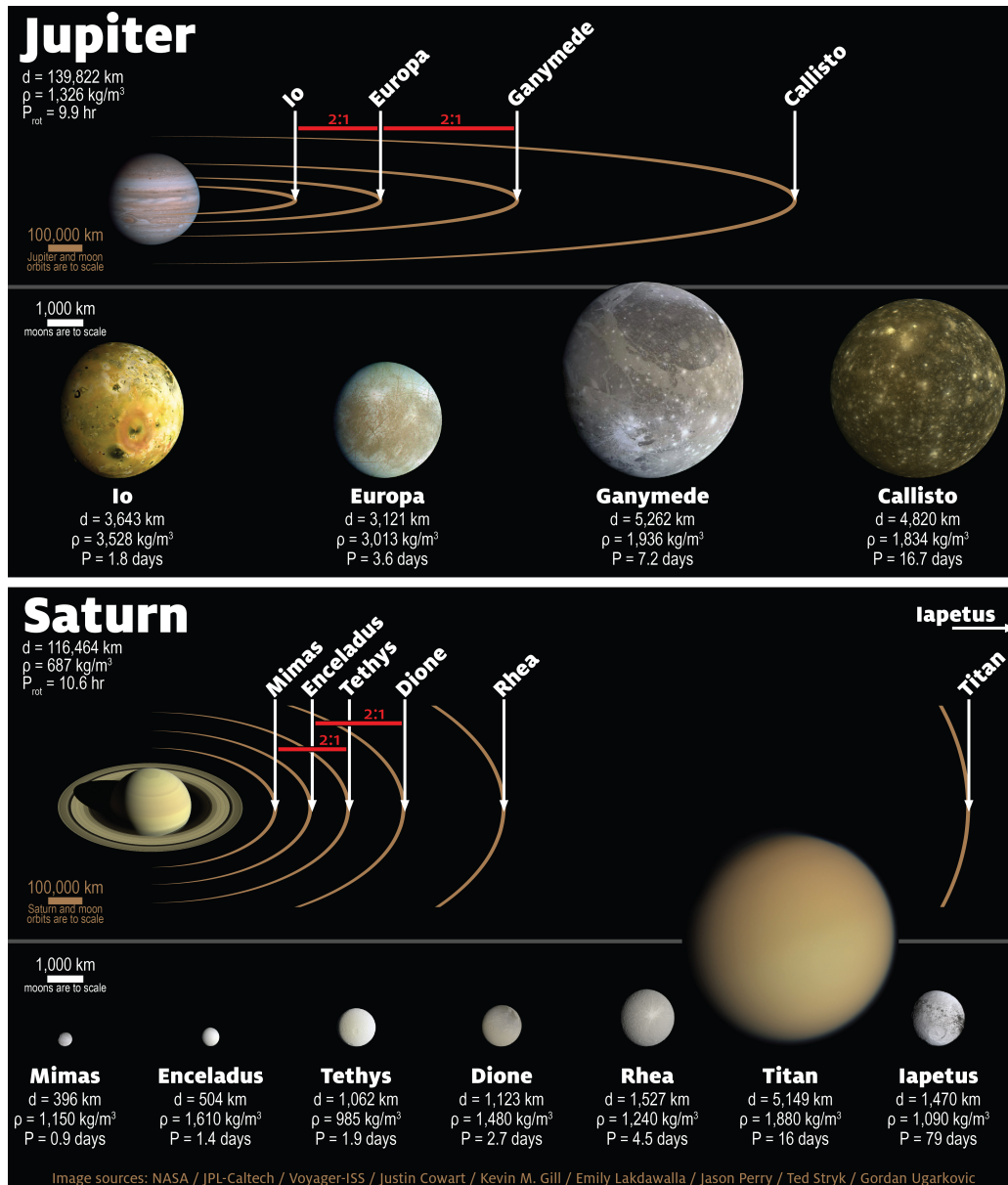


Figure 1.2: Schematic of the Jovian and Saturnian systems. The top panels show the orbital architecture of the system, with the host planet and orbits to scale. Relevant mean-motion resonances are identified in red. The bottom panels show the satellites to scale with one another. We focus on the major satellites. Listed physical parameters include the diameter (d), bulk density (ρ), and rotational period (P)—which for all of the satellites is equal to their orbital period, as they are all tidally locked with their host planet.

To explain these measurements, Fuller et al. (2016) proposed that a mechanism called “resonance locking” (Witte and Savonije, 1999) produces accelerated orbital migration via dynamical tides

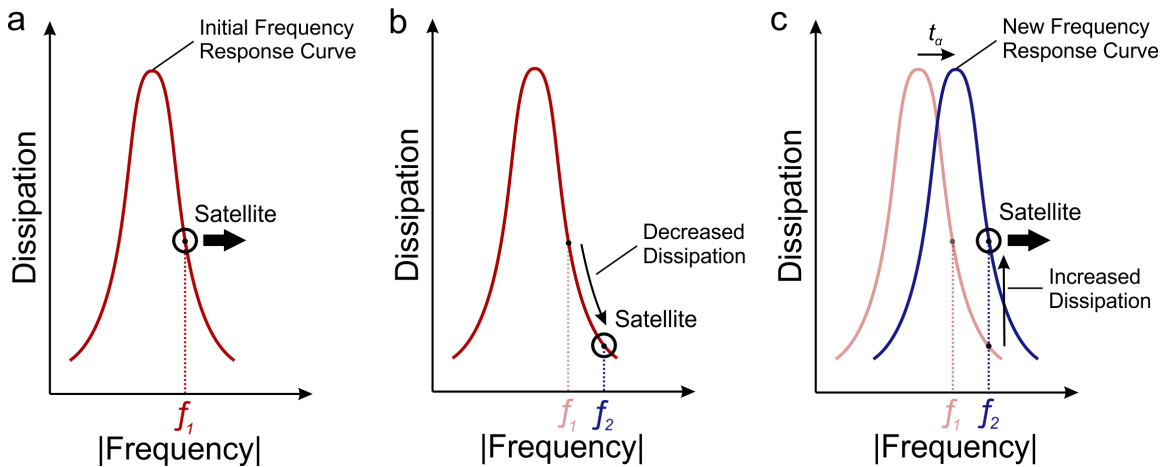


Figure 1.3: Resonance locking scenario. (a) Satellite is close to a dissipation peak at absolute synodic frequency f_1 and migrates outwards, increasing its frequency. (b) At frequency f_2 the satellite experiences less dissipation and stops migrating. (c) The peak evolves to higher frequency as Saturn evolves, so dissipation in the satellite increases again. Hence, the outwards migration rate of the satellite is controlled by the timescale for Saturn to evolve. Figure adapted from Nimmo et al. (2018).

(Figure 1.3). Although neglected in previous studies, the internal structures of gas giant planets may evolve on timescales comparable to their age.

Such evolution causes planetary oscillation mode frequencies to gradually change, allowing resonance locking, in which a planetary oscillation mode stays nearly resonant with the forcing produced by a moon, greatly enhancing long-term tidal dissipation and producing outward migration on a timescale comparable to the age of the solar system. Resonance locking predicts a similar migration timescale but a different effective Q for each moon. The theory also predicts nearly constant migration timescales as a function of semimajor axis, such that effective Q values were larger in the past, consistent with formation billions of years ago. This hypothesis can explain the long-term survival of the habitable ocean in Enceladus and the present-day heat flux without requiring Enceladus to have formed recently (Nimmo et al., 2018).

1.2.4 Exoplanets

The discovery of seven roughly Earth-sized planets orbiting TRAPPIST-1 (Gillon et al., 2017) has raised interest in tidal heating of exoplanets. The planets orbit the low-mass star with semi-major axes <0.1 au, with periods of a few Earth days, and the orbits have non-zero eccentricities, so tidal forces vary with time, resulting in heating of their interiors (Luger et al., 2017). Barr et al. (2018) concluded that planets “b” and “c” receive sufficient tidal heating to maintain magma

oceans in their silicate mantles. Tidal heating could significantly enhance the habitable volume in the galaxy by warming exoplanets and their satellites (Dobos and Turner, 2015).

Highly volcanic exoplanets are considered high priority targets for future investigation (Henning et al., 2018). They are likely to be even more diverse than volcanically active worlds in our solar system, with a wide range of compositions, temperatures, activity rates, volcanic eruption styles, and gravitational magnitudes. These are likely to be relatively easy rocky exoplanets to characterize due to their preferential occurrence in short orbital periods, their bright flux in the infrared, and spectroscopy of volcanic gases. Henning et al. (2018) suggested that highly volcanic worlds could become second only to habitable worlds in terms of scientific and public interest.

1.3 Io: Proposed Tidal Heating Processes and Hypothesis Tests

Io's intense volcanic activity is a consequence of tidal dissipation and heating within its interior, but the distribution of heating within Io's solid and/or fluid layers remains a subject of debate. Initially, it was assumed that tidal dissipation would occur purely within solid materials, concentrating heating within the deep mantle, asthenosphere, or a combination of both regions (Beuthe, 2013; Peale et al., 1979; Segatz et al., 1988; Tackley et al., 2001). If dissipation concentrates in the deep mantle, tidal heat dissipation would preferentially occur along the polar axis with heat flux focused in a degree-2 pattern at the poles and minima located along the tidal axis (i.e., 0° and 180° longitude). In contrast, if dissipation concentrates in the asthenosphere, tidal heating would concentrate at low-latitudes, with minima at the poles. Figure 1.4 illustrates these end-member scenarios.

To determine if solid-body tidal heating preferentially occurs within Io's deep mantle or asthenosphere, studies have compared the model predictions to observed patterns of volcanism using a range of geospatial analysis techniques. These comparisons assume that there would be a high degree of correlation between locations of heat production and surface expressions of volcanism. This assumption is supported by the observation that conduction alone cannot explain Io's global thermal emission, and therefore thermal energy must be transported via a heat pipe mechanism (Kankanamge and Moore, 2019; Moore, 2003; O'Reilly and Davies, 1981). However, if Io has a subsurface magma ocean, or a globally extensive region with a high melt fraction, then volcanic eruptions could occur at any locality, with lithospheric weaknesses playing an important role in the spatial distribution of volcanism.

Previous studies examining the global distribution of volcanism on Io (e.g., Carr et al., 1998; Davies et al., 2015; de Kleer and de Pater, 2016b; Hamilton et al., 2013; Kirchoff et al., 2011; Lopes-Gautier et al., 1999; McEwen et al., 2004; Radebaugh et al., 2001; Rathbun et al., 2018; Schenk et al., 2001; Shoji and Hussmann, 2016; Tackley et al., 2001; Veeder et al., 2011, 2012; see Section 2.1.5) observed that volcanic centers on Io are broadly distributed, but exhibit a

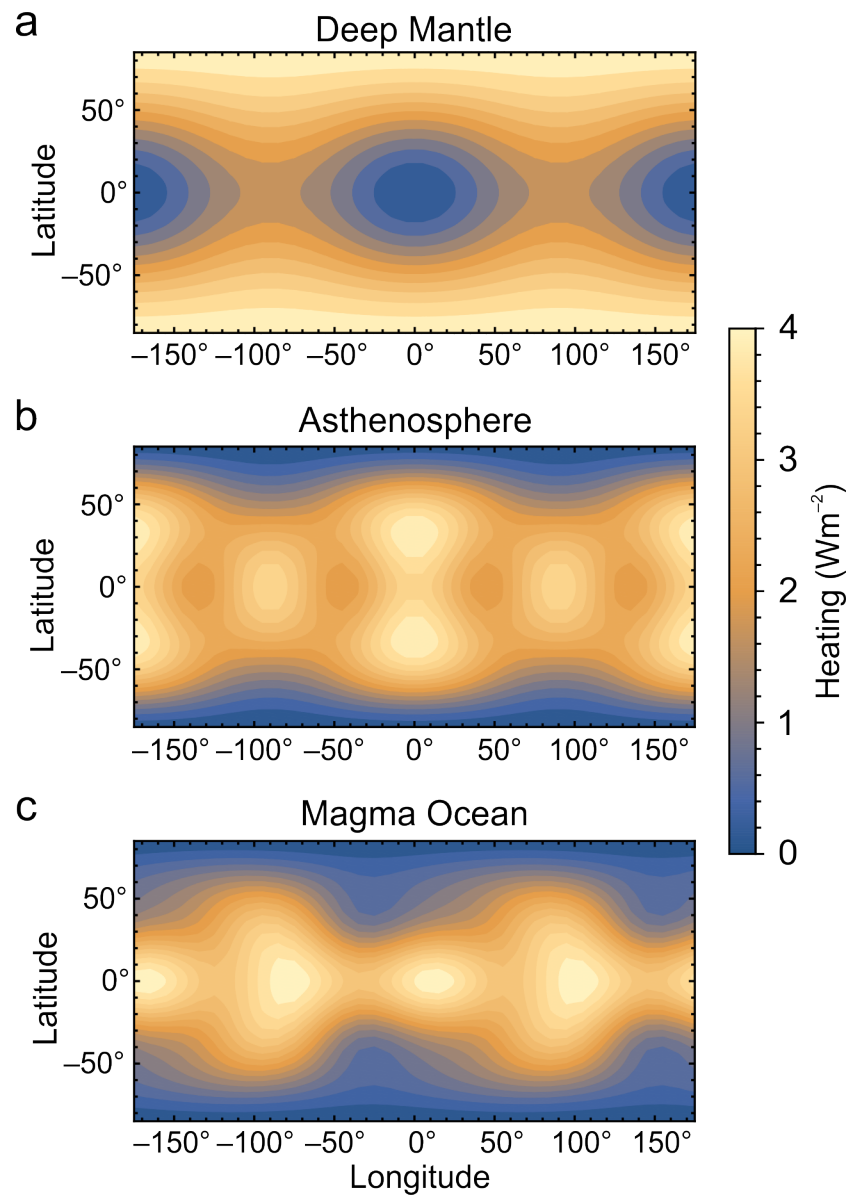


Figure 1.4: Expected patterns of surface heat flux on Io for three cases: top: deep-mantle tidal dissipation; middle: asthenospheric tidal dissipation; bottom: tidal dissipation within a relatively fluid asthenosphere or magma ocean. These surface heat flux patterns were calculated using the propagator matrix technique, based on Segatz et al. (1988) and Tobie et al. (2005), assuming: (1) a spherically symmetric incompressible body, (2) Maxwell rheology, and (3) radial heat flow to the surface. In the deep-mantle end-member heating case (top) the shear modulus, μ , is 3.5×10^9 Pa and viscosity, η , is 10^{15} Pa \cdot s. In the asthenospheric end-member case (middle), $\mu = 4 \times 10^4$ Pa and $\eta = 10^{10}$ Pa \cdot s, assuming a 50-km-thick asthenosphere. The top and middle figures are adapted from Hamilton et al. (2013) and the bottom figure is adapted from Tyler et al. (2015) while also taking into account the effect of the overlying elastic shell using the method of Matsuyama et al. (2018). A 50:50 combination of the deep-mantle and ocean heat-flow distributions can provide a reasonable match to the distribution of known hotspot heat flow (see Figure 2.4), according to Tyler et al. (2015).

concentration at low-latitudes (see Section 2.1). While it is difficult to assess how much of this is due to the dearth of polar observations, this generally supports the idea that tidal heating is dominated by dissipation in the asthenosphere. However, many of these studies note the absence of the longitudinal pattern in volcanism around the equator expected from the standard solid asthenospheric heating model (Figure 1.4, center). The apparent eastward offset of observed patterns of volcanism relative to the tidal axis led Hamilton et al. (2013) to suggest that fluid tidal dissipation could account for the observed offset. Tyler et al. (2015) explored this issue in more detail and determined that fluid tidal dissipation can explain the eastward offset in observed volcanism, but that a component of deep-mantle heating is still required to explain the occurrence of high-latitude volcanism (Figure 1.4, bottom). More sophisticated modeling, as well as new observations particularly of the polar regions, are needed to better constrain where dissipation is occurring within Io's interior.

To first order, determining how and where tidal dissipation occurs within Io depends upon whether or not its interior includes a magma ocean (Figure 1.5; Section 2.2). If there is no magma ocean within Io, dissipation would occur purely within solid rock (i.e., likely within a combination of the asthenosphere and deep mantle). The shell would be well-coupled with the interior and volcanism should be highly correlated with the locations of underlying tidal heating, modified only slightly by processes of melt transport through the lithosphere. In contrast, if a magma ocean is present within Io, dissipation could occur within the fluid layer as well as underlying solid layers. A globally continuous melt layer would also decrease the likelihood that surface expressions of volcanism would be directly correlated with underlying locations of enhanced tidal heating because volcanic systems could tap magma from anywhere within the magma ocean. In addition, the efficient decoupling of the shell from the interior would make non-synchronous rotation of the shell more likely. As discussed in Section 2.3, the presence or absence of a magma ocean can be ascertained with considerable confidence from geophysical observations (especially the induced magnetic field, the k_2 Love Number of the tidal gravity field, and libration amplitude).

If Io does not have a magma ocean, the question is whether tidal dissipation occurs mainly within the deep or shallow mantle (Figure 1.6, left). Deep- versus shallow-mantle heating could be distinguished based on the distribution of active volcanoes and the magma temperatures. For instance, enhanced heat flux at high-latitudes with high eruption temperatures associated with rapid adiabatic magma ascent would favor the deep-mantle heating end-member, whereas enhanced low-latitude volcanism with lower eruption temperatures would favor shallow heating. However, testing these scenarios would require improved imaging of Io at high latitudes using both visible and thermal infrared measurements to constrain the nature of near-polar volcanic systems and their contribution to Io's overall thermal emission (Davies et al., 2015; Hamilton et al., 2013).

Alternatively, if Io includes a melt-rich interior layer, then it would be possible for fluid tidal dissipation to occur within Io's interior (Figure 1.6, right), with the magnitude of tidal heating

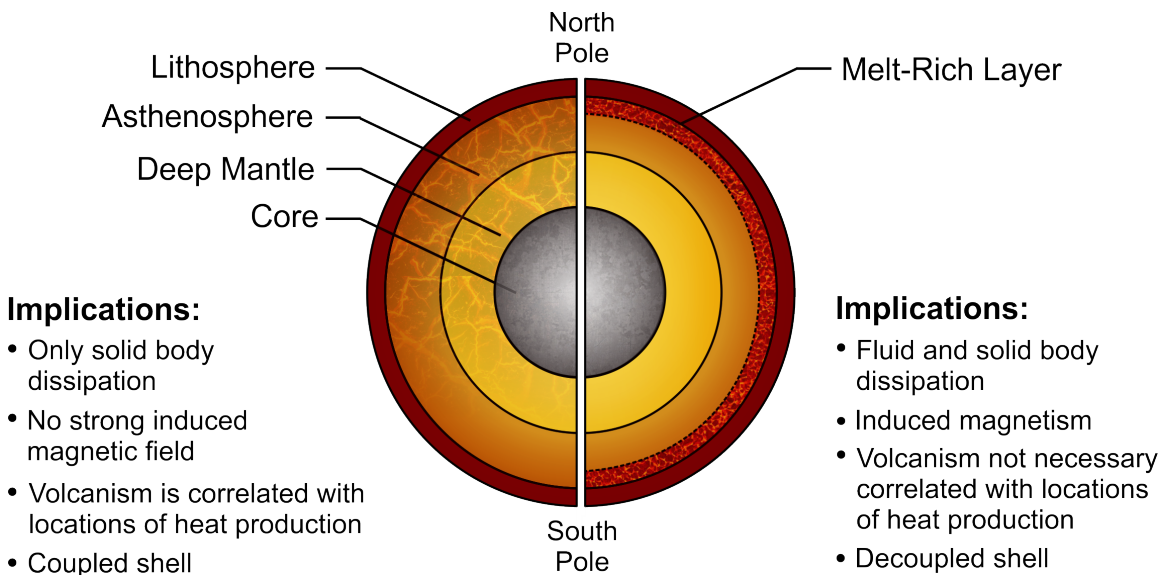


Figure 1.5: Schematic illustration of the structure of Io's interior, with arbitrary layer thicknesses, if it were solid (left), or if it included a magma ocean (right). Implications of each scenario are summarized. Adapted from Hamilton et al. (2018).

being strongly controlled by resonances that depend largely on the thickness of the melt layer, h , and its dissipation factor, Q (Tyler et al., 2015). A layer with a silicate melt fraction $>20\%$ and $h > 50$ km could generate a strong induced magnetic field, as documented by Khurana et al. (2011), but it is unclear if this layer is a magma ocean that behaves as a continuous fluid that decouples the shell from the interior, or if the layer is a melt-rich “magmatic sponge” with interconnected silicate melt and interconnected silicate solid (Section 2.3). A third possibility to explain strong magnetic induction is $<20\%$ melt with enhanced conductivity due to dissolved volatiles (Ni et al., 2011; Pommier et al., 2008; Sifré et al., 2014). In all three cases, a strong magnetic induction signal would be expected, but only the liquid magma ocean scenario would be expected to generate a high k_2 value (0.5; Bierson and Nimmo, 2016) and high amplitude librations (Section 2.3.6), making these important future measurements. In terms of the expected location of volcanic activity associated with fluid-body dissipation, models predict enhanced heating at low latitudes (Tyler et al., 2015), but if the melt accumulates into a fully connected reservoir at a global scale, then volcanic eruptions could be sourced from any location, which would invalidate the assumption that volcanic centers would be well correlated with locations of interior heating. Instead, eruptions might be sourced near lithospheric structures that permit ascent of magma (e.g., Jaeger et al., 2003). Additionally, while the maximum temperature of the magma can be predicted based on equilibrium states for heat production and extraction within Io (Moore, 2001), these models assume only solid-body heating, which breaks down when the dissipating material no longer behaves as a solid. Consequently, if fluid tidal heating were to occur, it may be possible to “superheat” the melt and produce high temperature eruption

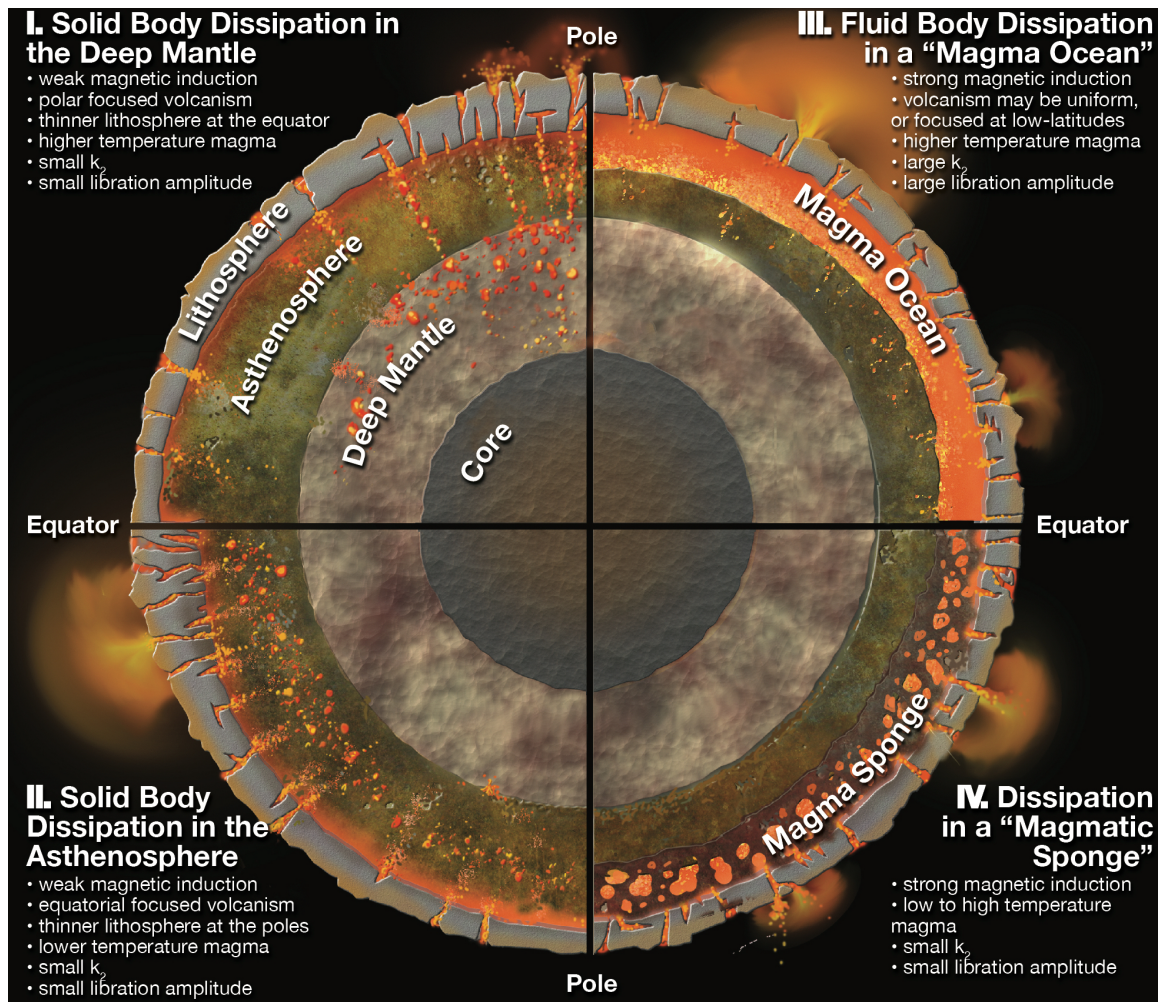


Figure 1.6: Schematic illustration of the structure of Io's interior, with arbitrary layer thicknesses, considering deep- (top) and shallow-mantle (bottom) end-member tidal dissipation scenarios within a solid interior (left panels) versus how dissipation processes would be affected by either a magma ocean, or globally extensive high-partial melt layer (i.e., a magmatic sponge; right panels).

products, with temperature distributions that are not necessarily correlated with source depth or composition. Lastly, it is possible that a combination of fluid and solid tidal dissipation occurs within Io, as suggested by Tyler et al. (2015). The key observations summarized in Figure 1.6 would provide important new information for resolving the issues surrounding whether or not Io has a magma ocean and how dissipation may be partitioned between Io's solid and fluid layers.

1.4 Europa and Enceladus

1.4.1 Europa

Interior structures of ocean worlds are illustrated in Figure 1.7.

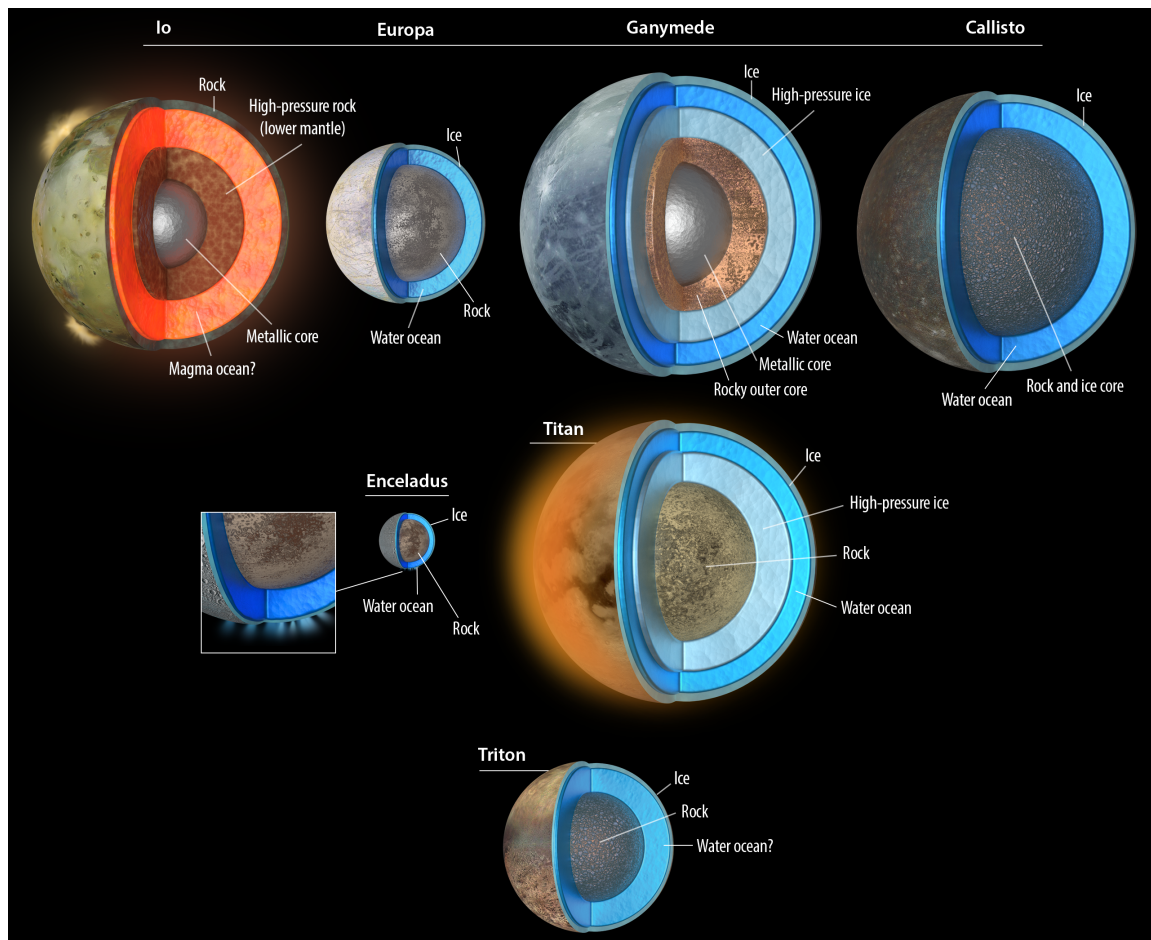


Figure 1.7: Schematic illustration of the solar system's ocean worlds. All worlds are shown to scale with one another, although the size of the interior layers are only approximate.

The detection of an induced magnetic field on Europa provides evidence for a salty subsurface ocean (Kivelson et al., 2000). However, the ocean and shell thicknesses are only weakly constrained. A combined ocean and shell thickness in the range of about 80 to 170 km was estimated from the mean moment of inertia inferred from gravity data using the Radau–Darwin approximation (Anderson et al., 1998). Thus, tidal dissipation models must consider a wide range of shell and ocean thicknesses. Multi-frequency magnetic induction from Europa Clipper is expected to address this question (Raymond et al., 2015).

Models indicate that tidal dissipation in the subsurface ocean is orders of magnitude smaller than radiogenic heating in the silicate mantle unless the ocean is very thin (thickness <0.5 km) and has a large linear drag coefficient (Matsuyama et al., 2018). However, the presence of a subsurface ocean has a large effect on overall tidal dissipation because it decouples the deep interior from the icy shell, increasing tidal deformation and energy dissipation in the icy shell, and decreasing tidal dissipation in the silicate mantle. As a result, most of the tidal heating is produced in the icy shell, where it can be orders of magnitude higher than radiogenic heating in the silicate mantle (Tobie et al., 2005). Most of the tidal dissipation occurs at the bottom of the icy shell due to the strong temperature dependence of the energy dissipation rate (Ojakangas and Stevenson, 1989).

1.4.2 Enceladus

The Saturnian moon Enceladus is another archetypal example of tidal dissipation. The intensity of cryovolcanic eruptions from the south polar fractures are timed with the tidal cycle and are strongly indicative of tidal heating (Hedman et al., 2013), but there are many questions related to the dynamics and mechanics of the process (Nimmo et al., 2018). Four key questions have been put forth:

1. **Is Enceladus in equilibrium?** The use of astrometry and thermal imaging (particularly over multi-decadal timescales) can potentially answer this question by comparing the tidal evolution of Enceladus' orbit with its heat flow, and assessing temporal variability in the heat flow (see also Section 2.4 below).
2. **What are the properties of the core?** Determining how close to hydrostatic the rocky core is (using long-period librations, surface tracking, and high-order gravity measurements) and its isotopic equilibrium temperature could determine if the core is the source of heating at Enceladus.
3. **How is the ice shell deforming?** The potential future use of radar to measure lateral flow and dynamic topography and the identification of non-synchronous rotation, true polar wander, or nutation will help constrain if convection is active. Phase lag—which could be obtained from tidal tomography using continuous temperature derived from chemical or isotopic equilibria and/or synthetic aperture radar (SAR) interferometry—can identify inelastic processes in the shell.
4. **Do Dione and Mimas have oceans?** Future exploration may answer this question and identify whether or not Enceladus is anomalous.



2. Key Science Questions and Measurements

During the KISS study, much time was spent defining and discussing science questions, and it became evident that these could be condensed into a short list of overarching questions. Below we discuss these five key questions and the measurements or modeling needed to address them.

2.1 Question 1: What do volcanic eruptions tell us about the interior?

2.1.1 Introduction to Question 1

Volcanism is a fundamental geologic process that has shaped the evolution of bodies across the solar system, from Mercury to Pluto. Incontrovertible evidence for active eruptions in the outer solar system has been found on Io and Enceladus (Figure 2.1). In both of these cases, plumes of condensing gas blasting out from discrete vents have been clearly resolved in iconic images from nearby spacecraft. Possible eruptions have also been seen on Neptune's large moon Triton (Soderblom et al., 1990), initially interpreted as a seasonal process driven by solar heat but recently reconsidered to be volcanism driven by obliquity tides (Nimmo and Spencer, 2015). Suggestions of plume activity at Europa have come from Hubble Space Telescope (HST) observations (Roth et al., 2014; Sparks et al., 2016), as well as reinterpretation of Galileo plasma data (Jia et al., 2018), and interpreted as volcanic in origin. Surface features that are suggestive of cryovolcanism (e.g., Kargel, 1995) are found on Ceres, Europa, Ganymede, Dione, Tethys, Titan, Miranda, Ariel, Pluto, and Charon. Active silicate eruptions are found on Earth and Io, and perhaps Venus as well, but we restrict further discussion to worlds with potential tidal heating.

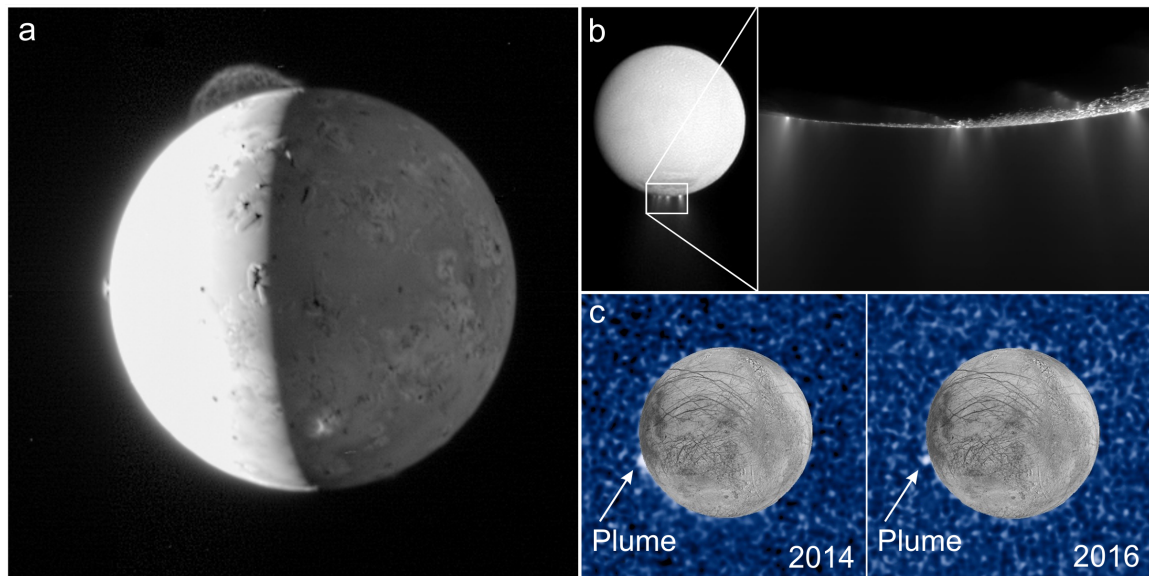


Figure 2.1: Plumes detect on Io (left, from New Horizons), Enceladus (top right, from Cassini), and Europa (bottom right, from HST). NASA images from Planetary Photojournal.

Volcanism is especially important for the study of the interiors of planetary bodies. It provides samples from otherwise inaccessible depths, as well as evidence that there is sufficient internal energy to melt the interior. The style of eruption places important constraints on the density and stress distribution in the subsurface. Furthermore, the evolution of volcanism across time and space provides key insights into the thermal and chemical evolution of a planetary body.

The basic state of geologic materials, as well as rheologic parameters such as viscosity, is strongly dependent on chemical composition and temperature. Pressure plays an important but easily predictable role. Observing the composition and temperature of the fluids erupting in volcanic and cryovolcanic eruptions provides valuable information as to the state of the upper tens to hundreds of kilometers that are tapped by volcanic activity. For tidally heated bodies, detailed observations of the eruptive products can place strong constraints on the temperature and viscosity structure with depth, which is a critical piece of information for modeling the magnitude of the tides as well as the distribution and extent of tidal dissipation.

2.1.2 Eruption Temperatures

While eruption temperature is a greatly desired quantity, it is difficult to precisely measure via remote sensing. For the silicate volcanism on Io, thermal emission from active volcanic eruptions can be readily detected even with telescopes on Earth. These emissions are often reported in terms of surface temperatures (and areas). However, the surface temperatures reported are not the temperature of the erupting fluids; models show that they are likely hundreds of K lower than

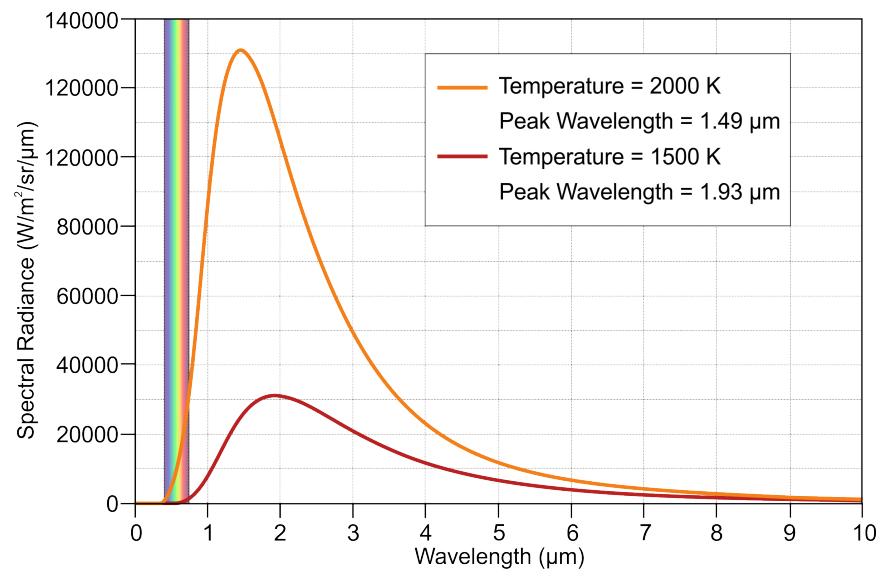


Figure 2.2: Thermal emission of a blackbody for ultramafic (~2000 K) and mafic (~1500 K) eruption temperatures, assuming an emissivity of 1. The difference is most readily measured near 1 micron, on the steeper, short-wavelength side of the spectrum.

the actual eruption temperature because the lava cools extremely rapidly (Carr et al., 1998). In fact, only a small amount of lava exposed at the surface is at the eruption temperature. Thus, lava-cooling models must be used to convert the distribution of surface temperatures into an estimate of eruption temperature (e.g., Davies, 2007). These cooling models are dependent on an accurate understanding of the style of the eruption and hence the dynamics of the lava at and away from the vent. The style of eruption can be inferred with some confidence from repeated observations over months and years in the near-infrared (2–5 μm; Davies et al., 2010), but is best determined via repeat imaging with sufficient spatial resolution to directly observe the style of volcanic activity. Previous imaging of eruptive activity on Io indicates that 200 m/pixel suffices for the most vigorous eruptions, such as large lava fountains (McEwen et al., 2000), but ~20 m/pixel is more appropriate for quiescent activity like active pahoehoe lava flows (Keszthelyi et al., 2001).

Even when the volcanic activity is spatially resolved, each pixel will include material at a range of temperatures. To derive a meaningful temperature from the thermal emission, data at multiple wavelengths is required. The highest temperature component is best constrained with data collected along the steep, short-wavelength, section of the thermal emission spectrum (Figure 2.2). For silicate lavas, this means data collected in the visible to nearest infrared wavelengths. Data collected at longer wavelengths are essential for understanding the total thermal emission and time history of an eruption but provide much weaker constraints on eruption temperature. Measuring the temperature of active cryovolcanism faces analogous challenges, but the lower temperatures mean that the ideal wavelengths shift to the thermal infrared (~5–100 μm).

The eruption temperature can be used to distinguish between fundamentally different types of fluids, such as silicates versus sulfurous materials versus aqueous fluids. It has been used to suggest ultramafic rather than just mafic compositions on Io (Davies et al., 2001; de Kleer et al., 2014; McEwen et al., 1998), but the Galileo data has several severe limitations and inferring magma composition from temperature relies on several assumptions whose validity has not been tested. For example, the link between temperature and mafic/ultramafic composition relies on the assumption that Io has a chondritic bulk composition. Furthermore, it is difficult to rule out significant heating of the rising magma by processes such as viscous heating and even electrical currents (Kargel et al., 2003; Keszthelyi et al., 2007). It is therefore extremely important to have an independent estimate of the composition of the erupting materials.

In general, near- to mid-infrared spectroscopy is the preferred method to remotely determine the composition of both aqueous and silicate materials. It has proven useful on icy satellites including Europa and Enceladus (e.g., Brown et al., 2006). Even small amounts of ammonia, sulfates, and other compounds can be readily detected as mixtures within water ice (e.g., Clark et al., 2013). However, on Io, near-infrared spectroscopy may be confounded by the glassy nature of the warm lava surfaces and the sulfurous coating on cooled lavas. Alternative methods, such as gamma ray spectroscopy, are unable to collect useful data during a limited number of high-speed flybys. Sampling the plumes above eruptions could provide detailed compositional information on volcanic gases, but not direct measurements of the chemistry or mineralogy of the lavas.

The most promising method to determine the composition of Ionian silicate lavas is via thermal infrared spectroscopy to measure the location of the Christiansen frequency, which is directly tied to silica content (Logan et al., 1973; Maturilli et al., 2014; Salisbury and Walter, 1989). This method has been demonstrated on the Moon, where returned samples are available (Greenhagen et al., 2010). Ongoing laboratory studies on how these spectral features are manifested when the material is hot are essential for properly interpreting this type of data (Helbert et al., 2013; Lee and Ramsey, 2016).

Ultimately, in situ compositional measurements from landed instruments are desired. The types of instruments used on Mars should be appropriate for Io (Grotzinger et al., 2012). For icy surfaces, mass spectrometry of evolved gases would be ideal, possibly supplemented with electrical conductivity measurements and differential calorimetry (Pappalardo et al., 2013). Raman spectroscopy shows promise for both silicate and icy worlds (Tarcea et al., 2008).

2.1.3 Eruption Styles

Volcanic fluids (magma) rise to planetary surfaces, where they erupt (becoming lava). Ascent may be driven by the density difference between the magma and the material above it (be it rock or ice). Alternatively, magma may be lifted to the surface by excess hydrostatic or dynamic pressure on the magma origination or storage location. The latter process explains the eruption

of dense basalts through a less-dense anorthosite on the Moon (Wilson and Head, 1981). The mechanism of an eruption depends on the rheology and thermodynamics of the erupting material, and whether or not the magma contains exsolving volatiles or undergoes phase changes as pressure decreases during ascent. Understanding the eruption mechanism and style of eruption allows quantification of heat transport from the planetary interior, and constrains interior conditions needed to generate the melt. Mapping surface changes and measuring thicknesses of deposits allows quantification of erupted volumes.

On Io, there is a diverse set of eruption styles that are generally indicative of low-viscosity, high temperature lavas with different volatile contents (e.g., Davies et al., 2010), with powerful, voluminous volcanic activity forming lava fountains, large plumes, and extensive lava flows. Much activity takes place within paterae (caldera-like depressions). Such activity can be best classified through high-spatial-resolution imaging. Observing on timescales ranging from seconds to years, at ultraviolet through infrared wavelengths ($\sim 0.1\text{--}100\ \mu\text{m}$), captures the evolution of eruptions at local to global scales. Measurements of topography, including lava flow thicknesses, can be made using stereo imaging with a pixel scale $<5\ \text{m}$ to obtain a vertical precision of $<5\ \text{m}$. For large landforms (e.g., mountains, mesas, and paterae), $<50\text{-m}$ vertical precision is desired.

On icy worlds, the goals are essentially the same as for volcanic Io, even if temperatures are shifted lower. The style of active cryovolcanism can be mapped using visible and thermal mapping at the same spatial scales as for Io (Spencer et al., 2006). On icy worlds, radar sounding can investigate the structure of the icy lid through which the cryomagmas must ascend, as demonstrated in Antarctica (Carter et al., 2009), and planned for the Europa Clipper and JUICE missions.

2.1.4 Spatial Distributions of Volcanoes

Constraints on the spatial distribution of volcanoes on Io is determined primarily through global imaging of the surface. Global imaging from Voyager and Galileo is incomplete and should be done systematically at scales $\leq 100\ \text{m/pixel}$ and at multiple of visible and near-infrared wavelengths (from $0.4\text{--}5\ \mu\text{m}$). Images will need to be acquired: (1) at the appropriate photometric conditions for mosaicking so that images can be translated in radiometrically and geometrically accurate global basemaps; (2) including limb profiles that provide $<100\text{-m}$ resolution for observations of eruption columns; and (3) place special emphasis on polar regions that have been poorly covered in the past. Thermal mapping at wavelengths $5\text{--}100\ \mu\text{m}$ and resolutions $\leq 1\ \text{km}$ will also play a role in determining the spatial distribution of volcanic activity; thermal signatures will help distinguish between ambiguities in image data and provide a diagnostic for classifying volcano type. Other tools that may prove useful for assessing the spatial distribution of volcanoes include radar sounding and topographic mapping. See Section 1.3 for a review of previous work.

The slower pace of activity on the other tidally heated worlds means that measuring the spatial distribution of (cryo)volcanism necessarily relies on interpreting older deposits. For example,

while Enceladus currently only has plumes erupting from near its south pole, determining if such eruptions were more widespread in the past requires interpreting the surface geomorphology across the body (e.g., Bland et al., 2012). It is hard to put firm requirements on the scales and wavelengths of new observations needed to substantially improve earlier geologic studies because there tends to be a smooth relationship between the quality of the input data and the quality of the interpretations. However, the imaging requirements as stated for Io are a good baseline because they constitute a major improvement over existing datasets. One of the best ways to summarize the geologic history of a body will be in new global geologic maps. The map units should be delineated on the basis of age and lithology in a manner that allows the temporal and spatial distribution of geologic processes to be detailed.

2.1.5 Temporal Variability

The temporal variability of eruptions on tidally heated worlds has not been well constrained, but is best measured at the hundreds of active volcanoes on Io. The Galileo mission, particularly the Near-Infrared Mapping Spectrometer (NIMS), was able to track the output of many volcanoes over the more than six years of the mission. Ground-based telescopic observations have extended the time period of observations (Cantrall et al., 2018). While many of Io's volcanoes have had relatively constant or slowly varying thermal output, a few have exhibited massive, brief spikes in power ("outburst" eruptions) that are many orders of magnitude above levels typical of Io's volcanoes (Davies et al., 2010; de Kleer and de Pater, 2016a; Witteborn et al., 1979). Estimated effusion rates of tens to hundreds of m^3/s are likely typical of Io's volcanoes (Davies, 2003; Davies and Ennis, 2011; Davies et al., 2001; Keszthelyi et al., 2001), but outbursts, the most powerful class of ionian eruptions, can have fluxes of tens or hundreds of thousands of m^3/s , or even higher (Davies et al., 2001; de Pater et al., 2014).

Galileo NIMS observed thermal emission on timescales ranging from months to a fraction of a second. Most hot spots showed short-timescale stability, but in at least one case, at Marduk Fluctus, there were large changes in thermal emission (both waxing and waning) in the space of a few minutes over wavelengths from 1 to 5 μm ; this event was modeled as a large explosive eruption event that briefly generated large areas at very high temperatures and small clasts that rapidly cooled (Davies et al., 2018). The Cassini Imaging Science Subsystem (ISS) observed Io at low spatial resolution but high temporal resolution during a distant flyby in 1999 (e.g., Radebaugh et al., 2004). Some hot spots, including Pele, showed rapid variability, but this might be expected from an instrument sensitive only to the hottest (and therefore most rapidly cooling) surface present. Similarly, the New Horizons spacecraft was able to measure short-timescale variations on the scale of seconds to hours (Rathbun et al., 2014). None of the three volcanoes observed by New Horizons exhibited variations on the scale of seconds, and only East Girru had substantial variations over the course of minutes and hours, albeit at short infrared wavelengths.

Improved understanding of the temporal variations in the thermal output of individual volcanoes requires better spatial and temporal resolution. Based on terrestrial experience, the heat flux from lava fountains is expected to vary by factors of many over timescales of seconds and minutes as pulses of gas cause large bubbles of lava to burst and the height of fountains to wax and wane. Due to the way the pressure in magma chambers is relieved, eruptions on Earth typically build up over a period of hours and gradually shut down over a period of months. It is rare for volcanoes on Earth to persist at a relatively constant level for years or decades. If Io's volcanoes do not follow these general patterns, it is a strong indicator that the plumbing system that feeds them is different from those typically found on Earth, which in turn could point to an important difference in how tidally heated worlds lose their internal heat. To confidently reach this conclusion, a statistically meaningful number of Io's volcanoes need to be monitored at a frequencies ranging from seconds to months over hundreds of cycles.

2.1.6 Global Average Heat Flow

While short and medium-length timescales are useful for understanding eruption types and properties, observations over longer periods and at longer wavelengths are needed to understand variations in the global heat flow. Only ground-based observations have been able to track infrared emission over a timescale of decades. Veeder et al. (1994) used a decade of ground-based observations at wavelengths from 4.8 to 20 μm to determine how the total power output varied with time. They found that the average heat flow was 2.54 W/m^2 with a standard deviation over that period of only $\sim 10\%$. They considered this a lower limit because the Earth-based data are not sensitive to high-latitude heat flow (which might exceed the global average via deep-mantle tidal heating; Figure 1.4), nor any potentially significant conducted heat. The lower-limit endogenic power emitted by Io was estimated to be $1.05 \pm 0.12 \times 10^{14} \text{ W}$ (Veeder et al., 1994).

Veeder et al. (2009, 2011, 2012, 2015) estimated the total thermal emission from all active and recently active volcanic centers on Io, totaling 250 discrete sources (Figure 2.3). These volcanic centers accounted for 56.2 TW, or about 54% of Io's total thermal emission (using the estimate from Veeder et al., 1994). The resulting Io volcanic heat flow map (Figure 2.4; Davies et al., 2015) represents an estimate of the magnitude and distribution of volcanic heat flow—and, by inference, volcanic advection.

The Veeder et al. (1994) estimate is supported by Galileo data. Rathbun et al. (2004) determined Io's global heat flow from Galileo Photo-Polarimeter Radiometer (PPR) observations that covered 50% of the surface. They assumed that passive nighttime temperatures have a latitudinal dependence with a temperature of 95 K at the equator. By subtracting this background from the observations, they calculated a heat flow of 2.4 W m^{-2} if the area covered is representative of the entire surface and 2.1 W m^{-2} if Loki Patera is unique. These values are remarkably close to that of Veeder et al. (1994).

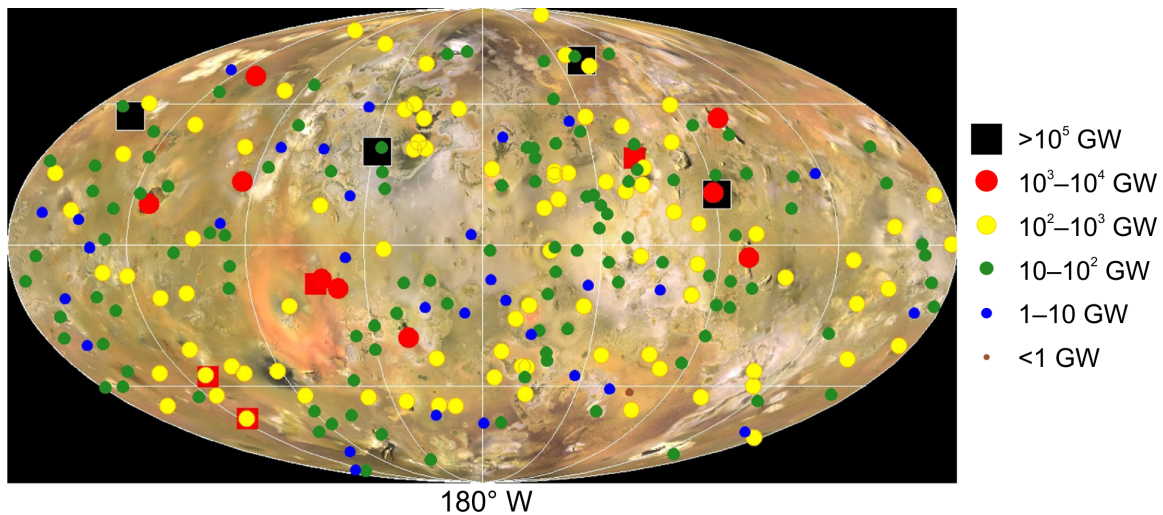


Figure 2.3: Thermal emission from Io's volcanoes. This Mollweide equal-area projection centered on 180°W longitude shows 250 active or recently active volcanoes that show measurable thermal emission, with the size and color of the symbol reflecting the magnitude of their heat flow contributions. The plot includes the locations of outburst eruptions at Surt, Tvashtar, Amirani, Pillan, Gish Bar Patera, Heno Patera, Rarog Patera and 201308C. Because of their transient nature outbursts are shown as black or red squares. From Davies et al. (2015), using data from Veeder et al. (2012, 2015).

Quantification of thermal emission from all of Io's volcanic centers by Veeder et al. (2015) reveals that resolved active silicate volcanism accounts for only about half of Io's total known heat flow (n.b., less than 1% of Earth's heat flow is from eruption of silicate lava; Turcotte and Schubert, 2002). It is therefore crucial to determine the nature of the other half or more of Io's heat flow. The process or processes must involve relatively low temperatures, perhaps subtle surface temperature variations caused by conduction from intrusions and heat transport by movement of low temperature sulfur and SO₂. Relatively old (nearly completely cooled) lava flows must also contribute low-temperature conducted heat flow (Stevenson and McNamara, 1988). Detection of low-temperature processes was difficult with Galileo measurements. The Voyager Interferometer Spectrometer (IRIS) observed Io from ~5–50 μm, but at low spatial resolution (Pearl et al., 1979).

All of the models of Io's heat flow discussed in this section required assumptions about re-radiated solar heat. This is critically important because a large fraction of Io's endogenic heat flow occurs at low temperatures, not easily distinguished from re-radiated insolation. The most rigorous remote-sensing-based approach would be to map Io's Bond albedo (sunlight reflected at all angles and wavelengths) and thermal inertia (from day and night thermal measurements), both at high resolution, to accurately determine the passive heat flow over Io at any time and place, then subtract that quantity from the total (passive + active) thermal emission from ~5–50 μm. This approach was followed using disk-integrated Voyager IRIS data of day and night hemispheres

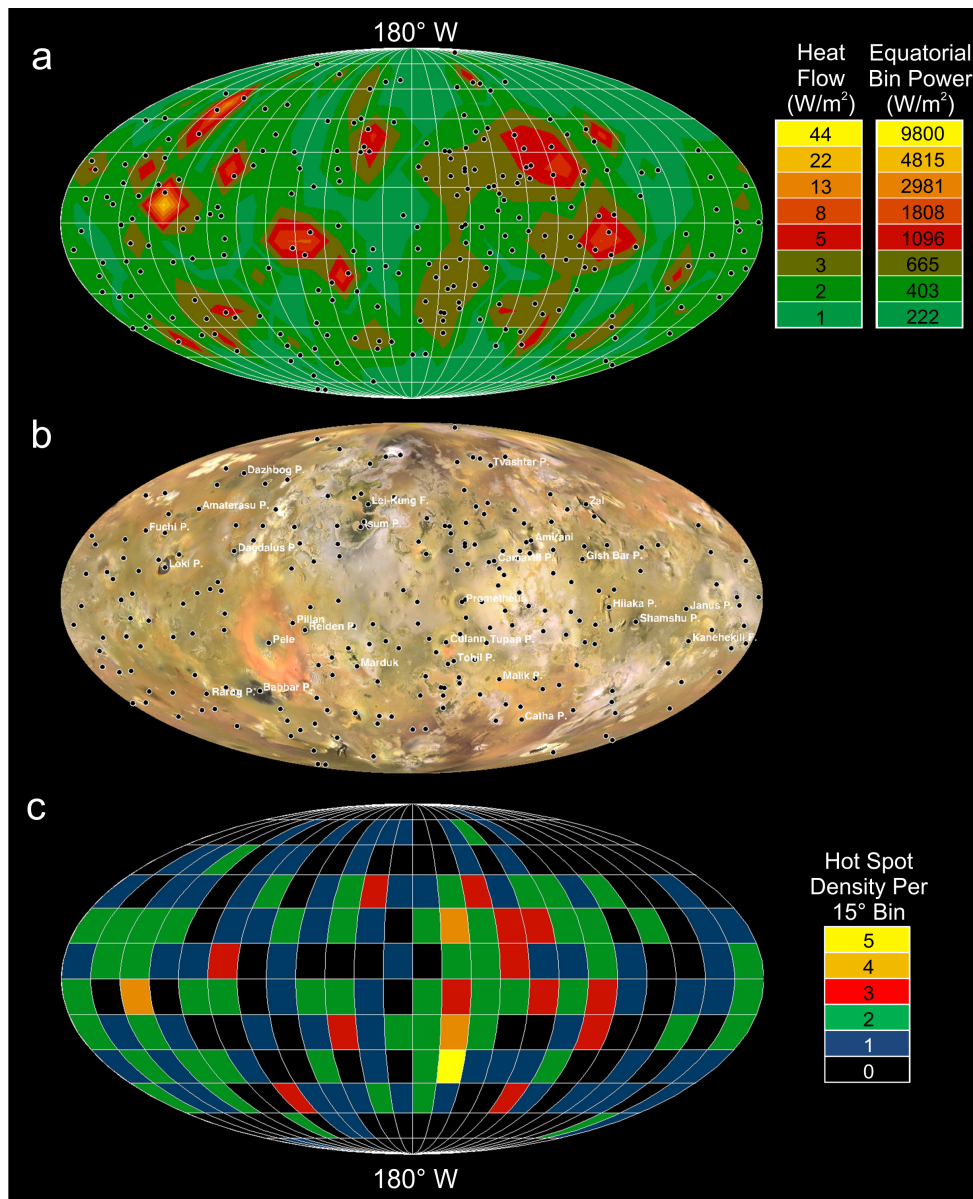


Figure 2.4: Mollweide equal-area projections of Io centered on 180 W longitude (the anti-jovian point). North is up. (a): heat flow map using hot spot data in Veeder et al. (2015). Heat flow is shown as the log of power at the scale on the right. This scale also shows power output for a 15×15 bin located on the equator with an area of $2.26 \times 10^{11} \text{ m}^2$. The background heat flow is taken to be 0.98 W/m^2 . (b): Io Voyager-Galileo mosaic (after Becker and Geissler (2005)) with 242 hot spot locations (excluding outbursts) shown as black circles. (c): Hot spots per 15 degree longitude and latitude bin, excluding outburst eruptions. Hot spots per bin range from 0 to 5. Hot spot density is color coded as shown in the bar at right. From Davies et al. (2015).

(McEwen et al., 2004; Spencer et al., 2002) along with a Galileo-based global value for Bond albedo (Simonelli et al., 2001), with a resulting global average heat flow of $2.1 \pm 0.7 \text{ W m}^{-2}$. The error bars were large due to subtracting two numbers that each have significant uncertainties, but the result is robust because it does not depend on assumptions about how heat is divided into endogenic and passive components. The Bond albedo map (Simonelli et al., 2001) is incomplete, and may have changed since the Galileo mission observations. Note that determining Bond albedo requires observations over a broad range of phase angles, not possible from Earth-based telescopes. A future spacecraft mission should strive to map Io's Bond albedo and thermal emission to accurately measure the endogenic component. Thermal emission data needs to include mid-day and nighttime maps for thermal inertia, or in and out of eclipse coverage for the Jupiter-facing hemisphere. New observations require sufficient spatial resolution to determine if this low-temperature heat flux is extremely diffuse (as expected from conduction through the lithosphere) or is focused at specific geologic structures (e.g., sulfur or sulfur dioxide flows). Additional observations may also be needed to better constrain the effect of the latent heat of sublimating SO_2 (Walker et al., 2012).

2.1.7 Differentiation and Crustal Recycling

While volcanism does not provide a direct view of the interior of a body, it provides some of the best constraints on different interior models. For example, volcanic processes operating for four billion years would be expected to strongly differentiate incompatible elements into a low-density crust, resulting in low-temperature, high-silica volcanism at the present time (Keszthelyi and McEwen, 1997). The ubiquity of mafic/ultramafic volcanism effectively negates this model and requires extremely efficient recycling of the crust into the mantle. A magma ocean would be compatible with this geochemical model for Io (Keszthelyi et al., 1999, 2007). Better information on the composition and temperature of the erupting materials will allow more sophisticated petrologic models for the magma ocean and mantle of Io to be tested. Similarly, it is rapid volcanic resurfacing that allows the heat pipe model for Io's lithosphere (O'Reilly and Davies, 1981), which permits the observed mountains on Io to exist. More detailed studies of the interaction between tectonic and volcanic features should allow more refined models of Io's crustal recycling to be tested.

2.2 Question 2: How is tidal dissipation partitioned between solid and liquid materials?

2.2.1 Introduction to Question 2

Gravitational forcing of a satellite produces tides, and the tidal energy associated with this process can be dissipated as heat in the solid and liquid regions of the satellite. This requires

a time-varying gravitational forcing, which can be produced by orbital eccentricity, obliquity, libration, and non-synchronous rotation. The total volume- and time-averaged tidal energy dissipation rate, including dissipation in all of the solid and liquid regions, can be obtained by setting it equal to the rate of work done by the tide. The total energy dissipation rate can then be written as a function of the forcing tidal potential and the response potential arising from the deformation of the satellite (Platzman, 1984; Zschau, 1978). This approach can only provide the volume-averaged tidal dissipation, and does not explain what processes cause the dissipation. Understanding the interior distribution of tidal dissipation requires modeling each layer separately.

Tidal energy dissipation is commonly described using a tidal quality factor:

$$Q = 2\pi E_{\max}/E_{\text{diss}} \quad (2.1)$$

where E_{\max} is the peak energy stored in the cycle and E_{diss} is the energy dissipated during a complete forcing cycle (e.g., Goldreich and Soter, 1966). As discussed above, because the total tidal energy dissipation rate depends on forcing and response potentials, Q can also be defined in terms of the phase delay of the response potential. However, the usage of Q for tidal dissipation in liquid regions is problematic because there is no peak energy stored in a liquid. It is possible to redefine Q in terms of the maximum kinetic energy of the ocean (Beuthe, 2016; Chen et al., 2014; Matsuyama, 2014; Tyler, 2011). Nevertheless, in addition to requiring a modification of the original definition, the modified definition also leads to counter-intuitive results, such as decreasing energy dissipation with decreasing Q because the kinetic and dissipated energies are coupled (Matsuyama, 2014).

2.2.2 Constraints from Laboratory Experiments

The tidal quality factor of a solid material, Q_{μ} , due to dissipation in shear is well defined at small scales. Laboratory experiments are designed to measure the mechanical behavior of materials over a range of conditions and frequencies (Faul and Jackson, 2015; McCarthy et al., 2011). The response of Earth and planetary materials depends on many microstructural characteristics as well as on the timescale of forcing. At high frequency materials respond via instantaneous elastic deformation. At very low frequency quasi-steady-state forcing, the response is permanent viscous deformation. In between these timescales the response is time-dependent, but fully recoverable anelastic deformation. Depending on the tidal period of an orbiting body, the response of the material within may be viscous and/or anelastic (McCarthy and Cooper, 2016). Intrinsic mechanisms of anelasticity, called internal friction or attenuation (the inverse of Q_{μ}), are accommodated by the thermally-activated motion of defects at the lattice and grain scale. Different mechanisms of dissipation have different timescales of response and different dependences on stress, temperature, pressure, as well as the grain size and melt content (and location) of the material. This property is measured by applying a sinusoid of stress to a sample

and measuring the strain (also a sinusoid), such that the tangent of the phase lag between the two is $1/Q_\mu$ and the ratio of the amplitudes is the relaxed modulus. Existing lab studies on olivine, ice, and rock analogues have isolated individual mechanisms, particularly at low stress, low amplitude conditions. Under those conditions, dissipation in polycrystalline materials occurs by mass diffusion at grain boundaries and the attenuation spectra displays a modest frequency dependence over a broad frequency range. The form of intrinsic attenuation requires, at a minimum, a mathematical description that includes an anelastic term, such as in the Extended Burgers or Andrade modes (Renaud and Henning, 2018).

Although decades of experimental studies have measured the anelastic behavior of Earth and planetary materials and there is consensus in the experimental community about the low stress, low amplitude response over a broad range of conditions, such research has been primarily focused on constraining seismic wave attenuation. Since seismic waves have much smaller stress amplitudes and are much higher frequency than tidal forcing, there are still significant gaps in our understanding of tidal dissipation mechanisms. For instance, it is not clear under what conditions tidal stress could alter the existing grain size and/or melt distribution within the material being stressed. Additional experiments focusing on applicable planetary conditions would elucidate the low frequency, high amplitude (potentially non-linear) mechanisms of anelasticity active in tidally-stressed planetary interiors.

2.2.3 Dissipation in Solid Regions

In solid regions, tidal dissipation occurs due to anelastic deformation, as described above. In principle, one should be able to derive the total energy dissipated from a measurement of the phase delay in the tide. However, this requires a precise definition of the phase delay and its relation to Q . The phase lag requires a precise definition because it can be defined based on the radial displacement, tangential displacement, or gravity, which have different phase lags (Zschau, 1978). Although the material Q_μ can be measured in laboratory experiments as described above, Q_μ is not the same as Q due to self-gravity effects, even if the satellite is homogeneous and composed of the same material. For real satellites with multiple interior layers, the total Q depends on the Q_μ of each of the layers and the effect of self-gravity must be taken into account. Thus, the use of Q is also problematic when describing tidal dissipation in solid regions. Q is not a fundamental quantity, but a phenomenological factor whose definition depends on the particular context. Tidal energy dissipation should be characterized using fundamental quantities (e.g., the actual energy dissipation rate or a well-defined phase delay) instead of Q .

As discussed above, the work done by the satellite tide provides the total volume- and time-averaged tidal energy dissipation rate, including dissipation in all the solid and liquid regions. The tidal energy dissipation of a solid region alone can be computed by integrating the energy dissipation rate per unit volume, which is given by the product of the stress and strain. This

method provides the spatial pattern of tidal dissipation, which can be compared with the pattern due to dissipation in liquid regions. Tidal energy dissipation requires anelastic deformation, and the computation of the stress in this case requires the introduction of a complex shear modulus (e.g., Segatz et al., 1988; Tobie et al., 2005). This is typically done assuming a simple Maxwell rheology; however, as discussed above, laboratory experiments suggest that more complicated rheologies (e.g., extended Burgers or Andrade) are required (Bierson and Nimmo, 2016; Faul and Jackson, 2015; McCarthy and Cooper, 2016; Renaud and Henning, 2018). Additionally, the shear modulus depends on grain size, and therefore we need laboratory experiments on grain size under oscillatory stresses with frequencies and amplitudes similar to those of tidal stresses.

2.2.4 Dissipation in Fluid Regions

In fluid regions, tidal energy dissipation occurs due to the excitation and damping of waves and turbulence, and the energy dissipation rate depends on the nature of the fluid motions and the damping mechanisms. Fundamentally, fluids dissipate energy through a loss of momentum due to friction. This friction, or drag, can manifest itself in several ways at different scales. Both turbulence and viscosity lead to friction in a fluid medium. Viscous dissipation, which is dominant in laminar flow, occurs at the molecular level. In contrast, turbulent dissipation can occur over many different length scales. For water oceans, turbulent processes are the main control on dissipation because the molecular viscosity of water is too small to be significant, especially for the typical length scales relevant to planetary oceans. Magma oceans may have (effective) viscosities considerably higher than water depending on the degree of partial melt, porosity/permeability, and temperature of the fluid and solid medium.

The dynamical behavior of a subsurface ocean has never been observed on any scale, so the dominant dissipative mechanisms are essentially unknown. Below, we outline some possible mechanisms to dissipate tidal energy in subsurface water and magma oceans.

2.2.4.1 Turbulent Dissipation

Subsurface water oceans are expected to be very turbulent based on the Reynolds number of the ocean. It is unclear, however, what the dominant scale of this turbulence is, making it difficult to quantify. Certainly, Earth's oceans contain mesoscale eddies that contribute significantly to the effective viscosity of the ocean, and at some scale these eddies are eventually dissipated, leading to both heating and ocean mixing (Nikurashin and Ferrari, 2013; Zhai et al., 2010). At present, turbulent eddy dissipation has not been investigated in detail for subsurface water oceans, which may impact both the dynamics and heating of these oceans.

Turbulence, and therefore dissipation, is also likely to occur at any oceanic boundaries. Interaction of the flow field with a solid interface leads to small-scale turbulence, which is thought to scale

with the square of the velocity. This kind of friction is termed bottom drag, and is not usually resolved in numerical simulations. For Earth, the solid boundaries include the ocean floor and the continents, where shallow and laterally confined regions of the ocean, such as the continental shelf and inlets, become a significant source of energy dissipation (Egbert and Ray, 2001). Icy satellite oceans do not have continents, as far as we know, so the ocean is proposed to be bounded only by the ice shell above and the silicate or high-pressure ice layer below. This would mean that the ocean contains no shallow regions, which reduces the effect of turbulent boundary layer dissipation relative to Earth's oceans. Bottom drag is typically used in numerical studies of Earth's ocean tides (e.g., Egbert and Ray, 2001; Jayne and St. Laurent, 2001), and has also been applied to icy satellite oceans in scaling analysis and numerical modeling (Chen et al., 2014; Hay and Matsuyama, 2017, 2019).

2.2.4.2 Internal Friction

Friction may also occur between two adjacent fluid parcels moving relative to one another. This source of friction is often termed Rayleigh or linear drag (Neumann, 1968). Several studies of icy satellite ocean tides use this approach to modeling dissipation in the ocean because it scales linearly with velocity (e.g., Beuthe, 2016; Matsuyama et al., 2018; Tyler, 2011). Physically, this form of friction is probably most appropriate for modeling dissipation due to internal (buoyancy) waves, where there is one fluid layer moving relative to another. Internal waves are thought to be an important process in Earth's deep oceans, dissipating up to 30% of the tidal energy budget (Egbert and Ray, 2000; Green and Nycander, 2013; Jayne and St. Laurent, 2001; Nycander, 2005). The dynamical properties of internal waves depend on both the density structure of the ocean and small-wavelength topography at the ocean top and bottom, which are significant unknowns for icy satellite subsurface oceans. It is worth noting that friction associated with laminar fluid flow through a permeable layer also scales linearly with the fluid's velocity, where the magnitude of friction is controlled by the viscosity of the fluid and permeability of the solid (Das et al., 2018).

2.2.4.3 Magma Ocean Dissipation

If partial melt in a silicate layer is confined to interconnected pore-space, then fluid velocities will likely be small and the flow will be laminar. Consequently, viscous dissipation will be the dominant form of heating in the partial melt. If, however, the amount of partial melting is high enough to mechanically detach the shell from the interior, then most of the fluid's dissipation will likely occur through one or more of the turbulent processes described above. This has been examined for boundary layer bottom drag dissipation in the lunar magma ocean (Chen and Nimmo, 2016), and linear internal friction in a surface magma ocean on Io (Tyler et al., 2015).

2.2.4.4 Observational Constraints

Subsurface oceans produce spatial patterns of tidal dissipation that are different from those produced by solid body dissipation in the shell or deep interior (e.g., Chen et al., 2014; Hay and Matsuyama, 2019; Matsuyama et al., 2018; Soderlund et al., 2014; Tyler et al., 2015). The best way of determining if a subsurface ocean is the dominant region of tidal dissipation in a planetary interior is therefore by measuring the global distribution of heat flux. Additionally, spatial variations in shell thickness, which are presumably related to the spatial distribution of tidal dissipation, will also aid in determining how and where tidal energy is dissipated in the fluid and solid regions of the interior.

2.2.5 Need for Advanced Theory

Models that describe spatially variable tidal forcing, including the potential depth dependence of such forcing, already exist (see discussion above), but it remains unclear whether these models explain observed tidal heating. One of the main difficulties relates to whether the range of rheologies being modeled appropriately approximates the rheologies of the bodies of interest. Some improved constraints are likely to result from new laboratory experiments (see Section 2.2.2), but other improvements in modeling may require consideration of more complex, heterogeneous systems, including accounting separately for various microscopic physical processes such as solid-solid friction during fault slip or small-scale fluid flow within a solid matrix or the effect of grain size on creep. This type of process modeling is more challenging, and would stand in contrast to the most common modeling practices, in which these processes are only implicitly modeled through the use of phenomenological models like Maxwell viscoelasticity. Without better observational constraints on which small-scale physical processes dominate the large-scale observed viscoelastic deformation, there may continue to be significant unresolved tradeoffs in determining which regions dominate tidal heating.

In addition to testing how tidal heating models depend on specific assumed physical processes rather than on phenomenological choices, we also suggest that theoretical progress would be spurred if simple heuristics or other simplifications of tidal dissipation modeling could be created that would help both other theorists and observers to more easily understand what the main benefits and limitations of various modeling strategies are. As it is today, even some of the most basic conclusions of tidal modeling theory (such as whether the pattern of dissipation is expected to be mostly polar or equatorial) remain counterintuitive to most researchers, and progress in rejecting or supporting models is hindered by the fact that this evaluation is so challenging.

Finally, it would also be useful if models were to go farther toward making specific predictions regarding potentially observable features. For example, most existing tidal heating models do not make specific predictions about the amount of electromagnetic induction expected or the specific

thicknesses of layers (e.g., core, ocean, shell) expected due to the physical processes assumed in the modeling. Again, partly this is because many models are phenomenological, and thus may not be able to predict such quantities, and partly it is due to the fact that the prediction of these quantities often requires more sophisticated modeling than is currently done. However, without having such predictions in advance of the observations we hope to obtain from future spacecraft missions, it will be virtually impossible to reject or confirm hypotheses about the physics.

2.3 Question 3: Does Io have a melt-rich layer, or “magma ocean”, that mechanically decouples the lithosphere from the deeper interior?

2.3.1 Introduction to Question 3

Section 1.3 extensively introduces this topic, but here we provide more information and especially focus on measurement techniques. To understand the dynamics of Io—including where tidal heating occurs in the interior, how the volcanic systems function mechanically and evolve over time, and the longer-term thermal evolution of the moon—we need to better understand the interior structure.

2.3.2 What Do We Mean by a Magma Ocean?

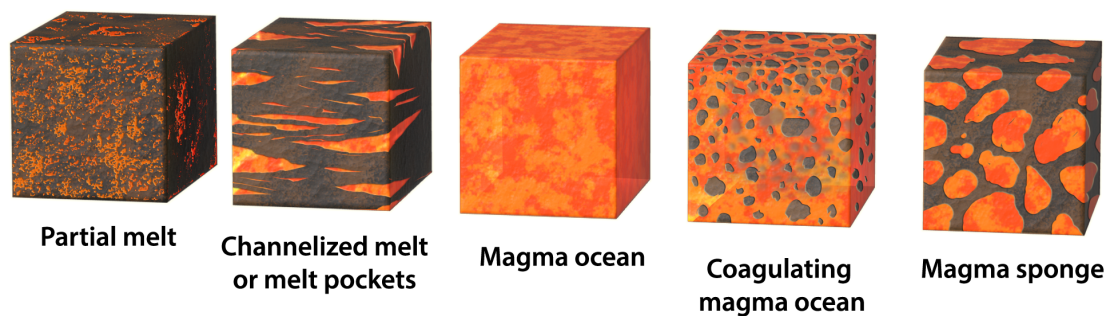


Figure 2.5: Schematic illustration of the possible physical configurations of melt within Io and other partially molten silicate worlds. The scale of each block is of-order one centimeter.

A solid heated by tides loses heat by convection and conduction, but if the heating is sufficient, then the material begins to melt. There are then two possibilities: the melt interconnects, or it fails to interconnect (Figure 2.5). The connected case is a two-phase medium that can be visualized as fluid-filled sponge in which you can get from any fluid element to another fluid element entirely on a fluid path, and the solid is likewise interconnected. Melt concentrated into channels may be a more realistic geometry (Kohlstedt and Holtzman, 2009), but explaining Io’s magnetic induction signature (Khurana et al., 2011) is thought to require interconnected melt.

This is the appropriate case to consider both for a water-ice-dominated system (the icy satellites) and for a silicate-dominated system (e.g., Io). The sponge-like medium will have rigidity because of the interconnected solid and permeability (i.e., the ability of the liquid to migrate relative to the solid because of the pressure gradient arising from the difference in liquid and solid densities). If such a medium is heated still further, there are three possibilities:

1. The melt may separate from the solid and macrosegregate to form a large purely fluid body. If this were to happen everywhere within a body, a global layer of melt would form a “magma ocean.”
2. The two-phase assemblage may reach such a high melt fraction that the grains would no longer be fully connected to each other and medium would behave like a dense suspension. This medium would have a viscosity that is larger than that of pure liquid but typically by less than a few orders of magnitude. This is also a magma ocean, but one that requires very vigorous stirring to persist, since the crystals will have a different density than the solid and the crystals tend to grow.
3. The medium could stabilize to some melt fraction at which the sponge topology is still present, but the melt that escapes is carried away into some overlying solid medium by cracks or conduits (heat pipes) rather than aggregating into an extensive fluid layer. This could be called an “asthenosphere” because it may be substantially less viscous than the deeper regions but still enormously more viscous than the two previous magma ocean examples, because the rheology will be dictated by the ability of the crystals to deform.

The boundary between the dense suspension and the much more viscous sponge-like medium with rigidity is not infinitely sharp, but this intermediate region is likely to have very rapid melt escape and other instabilities that may greatly limit its stability in a thick layer under the action of gravity. We can quantify the distinction as follows: Consider a relatively stiff spherical lid, radius, R , overlying a fluid region of thickness, D , with a more rigid region at greater depth. Suppose that in the absence of any viscous drag, the lid undergoes a radial tidal displacement h . This means that the underlying fluid has been drawn up a height h , creating a hydrostatic head ρgh in the tidal period, P . The horizontal flow needed to allow this radial motion is $w \sim (R/D)(h/P)$. If the fluid has a viscosity η , then the pressure gradient needed to drive this flow is $\eta w/D^2$. This must be small compared to $\rho gh/R$ in order that the viscosity would not impede the tidal deformation. We therefore require that $\eta R^2/PD^3 \ll \rho g$. For Io, this yields $\eta \ll (10^{12} \text{ Pa} \cdot \text{s})(D/100 \text{ km})^3$. This is well above the value of a dense suspension ($<10^5 \text{ Pa} \cdot \text{s}$) except for D small compared to 100 km, and probably below likely values of an asthenosphere ($>10^{16} \text{ Pa} \cdot \text{s}$).

According to this definition, a large tidal Love number k_2 indicates a magma ocean except in the unlikely case that an asthenosphere could have a very low viscosity, perhaps because it has very small grain size. This applies equally to water ice as to silicates, but note that the flow of water in an ice partial melt is approximately four orders of magnitude faster than the flow in a

silicate partial melt of the same grain size because of the much lower viscosity of water. As a consequence, a water ice low viscosity “asthenosphere” is highly improbable.

A low k_2 and libration amplitude (Section 2.3.6) implies the absence of a fully fluid magma ocean (Table 2.1). A thin (<20 km) magma ocean is plausible except that it might not explain the induction data. The low partial melt asthenosphere also may fail to match the induction signature, if confirmed. The observed induction signal for Io could be explained with an asthenosphere with ~20% partial melt, but that may not be stable because of very fast melt escape.

Hypothesis	k_2	Libration Amplitude	Magnetic Induction
Solid Io (few % melt)	Small (~0.1)	Low (<400 m)	Weak
Asthenosphere with ≥20% melt	Small	Low	Strong
Thick magma ocean (≥ 20 km)	Large (~0.5)	High (>800 m)	Strong
Thin magma ocean	Large	High	Intermediate

Table 2.1: Simple Tests for Io’s Interior Structure

2.3.3 Magnetic Induction

Tidal heating of Io is the best (or only reasonable) hypothesis for the high temperature volcanism observed on its surface. As discussed below, the electrical conductivity of a rock depends strongly on its temperature and the melt fraction (Pommier, 2014). Electromagnetic sounding exploits this conductivity/temperature relationship to derive temperature profiles inside planetary bodies. Electromagnetic induction sounding from space is now a well-established technique for the studies of the interiors of the Earth and the Moon (Constable and Constable, 2004; Hood et al., 1982). Using naturally occurring magnetic signals present in space in the frequency range of minutes to several hours, induction studies have not only provided temperature profiles inside these planetary bodies, but have also furnished bounds on their plausible mineralogies (Civet et al., 2015; Khan et al., 2006), because the rock composition also affects electrical conductivity. The induction technique was exploited for a planetary satellite by Khurana et al. (1998), who utilized the high conductivity of salty liquid water (compared to that of solid ice) to provide a definitive confirmation of a liquid water ocean in the icy moon Europa using magnetic field data from Galileo spacecraft flybys. Since then, the technique has been used to infer water oceans in Callisto and Ganymede (Kivelson et al., 2002; Zimmer et al., 2000) and a magma ocean in Io Khurana et al. (2011). Recently, Johnson et al. (2016) used the induction technique to place limits on the size of the conducting core of Mercury.

The time-varying inducing field in the rest frame of Io is created by the tilted rotating magnetic dipole and magnetospheric current sheet of Jupiter. The strongest signal is at the synodic rotation period of Jupiter (12.95 hr) with an amplitude of ~850 nT but another signal at the orbital

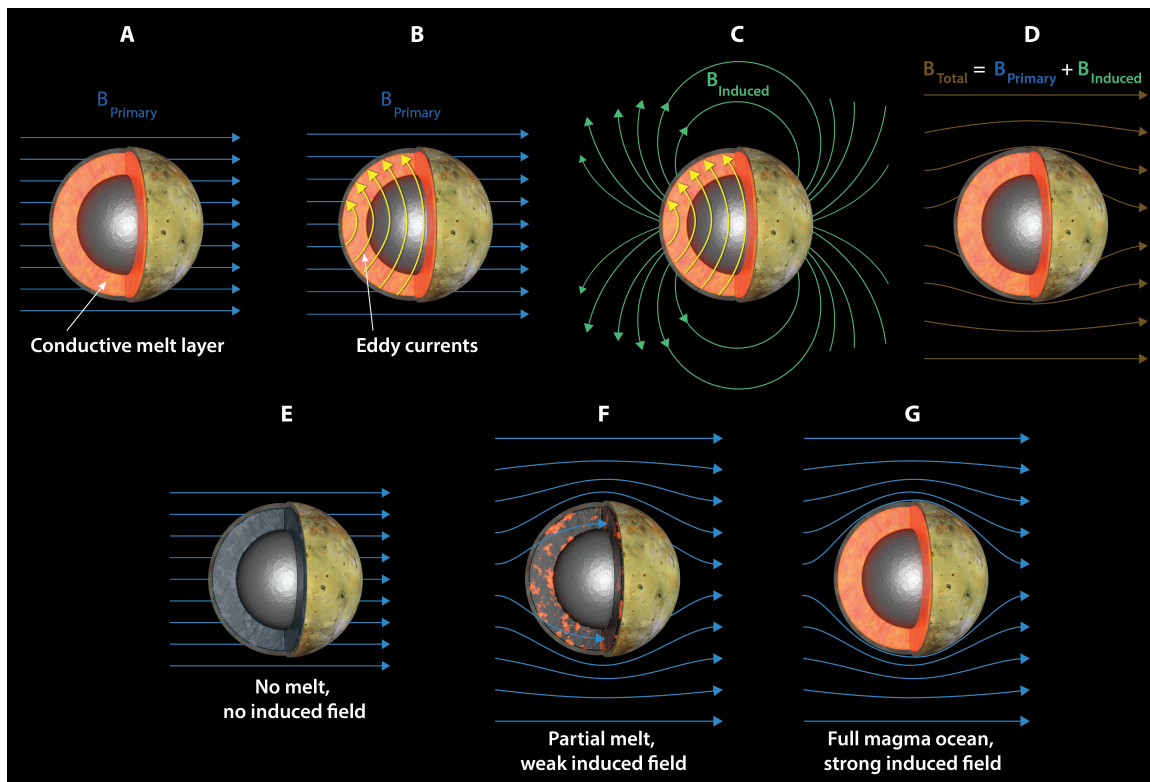


Figure 2.6: Schematic illustration of the principles behind electromagnetic sounding of Io’s interior. Io experiences a time-varying external magnetic field (A), which produces eddy currents in Io’s conductive layers (B), which drives an induced magnetic field (C). The observed magnetic field around Io is a combination of these processes (D). The magnitude of the induced magnetic field is a function of the physical and electromagnetic properties of Io’s interior (E–G).

period of Io (42.46 hr) is also quite strong (amplitude of 50 nT). Conducting regions in Io, such as a magma melt layer or hot mantle rocks, generate eddy currents in response to the oscillating primary field (see Figure 2.6). The secondary field generated by these eddy currents shields the interior of Io from the primary field and its study provides a window into Io’s internal structure.

The strength and form of a moon’s response depends on the shape, size, location, and conductivity of its conducting layers and also on the form and frequency of the primary field. As discussed by Khurana et al. (2009), in the presence of a time-varying uniform field (external harmonic of degree-1), a spherical conductor generates a dipolar response (internal harmonic of degree-1) at the same frequency. Jupiter’s magnetic field over the length scale of Io is essentially uniform; therefore, a global scale conductor such as a magma layer creates a dipolar field. The depth to which a signal penetrates a body is characterized by its skin depth, $s = (\omega\mu\sigma/2)^{-1/2}$, where ω is the signal frequency, μ is the permeability of free space, and σ is the conductivity of the body.

Thus, longer-period waves are able to penetrate deeper into a structure. Multi-frequency sounding exploits this fine-tuning ability of induction signals to probe different layers of a conductor.

The main mechanism of conductivity in solid rocks is temperature-induced semi-conduction involving mobility of charge carriers aided by point defects (Nover, 2005). For forsterite (a magnesium-rich olivine), electron mobility and—more important—ionic conduction by magnesium vacancies are additional sources of conductivity. For iron-bearing olivines, small polaron hopping (polarization from lattice deformation) of holes from Fe^{3+} to Fe^{2+} on the Mg sublattice increases the conductivity of the olivine. In solid rocks, the conductivity, σ , and temperature, T , are related by an Arrhenius relationship: $\sigma = \sigma_0 e^{-E_a/kT}$ where E_a is the activation energy. The exponential rise in conductivity is such that dry mafic rocks which have room temperature conductivities of 10^{-10} S/m or less can have conductivities as high as 10^{-3} S/m at 1200°C . Molten mafic rocks have much higher conductivities (ranging between 0.1 and 30 S/m) because of the high mobility of alkaline ions in the liquid phase (Maumus et al., 2005). For partial melts, the conductivity of the aggregate is determined by the conductivity of the melt phase and its interconnectivity. Schilling et al. (1997) showed that even a melt fraction of a few percent can increase the conductivity of solid/melt aggregate by an order of magnitude. No significant increase in the conductivity occurs beyond a melt fraction of $\sim 20\%$ because the melt interconnectivity is expected to be almost total.

The Galileo magnetic field data from four different close Io encounters showed that the induced field is global, dipolar and almost out of phase with the inducing field (suggesting that the thickness of the conducting layer exceeds the skin depth of the signal). Detailed modeling (Khurana et al., 2011) shows that a completely solid mantle provides an insufficient response and provides inadequate fits to the observations. However, a global subsurface magma shell located ~ 50 km beneath the surface, with a thickness exceeding 50 kilometers and a rock melt fraction of 20% or more has sufficient conductivity to be consistent with the observations. The fact that the observed induced field is time-varying and keeps an out of phase relation with the inducing field during each of the flybys confirms that the observed field is not a permanent dynamo generated field.

Because of the sparseness of Galileo data, all of the Io studies so far have used only the synodic period of Jupiter as a sounding signal and have ignored the contribution of the much longer orbital period signal to the observed induction. Future investigation of Io from either a multiple-flybys mission or an orbiter should exploit longer period signals to uniquely characterize the thickness and conductivity of the melt layer in Io. Future missions should also better characterize the primary inducing field at multiple frequencies, and better characterize effects of the plasma environment (see Section 2.3.10).

The interpretation of Khurana et al. (2011) that a strong electrically conducting layer in Io is required to explain the Galileo data has been questioned (Blöcker et al., 2018; Roth et al., 2017). New flybys with a magnetometer experiment coupled with capable plasma measurements

(Westlake et al., 2016) and modeling (Section 3.2.10) are needed to resolve this question, along with measurements such as k_2 , h_2 , or libration amplitude.

2.3.4 Tidal Love Numbers k_2 and h_2

The potential Love number k_2 is a powerful tool for understanding the internal structure of any tidally heated world. k_2 measures how the bodies’ gravitational potential responds to an external forcing potential. For a tidally heated world there are two distinct values of k_2 . The fluid k_2 is a measure of the long term response of the body to the external potential. For a hydrostatic body this can be related to the moment of inertia of the body via the Darwin–Radau equation. The fluid k_2 has been measured for Io by Anderson et al. (2001). Conversely the tidal k_2 measures how the body potential responds on a tidal timescale. For a homogenous body, the tidal k_2 is given by:

$$k_2 = \frac{3/2}{1 + \frac{19}{2\rho g R}\mu} \quad (2.2)$$

Here, μ is the inverse of the complex compliance. The imaginary part of k_2 gives the phase lag between the forcing potential (from the host planet) and the satellite response. This scales to the energy dissipated in the moon by:

$$\dot{E} = -\text{Im}(k_2) \frac{21}{2} \frac{R^5 n^5 e^2}{G} \quad (2.3)$$

In many sources, the term $\text{Im}(k_2)$ is given by the equivalent expression k_2/Q where Q is the dissipation factor. For Io, $\text{Im}(k_2)$ has been estimated from astrometry by Lainey et al. (2009). Their value of 0.015 is consistent with surface heat flow estimates.

Measuring the real part of the tidal k_2 gives a strong constraint on the structure of a tidally heated world. Bierson and Nimmo (2016) suggested that measuring k_2 of Io would test whether Io just has a high partial melt mantle or a full magma ocean (see Section 2.3.2).

While the tidal Love number k_2 describes the added contribution to an imposed gravity field of degree-2 due to an internal redistribution of mass, the body tide Love number h_2 expresses the radial surface deformation. Both Love numbers, h_2 and k_2 , are affected in similar, but not identical ways, by the mechanical structure of the interior. Therefore, each of the tidal Love numbers alone can confirm or reject the hypothesis of a liquid layer decoupling the crust, but the simultaneous determination of both Love numbers significantly reduces the ambiguity of interior models and the dependence on rheological properties (e.g., Wahr et al., 2006; Wu et al., 2001). On an Io without a magma ocean, h_2 is at the order of 0.1. In the case of a full magma ocean, mechanically decoupling the deeper interior, h_2 is much higher (i.e., ~ 0.5 – 1.0). The same applies for most icy satellites affected by tidal forces in the case of the presence or absence of a liquid

water ocean. However, compared to k_2 , h_2 is often more difficult to measure. While k_2 can be measured by radio science (every spacecraft carries a radio telecom system), the measurement of h_2 requires an altimeter and good knowledge of the spacecraft position in orbit. Due to its geodetic accuracy, laser altimetry is the natural choice to probe the surface for tidal deformations (e.g., Mazarico et al., 2014); however, combinations of radar and stereo images are in principle also suitable (Steinbrügge et al., 2018). The h_2 Love number can be retrieved by inversion from spherical harmonics (Koch et al., 2008, 2010) or by a differential measurement at cross-over locations (e.g., Mazarico et al., 2014; Steinbrügge et al., 2015, 2018).

2.3.5 Combining Gravity and Topography

Measurements of gravity and topography provide an additional constraint on internal structure. In either the case of an asthenosphere or a magma ocean, topography of Io is expected to be compensated due to the presence of a lower-viscosity layer at depth. The compensation can be assessed by comparing the amplitude of gravity to that of topography. Admittance is the ratio of gravity to topography computed for a specific wavelength (e.g., Watts, 2001). If gravity and topography are expanded in spherical harmonics, the admittance for uncompensated topography with units of mGal/km is:

$$Z_n = \frac{GM}{R} \frac{3(n+1)}{2n+1} \frac{\rho_{\text{lid}}}{\bar{\rho}} \quad (2.4)$$

where n is the spherical harmonic degree, ρ_{lid} is the density of the lid, $\bar{\rho}$ is the mean density, R is the radius of the body, G is the gravitational constant, M is the mass of the body. In case of Airy-compensated topography, the admittance is:

$$Z_n = \frac{GM}{R} \frac{3(n+1)}{2n+1} \frac{\rho_{\text{lid}}}{\bar{\rho}} \left(1 - \left(\frac{R - h_{\text{lid}}}{R} \right)^{n+2} \right) \quad (2.5)$$

where h_{lid} is the thickness of the lid. It can be seen that compensation causes the reduction of admittance by a factor of

$$\left(1 - \left(\frac{R - h_{\text{lid}}}{R} \right)^{n+2} \right) \quad (2.6)$$

Equation 2.5 is valid for a thin compensated layer ($h_{\text{lid}} \ll R$). The admittance reduction happens preferentially at low degrees. The cause for the reduction of admittance can be understood by a simple example of a floating iceberg, where the positive gravity of the above-water part of the iceberg (a mountain) is compensated by a negative gravity anomaly of the underwater part of the iceberg that has displaced the higher density water and thus presents a negative density anomaly. The underwater part of the iceberg in this example is analogous to a thicker crust (or

“crustal root”) associated with a topographic high. Webb and Stevenson (1987) proposed that the presence of hot magma ocean will cause lateral flow at the bases of crustal roots due to a decrease in the viscosity. This can lead to relaxation of the crustal roots, and can thus increase the gravity–topography admittance above the isostatic values (unless the mountains subside). Likewise, elastic support of surface loads would also increase the admittance.

2.3.6 Seismology

Given the extensive volcanism on Io and large amounts of tidal energy, Io is likely very seismically active. Using scaling relationships for tidally active worlds derived initially for Europa (Panning et al., 2018), but generalized for any tidally active world (Hurford et al., 2018), the cumulative seismic moment release rate on Io is likely within an order of magnitude or two of the rate on Earth, implying significant potential for passive observation of seismic signals.

Multiple seismic techniques using both body and surface waves are very powerful for identifying layered seismic velocity structure, and an asthenosphere (with reduced but non-zero shear velocity) is seismically distinct from a magma ocean or dense suspension (shear velocity of zero with no interconnected solids). In fact, the presence of a magma ocean below a rigid lid would produce many distinct seismic phases (such as flexural waves and Crary waves) identified for detecting the thickness of an ice shell on ocean worlds like Europa (Kovach and Chyba, 2001; Panning et al., 2006; Stähler et al., 2018).

With current technology, seismic observations would likely require some sort of landed mission. Networks of seismic instruments are powerful, but preparation for the Interior Exploration using Seismic Investigations, Geodesy and Heat Transport (InSight) mission to Mars has demonstrated the potential for single-station approaches if only a single lander can be feasible (Böse et al., 2017; Panning et al., 2015).

2.3.7 Libration Amplitude

The orbits of Io and Europa are eccentric; this causes the orbital speed to be variable. The rotation of the body is, on the other hand, nearly uniform. Therefore, the subjovian point moves backwards and forwards in the satellite-fixed frame. Longitudinal libration arises due to the torque from Jupiter on the static tidal and rotational bulge misaligned with the direction towards Jupiter. This time-variable gravitational torque modifies its rotation rate (e.g., Comstock and Bills, 2003; Van Hoolst et al., 2013). If there are liquid layers within Io or Europa, or a liquid core, the Jupiter torque on the different internal layers must be considered, and the libration will also be affected by the internal gravitational, pressure, viscous, and electromagnetic torques between those layers. Typically, modeling the rigid response of a body is a sufficiently good approximation for a body without liquid layers. When liquid layers are present, the torque exerted by the primary on the

time-varying tidal bulge (as opposed to the static bulge) can also affect the amplitude of libration. The ratio of the term related to the tidal deformation and the gravitational torque is equal to 0.10 for Io given the maximum theoretical limit on the Love numbers (Baland and Van Hoolst, 2010). Therefore, the effect of zonal tides on libration could be up to 10%.

If the solid layers of the satellites with subsurface oceans are considered infinitely rigid, the libration amplitude is at least one order of magnitude larger than for an entirely solid moon (Van Hoolst et al., 2013). This rigid shell assumption is likely valid for tiny Enceladus (Thomas et al., 2016; Van Hoolst et al., 2016). However, ice shells of large satellites will deform elastically, and this could keep the libration amplitude at the level of the libration of the solid satellite (Van Hoolst et al., 2013). Hence, the interpretation of libration expected to be measured by Europa Clipper (Turtle et al., 2016) may prove ambiguous. Io is quite different because the lithosphere is composed of silicate rock, which is intrinsically more rigid than ice and must support mountains up to 17 km high. Reasonable values for the rigidity (>30 GPa) and thickness (~ 50 km; Khurana et al., 2011) of Io's lithosphere lead to libration amplitudes of 500 m or larger (Van Hoolst et al., 2018).

For Io, the rigid libration amplitude is 245 m (Comstock and Bills, 2003). If the entire mantle is solid and the core is liquid, as assumed for Io in Baland and Van Hoolst (2010), we can constrain the size of the core by combining the gravity observations with a libration measurement. As can be seen in Figure 2.7, libration amplitude becomes highly sensitive to the mantle (top) layer thickness if it becomes small. Assuming the core densities between 5000 and 8000 kg/m³ and given the observed gravity field, the libration amplitude for the no-magma-ocean case is between 275 and 300 m.

The presence of a magma ocean that decouples the lid can lead to a large amplitude of libration (Baland and Van Hoolst, 2010; Van Hoolst et al., 2018). Figure 2.8 shows the libration amplitude in the case of a magma ocean as a function of the crustal lid thickness and rigidity. In this case, libration amplitude is strongly sensitive to both of these parameters. Although a partially molten crust might have a rigidity lower than the ~ 50 GPa associated with solid rock, the crust still has to support mountains 17 km high. Figure 2.8 shows that unless the crustal rigidity is <10 GPa, measuring the amplitude of libration provides a stringent test of whether a mechanical magma ocean exists beneath Io's surface.

Distinguishing libration without (≤ 300 m) and with a magma ocean (>500 m with a lithosphere very likely <100 km thick) can be accomplished with repeat imaging at ≤ 300 m/pixel, navigated to Io limb fits, and timed to true anomalies near the maximum negative and positive libration amplitudes.

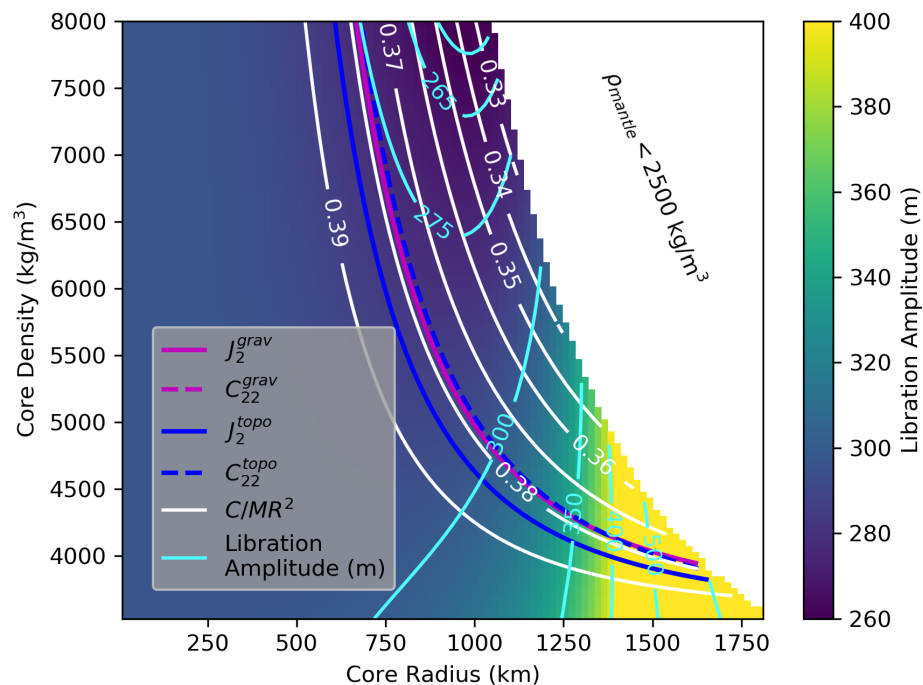


Figure 2.7: The amplitude of libration (background color and cyan contours) as a function of core radius and core density assuming a two-layer model of Io with a liquid core and solid and rigid mantle. The solid and dashed blue and purple contours show the solution for the two-layer model given the observations of Io’s J_2 and C_{22} gravity coefficients (Anderson et al., 2001) and shape data (Oberst and Schuster, 2004). The white contours show to the normalized polar moment of inertia. The white region in the upper right corresponds to the part of the parameter space where crustal density is below 2500 kg/m^3 .

2.3.8 Experimental Work Needed: Dissipation in High Melt Fraction Environments

Understanding the structure and dynamics of a melt-bearing planetary interior subject to heating processes such as tidal forcing is critical to our knowledge of terrestrial planetary evolution and possibly of some rocky exoplanets. This knowledge comes from field measurements (e.g., induction, seismic), computational simulations (geodynamics), as well as laboratory studies (e.g., mineral physics and experimental petrology). This section focuses on the latter. Laboratory investigations can provide direct information and fundamental knowledge about the structure and dynamics of a melt-bearing interior. The relevance of laboratory experiments will mostly depend on the constraints obtained on the bulk composition of Io and/or the chemistry of eruptive products, as these data will define the starting materials for laboratory studies. The

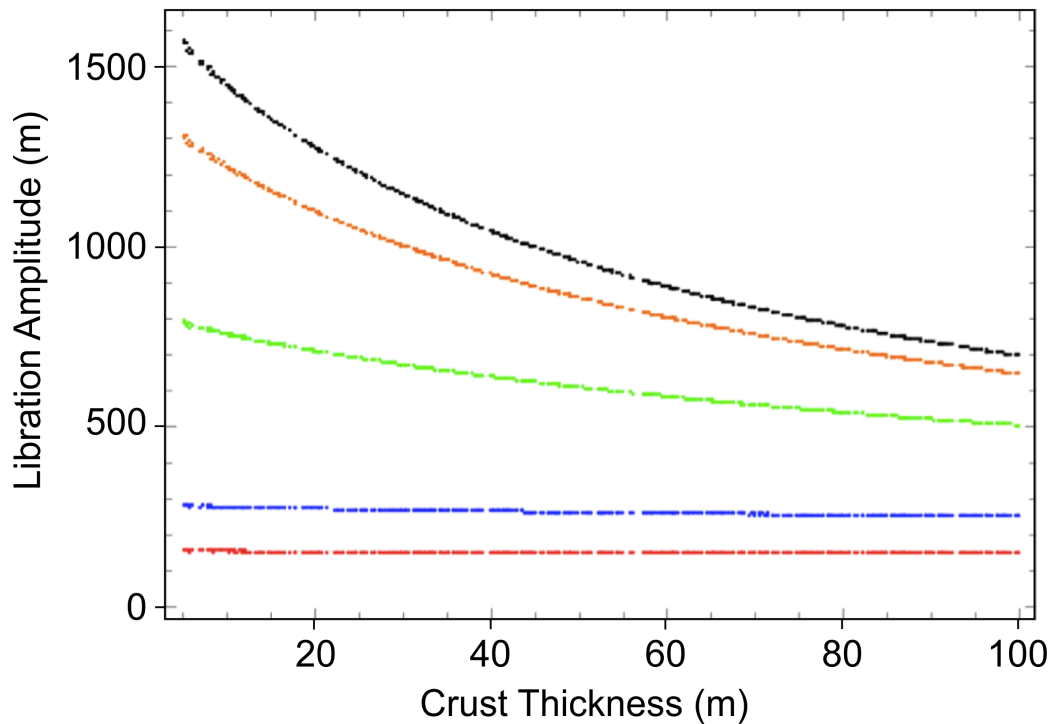


Figure 2.8: The amplitude of libration of a solid crust over a liquid magma ocean, with various assumed crustal rigidities. Crustal rigidities assumed are from top to bottom: 60, 50, 30, 10, 5 GPa. The expected libration amplitude for a fully solid lo mantle is 275–300 m (see Figure 2.7). Calculation methodology is based on Van Hoolst et al. (2018).

experiments mentioned below represent a non-exhaustive list of laboratory studies that are relevant to investigations of lo's melt-bearing mantle.

Evidence for strong coupling between deformation and melt segregation in a partially molten mantle comes from laboratory measurements as well as field and theoretical studies (e.g., King et al., 2010; Le Roux et al., 2008; Stevenson, 1989; Takei and Katz, 2013). Modeling melt segregation and transport in lo's interior requires understanding rock permeability, melt mobility and melt topology in response to stress. The rheological properties of a partially molten mantle can be investigated using deformation experiments (in torsion, compression) under hydrostatic and non-hydrostatic conditions (Gleason et al., 1999). Grain size should be an important parameter in these studies, as it influences fluid flow within the solid matrix (e.g., Wark and Watson, 2000). Although only a limited range of grain sizes can be used as part of experiments on polycrystalline materials under pressure, these studies are valuable to investigate melt segregation mechanisms at depth and can be used to develop grain size–stress piezometric relationships (e.g., Hirth and Kohlstedt, 2015). Melt distribution also depends on the confining pressure; at high pressures (>1 GPa, >200 km depth in lo), it was shown that melt distribution corresponds to a disequilibrium phenomenon that can be caused by the non-hydrostatic state of stress or the induced strain

(e.g., Bai et al., 1997; Jin et al., 1994). Recently, it was also demonstrated that compaction length has a strong influence on melt migration and extraction processes in a partially molten rock undergoing deformation (Qi and Kohlstedt, 2018). Understanding the rheological properties and dynamics of a melt-bearing mantle would strongly benefit from viscosity measurements under high pressure and temperature conditions (e.g., Liebske et al., 2005; Tinker et al., 2004) on molten analogues of Io’s mantle. These data would provide valuable constraints on planetary convection and cooling processes for numerical models of a magma ocean with variable melt fraction.

The physical properties of a melt-bearing layer are critical to understanding planetary evolution and also represent a necessary input to dynamic and thermochemical models. Knowledge of these properties is required to investigate melt mobility at depth. The physical properties of a melt-rich layer can be probed in the laboratory by measuring the transport properties of liquids or partial melts. Among all transport properties, electrical conductivity is uniquely suited to investigate the present-day state of a partially molten planetary interior like Io. Being sensitive to small changes in temperature, chemistry, and melt fraction, the electrical conductivity is a relevant property to investigate partial melt in planetary mantles. The combination of electrical experiments in the laboratory (using the impedance spectroscopy technique) and field electrical data (from electromagnetic measurements) has proved to be efficient at placing constraints (e.g., melt fraction, chemistry) on the present-day structure of melt-bearing planetary interiors (e.g., Khurana et al., 2011; Zhang and Pommier, 2017 (Section 2.3.3)). Electrical conductivity can be combined with deformation experiments (Caricchi et al., 2011; Pommier et al., 2015; Zhang et al., 2014) to help further our understanding of melt mobility during deformation caused by tidal forcing.

Seismic measurements (e.g., velocities, shear, and Young’s moduli) represent a relevant probe of the physical properties of a melt-bearing layer at depth and help place constraints on the melt fraction (Section 2.3.6). Melt affects seismic wave velocity directly (poroelastic effect) and indirectly (anelastic effect), and both laboratory experiments on partially molten rock analogues and geophysical studies have suggested that the presence of partial melt can be detected at depth using seismic measurements (e.g., McCarthy et al., 2011; Williams and Garnero, 1996). The study of partial melt in Io’s mantle would benefit from the combination of field observations and measurement of long-period Young’s modulus, as the latter is drastically reduced in partial melting regions (Li and Weidner, 2013). Torsional forced oscillation tests on partially molten rocks have also proven useful in characterizing microstructures of melt-bearing material under deformation (e.g., grain boundary sliding processes; Faul et al., 2004).

Constraints on the heat budget of Io could be provided using thermal conductivity data. Laboratory measurements of thermal conductivity on relevant materials are particularly useful in estimating the heat budget within the partially molten interior of terrestrial planets (e.g., Murakami et al., 2014), as well as in understanding the implications for planet-scale properties such as the

sustainability of an intrinsic magnetic field (Konôpková et al., 2016). For instance, thermal conductivity measurements of sulfur dioxide (surface frost) and Io's lava analogues could help us understand how heat is conducted across the lithosphere and how heat is transported in melt channels at depth.

Existing laboratory studies on partially molten rocks represent a robust basis on which to develop models of Io's mantle, and new experiments and/or techniques are needed to further our understanding of melt behavior at stress/strain conditions relevant to tidal forcing in Io. For example, tidal dissipation in high melt fraction environments could be probed using rheological investigations mimicking tidal forcing, possibly using friction experiments at low differential stresses, as already developed to measure the deformational behaviors of ice (McCarthy and Cooper, 2016). Also, microwave-heating laboratory experiments (Limare et al., 2015) could be used to simulate mantle convection and to calculate the mantle potential temperature.

2.3.9 Petrology

Combined evidence provided by geophysical observations, laboratory studies, and geochemical analyses of Io's surface rocks are required to develop realistic petrological models of Io's interior. The composition of the mantle of Io can be explored within complex (natural) systems based on the chemical analyses of surface lavas, but also within simplified (synthetic) systems. As a first approximation, the mantle composition can be assumed to be dictated by equilibrium, and as previously done for the lunar mantle, could be computed from thermodynamic data for a given model pressure, temperature, and bulk composition by Gibbs energy minimization (e.g., Khan et al., 2014). Thermodynamic properties can be computed for the phase assemblage obtained at each temperature and pressure of interest, using models such as pMELTS (Ghiorso et al., 2002) or Perple_X (Connolly, 2005). This has been done under the assumption that Io has a broadly chondritic bulk composition (Keszthelyi and McEwen, 1997; Keszthelyi et al., 1999, 2007). Computed petrologic models should be compared with experimental phase relations.

The bulk composition and mineralogy of Io's mantle is strongly influenced by physical properties such as the density of phases and melt viscosity. Addressing the hypothesis of sinking or floating solids and of melt upward or downward percolation requires models of the mantle density and viscosity as a function of depth and composition (e.g., Elkins Tanton et al., 2002). Combining different physical properties (e.g., sound velocity and electrical conductivity; Verhoeven et al., 2009) would significantly further our understanding of a melt-bearing interior and constrain petrological modeling studies, since different properties are not sensitive to the same parameters (e.g., temperature, melt fraction) in the same way. For instance, seismic velocities are less sensitive than electrical conductivity to melt chemistry, whereas the melt phase geometry affects seismic velocities more significantly than bulk electrical conductivity.

Magnetic induction is a powerful way to probe the abundance, distribution, and electrical properties of an interconnected melt phase inside Io (see Section 2.3.3). However, laboratory studies of the electrical conductivity of silicate melts rich in sulfur-bearing volatiles are lacking. If the effect is similar to that of hydrogen or carbon, then the electrical conductivity could increase by an order of magnitude when a few hundreds of ppm of sulfur is added to the melt (e.g., Ni et al., 2011; Pommier et al., 2008; Sifré et al., 2014).

2.3.10 Plasma Interaction and Magnetic Fields

Blöcker et al. (2018) have recently shown that the magnetic induction signatures attributed by Khurana et al. (2011) to a subsurface magma ocean could also be consistent with induction above the moon’s surface in Io’s conductive ionosphere. Multiple well-planned spacecraft flybys with in situ measurements of the magnetic fields and bulk plasma properties at Io can definitively show whether the magnetic induction signatures are due to a subsurface magma ocean, or Io’s ionosphere, or some superposition of the two. However, numerical modeling presents the most expedient method to accurately interpret the existing data and estimate the depth, thickness, and conductivity of Io’s magma ocean. We suggest two targets for future improvements in magnetohydrodynamic (MHD) modeling of magnetic fields and bulk plasma properties at Io: more realistic representations of Io’s magma ocean and the plasma interaction itself.

Io’s induced magnetic field is produced by magnetic induction, which occurs in an electrically conducting layer, typically modeled as a magma ocean beneath Io’s surface. Therefore, the induced magnetic field is sensitive to the conductivity of the layer and variations in the depth and thickness of the layer. MHD models incorporating a multi-layer representation of Io’s interior, such as that used by Khurana et al. (2011), can better constrain the conductivity and resulting melt fraction of a magma ocean by incorporating the results of recent experiments on the conductivity of Io-like materials (Pommier et al., 2018; Zhang and Pommier, 2017). Furthermore, it is unlikely that Io’s magma ocean is perfectly spherically symmetric; future modeling should be capable of representing an ocean with large-scale topographies rising up from the ocean “floor” or descending from the crustal “cap”. Because the induced field depends on the depth and thickness of the conductive layer, such topographies may be identifiable in future magnetic field observations by comparison with these models.

Future models for Io’s plasma interaction must be able to determine the relative contributions of magnetic induction versus the contributions of the magnetic signatures of Jupiter’s magnetospheric plasma interacting with Io’s neutral atmosphere and ionospheric plasma to the total magnetic field. Many of the points raised by Plainaki et al. (2018) with respect to improved modeling of Europa’s plasma interaction in MHD models apply to Io as well. In particular, recent models have demonstrated that inhomogeneities in Europa’s atmosphere attributed to water plumes produce significant magnetic field signatures (Blöcker et al., 2018; Jia et al., 2018). MHD models should

therefore be capable of representing inhomogeneities in Io's neutral atmosphere due to volcanic plumes.

2.3.11 Relevance to Ocean Worlds

A magma ocean is a close physical analog to a subsurface ocean thought to exist in multiple icy ocean worlds, such as Europa, Ganymede, Callisto, Enceladus, and Titan (e.g., Vance et al., 2018), as well as possibly Triton and Pluto (Nimmo and Pappalardo, 2016), Dione (Beuthe, 2016), and Ceres (Fu et al., 2017). In fact, one can consider a subsurface water ocean as a magma produced by the melting of water ice rather than silicates. The physical observations of k_2 , h_2 , librations, magnetic induction (at least in the presence of a saline ocean), and seismic properties in the presence or absence of a global magma or liquid water ocean are qualitatively similar. The primary difference between these two different types of global oceans is in the expected density contrast, where liquid water is known to be denser than the solid, while the opposite is typically true for silicate melts. This presents a dynamical challenge for the stability of a global magma ocean on Io that is not present for global subsurface water oceans. However, beyond this important petrological difference, most other measurement techniques and modeling described in this section can be directly carried over to icy worlds with global subsurface oceans.

2.4 Question 4: Is the Jupiter/Laplace system in equilibrium?

2.4.1 Introduction to Question 4

The Io–Europa–Ganymede system is a complex and delicately built tidal engine that powers Io's extreme volcanism and warms water oceans in Europa. Io's gravity generates a tidal bulge within Jupiter, whose dissipation transfers some of Jupiter's rotational energy into Io's orbit, moving it outwards and deeper into a 2:1 eccentricity resonance with Europa. This in turn increases Io's eccentricity, resulting in enhanced tidal heating. Ultimately, Jupiter's rotational energy is converted into a combination of gravitational potential energy (orbits of the satellites) and heat via dissipation in both Jupiter and the satellites. A similar picture applies to the Enceladus–Dione 2:1 resonance in the Saturn system, with Enceladus's geysers ultimately fueled by dissipation in Saturn.

However, we do not know whether the processes described above are currently in an equilibrium state, or whether tidal migration/heating rates and volcanic activity vary episodically. For instance, it is possible that Io is currently migrating toward Jupiter (Lainey et al., 2009), due to tidal damping of its eccentricity. As Io's eccentricity damps, tidal heating will diminish and its internal structure will cool and become less dissipative. Io will then migrate back outwards into the resonance with Europa, increasing its eccentricity once again. This cyclic feedback between

thermal and orbital evolution was modeled by Ojakangas and Stevenson (1986), who found typical oscillation periods of order 100 Myr. Hussmann and Spohn (2004) obtained similar periodic behavior for both Io and Europa. Likewise, Enceladus may also be experiencing periodic tidal heating (Ojakangas and Stevenson, 1986; Shoji et al., 2014).

Figure 2.9 illustrates these possibilities schematically. Io could be in equilibrium, where its eccentricity is constant and the total satellite heat output is also constant and equal to the rate at which energy is delivered by Jupiter. Alternatively, the system could be experiencing a period of anomalously high heat production, with satellite eccentricities higher than their long-term average values.

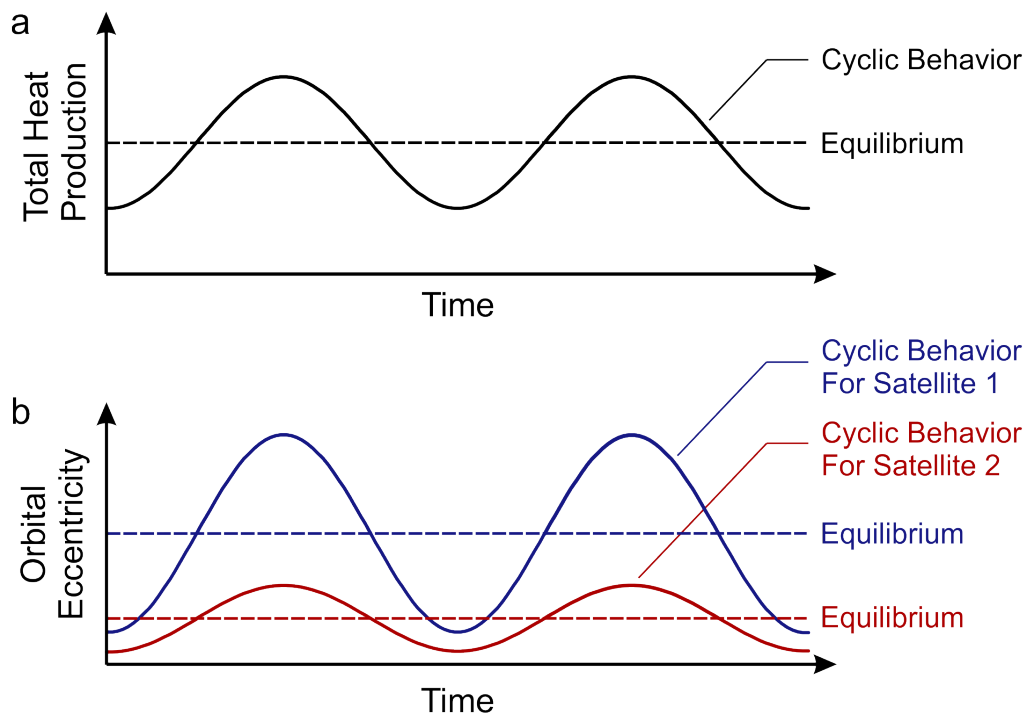


Figure 2.9: Schematic showing two possible situations for satellites in resonance. The system might be in equilibrium, in which $de/dt = 0$ for both bodies and the total heat produced is constant (and determined by dissipation in the primary). Or the system might be oscillating, with heat production varying around the long-term equilibrium value, and eccentricities also varying.

2.4.2 Definition of Equilibrium

Dissipation in and torques generated by the primary both depend on the k_2/Q of the primary, where k_2 is the tidal Love number and Q is a dissipation factor. Although Q_{primary} is often assumed to be constant, in the “resonance lock” scenario (Fuller et al., 2016), it is rather a derived property, controlled by the primary’s structural evolution timescale t and the period and mass of

the tide-raising satellite. Thus, for instance, the effective Q is lower (and orbital migration is faster) for larger or more distant satellites.

We will define equilibrium as the state in which the present-day rate of tidal heating equals the long-term rate. The long-term heating rate is set by k_2/Q of Jupiter, which controls the rate of energy delivery to the satellites; the instantaneous tidal heat production depends on the k_2/Q and eccentricities of the satellites, and l_0 in particular. In equilibrium, the total rate of heat produced in the satellites is independent of their k_2/Q values, because their eccentricities have adjusted to generate the amount of heat determined by Jupiter's k_2/Q (Meyer and Wisdom, 2007; Ojakangas and Stevenson, 1986). As a result, the rate of change of eccentricity is zero.

If the system is in equilibrium, the heating rate of l_0 (assuming it dominates the other two satellites) is:

$$\dot{E}_{\text{heat}} \simeq \frac{1}{t_{\text{tide}}} \left[\left(\frac{\Omega_1}{\Omega_2} - 1 \right) |E_{2,\text{orb}}| + \left(\frac{\Omega_1}{\Omega_2} - 1 \right) |E_{3,\text{orb}}| \right] \quad (2.7)$$

where Ω_1 and $E_{1,\text{orb}}$ are the orbital frequency and energy of l_0 , and Europa and Ganymede are indexed by 2 and 3. The tidal migration timescale, which can be measured via astrometry, is defined as:

$$t_{\text{tide}} = -\frac{E_{\text{orb}}}{\dot{E}_{\text{tide}}} = \frac{a_m}{\dot{a}_{m,\text{tide}}} \quad (2.8)$$

where a_m is the semi-major axis of a moon. The quantity t_{tide} is directly proportional to the primary Q/k_2 , and so Equation 2.8 is equivalent to the statement above that equilibrium tidal heating depends only on the primary k_2/Q .

Since all quantities except for t_{tide} and are well known, a measurement of $\dot{a}_{m,\text{tide}}$ will thus determine t_{tide} , assuming equilibrium. Thus, to determine whether the system is at equilibrium, we must measure both the heat flow of l_0 (assuming it dominates), and the semi-major axis change ($\dot{a}_{m,\text{tide}}$) of at least one of the moons.

2.4.3 Astrometry in the Jovian System

The orbital evolution of the Galilean satellite system due to tidal dissipation can be determined from the astrometrically observed positions of the Galilean satellites over an extended period of time by using an accurate model of their orbital motion. Lainey et al. (2009) used a full numerical model to solve tidal acceleration associated with tidal dissipation within both l_0 and Jupiter. Their model considered a constant k_2/Q value for Jupiter and neglected tidal dissipation within Europa and Ganymede. They obtained for l_0 's k_2/Q the value 0.015 ± 0.003 , implying a present-day tidal dissipation rate of about 10^{14} W, matching the observed heat flow.

The astrometrically-derived value of k_2/Q for Jupiter gives an evolution timescale for Io of $t_{\text{tide}} = 17$ Gyr (taking into account the angular momenta of Europa and Ganymede). This in turn yields an equilibrium heat production rate of about 0.5×10^{14} W via Equation 2.7 within a factor of ~ 2 of the observed heat flow.

2.4.4 Heat Flow Measurements

The ten-year averaged heat output derived by Veeder et al. (1994) is $\sim 10^{14}$ W, but there are a number of uncertainties. A future spacecraft mission should strive to map Io's Bond albedo and thermal emission (day and night for thermal inertia), including polar regions, to accurately measure the endogenic heat flow. See Section 2.1.7 for further discussion of this topic.

2.4.5 Stability of Laplace Resonance

A second way of verifying that the system is in equilibrium is to measure \dot{a} for all three moons in the Laplace resonance. If the system is in equilibrium, the tidal migration timescale t_{tide} must be identical for all three moons. Note that this criterion implies that k_2/Q_{Jupiter} will be different at the different satellite frequencies, as expected in the "resonance locking" scenario. Stability of the Laplace resonance implies a specific equilibrium between energy exchanges in the whole system, with implications for past and future evolution. This method requires measurement of \dot{a} for Europa and Ganymede as well as Io, and the Europa Clipper and JUICE missions are expected to provide this data (Dirkx et al., 2017).

V. Lainey and R. Park performed a covariance analysis associated with the expected measurements from all three missions. The stability of the Laplace resonance is defined by:

$$\frac{dn_1}{dt} - 2\frac{dn_2}{dt} = \frac{dn_2}{dt} - 2\frac{dn_3}{dt} = 0 \quad (2.9)$$

where n_1 , n_2 , n_3 are the (averaged) mean motions of Io, Europa and Ganymede, respectively.

They modeled the dynamics of the four Galilean moons in a very similar way to Lainey et al. (2009), except for the use of the Juno's derived gravity field (less et al., 2018), the addition of Amalthea as a perturbing body, and the use of the IAU nutation model. They solved for the initial states of the four Galilean moons, the mass of Jupiter and of each moon, and the polar orientation and precession of Jupiter. Jupiter's gravity field was solved simultaneously, but with constraints on its harmonics given by less et al. (2018). A constant da/dt parameter (that can be converted into dn/dt) was fitted for Io, Europa and Ganymede. They considered all observations in Lainey et al. (2009) and added the mutual events campaign of 2009 and 2016 (Arlot et al., 2014; Saquet et al., 2018).

1. *Simulation of Io data:* Ten flybys below from a candidate tour for Io Volcano Observer (McEwen, 2019) were considered, assuming ranging through each flyby. Ten data points per flyby dispatched over ± 30 minutes were considered with 2-m, 20-m and 200-m accuracy.
2. *Simulation of Europa Clipper data:* We considered the 43 flybys below (in Julian days) from candidate tour 16F11 strongly inspired by Park et al. (2011), which is one of Clipper's old reference tour designs and is sufficient for analyzing the impact of ranging data on the recovery of Europa's ephemeris relative to Jupiter. Ten data points per flyby dispatched over ± 30 minutes were considered with 10-m accuracy.
3. *Simulation of JUICE data:* They considered only the Juice final spherical orbit at 500 km altitude (denoted GCO500), which is to last for a nominal duration of 4 months. Following Dirkx et al. (2017), they fixed the 3GM range data schedule to a single nominal scenario: one 8 hour range tracking arc per day: $\sigma_r = 0.2$ m every 300 s. For simplicity, they considered only ranging data, and with a uniform sampling of 96 data points per day. They assumed 10-m precision of ranging.

Units in meter/year	Current	200-m	20-m
da/dt (Io)	1.934	1.281	1.132
da/dt (Eu)	13.632	9.031	7.976
da/dt (Ga)	3.720	2.469	2.189

Table 2.2: Scenario 1: Considering IVO radio science data and astrometry data.

The improvement on all three da/dt parameters is 34% and 42% for the 200-m and 20-m case, respectively. The uncertainties are much larger than any reasonable tidal scenario.

Uncertainty in meter/year	Juice and Clipper	Io, 200-m	Io, 20-m	Io, 10-m
da/dt (Io)	0.0296	0.0057	0.0045	0.0041
da/dt (Eu)	0.2089	0.0356	0.0273	0.0252
da/dt (Ga)	0.0604	0.0111	0.0091	0.0087

Table 2.3: Scenario 2: Considering IVO, Europa Clipper and JUICE radio science data and astrometry data.

The improvement on all three da/dt parameters exceeds $5\times$ (82%, 85% and 86%) for the 200-m, 20-m and 10-m cases, respectively. Such improvements are highly significant since they now allow quantifying the orbital expansions over the noise level. Indeed, the expected tidal acceleration signals are typically of few to several cm/year (Lainey et al., 2009; Peale, 1999). Furthermore, the results are not affected by biased tidal modeling since no assumptions are made on the dissipative mechanism at play within Jupiter (tidal lock, constant k_2/Q).

For comparison, Lainey et al. (2009) obtained -0.0039 , 0.019 , and 0.11 meter/year for semi-major axis variations of Io, Europa, and Ganymede, respectively. However, their variation rates should be considered as kinematical (as a computation obtained post-fit). The rates considered in the present study are directly related to physical accelerations experienced by each moon, before redistribution of energy via the Laplace resonance.

2.4.6 Summary

Astrometry in the Jovian system provides two heating estimates: instantaneous tidal heat production within Io (via Io's k_2/Q) of 10^{14} W; and the equilibrium heat flow driven by dissipation in Jupiter (via Jupiter's k_2/Q) of 0.5×10^{14} W. Direct measurements of heat flow at Io yield a mean value of 10^{14} W. Taken at face value, the present-day rate of heat loss and heat production at Io appear to be in balance. This suggests that any time lag between heat production and loss is small, as might be expected for a body where rapid melt advection dominates heat transfer (Moore, 2001). Conversely, Io appears to be producing twice as much heat as the expected long-term average value. In this sense, it is not in equilibrium, but would be on the declining-eccentricity segment of a cycle (see Figure 2.9). Similar variations in heating at Europa are therefore also expected, and might help explain its very young (~ 50 Myr) surface age (cf. Hussmann and Spohn, 2004). We caution, however, that the astrometric measurements in particular are subject to large uncertainties and involve assumptions (e.g., constant Q_{primary}) that need revisiting.

A similar analysis can be performed for the Enceladus–Dione resonance in the Saturn system. The equilibrium tidal heating rate (calculated with Equation 2.7 without the third moon terms) using astrometry is ~ 50 GW (with uncertainties of a factor of a few; Fuller et al., 2016), and the south polar heat flux from Enceladus according to (Howett et al., 2011) is ~ 16 GW (again with uncertainties a factor of a few). The uncertainties are thus sufficiently large that we cannot as yet be sure whether Io or Enceladus are in equilibrium. Better heat flow estimates are desirable for both Io and Enceladus, and future astrometry appears to be promising. In particular, improved ephemerides from spacecraft observations with precision ranging and improved models (e.g., taking resonance locking into account) will likely yield dividends over the next few years.

Fuller et al. (2016) posited that Titan and/or Callisto could have migrated outward via resonance locking. If so, they predicted $t_{\text{tide}} \approx 2$ Gyr, and $Q \approx 20$ for the Saturn–Titan tidal interaction, and $t_{\text{tide}} \approx 2$ Gyr, and $Q \approx 1$ for the Jupiter–Callisto interaction. A future measurement of such a low Q driving migration of Titan or Callisto would be strong evidence for resonance locking. This migration may have caused Titan to pass through mean motion resonances that excited its eccentricity to its current level (Ćuk et al., 2013, 2018). Astrometry of Callisto should be possible from the Europa Clipper and JUICE missions (Dirkx et al., 2016).

2.5 Question 5: Can stable isotopes inform long-term evolution of tidally heated bodies?

2.5.1 Introduction to Question 5

A major obstacle to our understanding of tidal heating is our almost complete lack of knowledge about the long-term evolution of tidally-heated systems in the solar system. Whether these satellites are currently in equilibrium, what their orbital and tidal energy dissipation histories have been over their lifetimes, and how long they have been geologically active are all central to interpreting current signatures, yet these are areas of major uncertainty (Section 2.4). Even the age of these satellites is a source of debate—recent models for the formation of Enceladus have date this moon to be as old as Saturn or as young as 100 Myr (Ćuk et al., 2016)!

An intrinsic difficulty in determining the long-term history of tidally-heated worlds is that their tidally-powered geological activity rapidly resurfaces them and alters visible signatures. Isotope ratios, which are insensitive to many of these alteration processes and hence preserve long-term records of processes, provide a potential window into these otherwise inaccessible periods of these objects' histories.

2.5.1.1 Background

Isotopic ratios have been measured on bodies across the solar system, and used to infer information on their evolutionary histories. The $^{12}\text{C}/^{13}\text{C}$ measured in methane on Titan has been used to determine the maximum length of time that methane has been present in the atmosphere (Mandt et al., 2009, 2012b; Nixon et al., 2012) and how much methane has been converted to organics that were then deposited on the surface (Mandt et al., 2012b). Observations of $^{14}\text{N}/^{15}\text{N}$ in HCN and N_2 in the atmosphere of Titan provides direct evidence of how photochemistry influences isotopes (Liang et al., 2007; Mandt et al., 2012a) and has been used to determine that Titan's nitrogen originated as NH_3 in the protosolar nebula (Mandt et al., 2014). The lower limit observed for $^{14}\text{N}/^{15}\text{N}$ in HCN in Pluto's atmosphere provides a potential tool for determining the origin of nitrogen on Pluto if the influences of condensation and aerosol trapping on isotopes can be constrained (Mandt et al., 2017). Applying the methods that have been used for Titan and Pluto can help advance understanding of how volatiles have evolved on Io.

2.5.1.2 Fractionation Processes and Escape

If processes lead to the preferential loss of certain isotopes, significant fractionation of a species may occur over the age of a satellite. However, to draw robust conclusions about mass loss from current isotope ratios, it is important to have a firm baseline understanding of the current and past processes that affect the fractionation of these species, as well as the primordial isotope ratios.

Broadly speaking, there are five realms that must be considered:

1. Formation: The primordial isotope ratios for an object depend on the isotopic signature of the material from which the object formed. In the case of a satellite, some insight into the primordial state may be gained from studying multiple objects in the system.
2. Interior: Fractionation in the interior reservoir leading to the direct outgassing of species with specific isotopic ratios.
3. Surface–Atmosphere: Fractionation during exchange between the surface and atmosphere. This exchange involves various processes that have specific fractionation signatures (e.g., sublimation and deposition), and in general can cause significant isotopic fractionation that differs from object to object due to temperature, pressure, and other factors.
4. Atmosphere: Fractionation gradients may be set up within an atmosphere.
5. Escape: Fractionation can occur during escape if the escape processes have a mass preference, or if escape occurs from a specific region of an isotopically-heterogeneous atmosphere.

In the case of Io, material escapes from the upper atmosphere primarily via non-thermal processes. In particular, for both Io's plumes and Europa's putative plumes, using published parameters, the majority of the plume material does not escape directly, but rather is a source term for the surface and/or atmosphere. Therefore, the key questions are first what the fractionation is at the surface, and second whether the surface isotopic ratios are preserved in the upper atmosphere (loss region), or whether other processes cause a vertical fractionation gradient between the surface and upper atmosphere. For example, there would be a 20% variation in fractionation of $^{34}\text{S}/^{32}\text{S}$ in SO_2 along a vertical column in Io's atmosphere if the density structure is purely due to gravitationally-induced diffusion. In other words, we need to know for each body whether we can make the assumption that the atmosphere is well mixed.

In the case of Io, most of the loss is from SO_2 , the dominant atmospheric constituent. This means that escape of S and O should be correlated, so if fractionation signatures are due to long-term mass loss, there should be correlated isotopic signatures for these two elements, which is a possible avenue for breaking degeneracies in fractionation signature interpretation. In particular, a major source of uncertainty is the unknown partitioning of S between Io's mantle and core; isotope measurements of other species would be a major step towards drawing robust conclusions about mass loss from S isotope ratios. An additional layer of complexity for the case of Io is that although SO_2 atmosphere is in a steady-state in the sense that sources = sinks, this is a dynamic steady-state (the timescale for Io to lose its entire atmosphere is ~100 days at current loss rates), and it is therefore not clear that the atmosphere is ever truly in equilibrium.

2.5.2 Measurement Potential for Tidally-Heated Satellites

Currently, isotopic studies on solar system satellites are limited to gas species that can be detected in situ with a mass spectrometer or remotely via spectroscopy, and in certain cases to surface frosts via reflectance spectroscopy. Of the satellites whose surface characteristics are clearly influenced by tidal heating, Io, Enceladus, and potentially Europa outgas from internal reservoirs, providing opportunities to compare the isotope ratios of these internal reservoirs with those of the bulk surface/atmosphere. On the icy worlds, measurements of D/H and O isotope ratios would allow for direct comparison with studies of these species across the solar system. On Io, sulfur isotope studies offer an additional avenue, and preliminary measurements of sulfur isotopes in SO₂ have already been made (Moulet et al., 2013). A comparison of sulfur isotope ratios between objects in the Jupiter system, including Europa and Jupiter itself, may provide information about the exogenic vs. endogenic nature of the S seen on these other bodies.

2.5.2.1 Radio Astronomy

Molecules with permanent dipole moments are detectable even in tenuous atmospheres at radio wavelengths via rotational transitions. The high spectral resolution of existing radio instruments allows for measurements of molecules containing different elemental isotopes. On Io, the first measurement of ³⁴SO₂ was made with the Atacama Pathfinder Experiment Telescope (APEX) 12-m antenna (Moulet et al., 2013). The high sensitivity, spatial/spectral resolution, and spectral coverage now offered by Atacama Large Millimeter Array (ALMA) at millimeter and submillimeter wavelengths provides the potential to search for and measure several new isotopologues, and even spatially resolve isotope ratios across satellites: ALMA currently can achieve ~20 resolution elements across the Galilean satellites, sufficient to resolve isotope ratios in plumes vs. bulk atmosphere on Io if there is sufficient signal from the rarer isotopes. While some isotopologues can be detected with high signal-to-noise, the majority of detections will have large uncertainties, which may limit interpretation unless the isotopes show large deviations from the expected ratios. A second major consideration with these measurements is that the ratio of emission line intensity from isotopologues does not necessarily match the species' abundance ratios due to differing opacities for different lines, which mean that various lines probe specific altitudes where the atmospheric temperatures may be very different. Experimentally, measurements of weaker non-optically-thick lines, or less abundant species, may have more straightforward interpretations. On the theoretical side, a better grasp on the atmospheric temperature profile would aid in interpretation of lines for species with different abundances and internal line strengths.

2.5.2.2 Reflectance Spectroscopy of Surface Frosts

Reflectance spectroscopy of Io's SO₂ surface frosts in the 3–5 μm range has also been used to infer the strengths of ³³S, ³⁴S, and ¹⁸O (Howell et al., 1989). On Io as well as the icy

satellites, the surface is the source for the (non-directly-outgassed) atmospheric material, and a comparison of atmospheric ratios between the surface frosts and atmospheric gasses would provide key information on fractionation due to the processes that remove material from the surface (sublimation, sputtering, etc.), and on potential vertical isotopic fractionation gradients in the atmosphere. Spatial mapping of isotope ratios across the surfaces of these objects may also probe the temporal axis, as the expected surface frost deposition age varies latitudinally. Isotopic ratios of icy surfaces in the Saturnian system have implications for the origin of Phoebe (Clark et al., 2019).

2.5.2.3 Mass Spectrometry

Bodies with tenuous or localized atmospheres such as Enceladus, Io, and Europa offer the possibility of direct sampling by spacecraft mass spectrometers or dust analyzers. Such measurements are expected to be of much higher sensitivity than remote-sensing observations (a factor of $>10^4$) and combined with high mass resolution can provide accordingly strong isotopic and compositional constraints. For example, Cassini measurements of vapor D/H ratios aided by chemisorption to increase virtual mass resolution at Enceladus (Waite et al., 2009) provide an important fiducial point for the outer solar system.

Recent years have witnessed significant progress on the miniaturization of mass spectrometers for a variety of applications (Mahaffy, 1999; Palmer and Limero, 2001). Mass spectrometer instruments developed specifically for space applications include time-of-flight, sector instruments, quadrupole arrays, quadrupole ion traps, and cylindrical ion trap mass spectrometers. The composition of planetary atmospheres, including isotopes, provides data on compounds and their concentrations, leading to new insights into theories of planetary formation and models of planet evolution. Although remote-sensing-based spectroscopic methods can be used to infer atmospheric composition, in situ mass spectrometry provides the ability to definitively identify a variety of atmospheric constituents across a wide range of concentrations that can approach eight orders of magnitude. Mass spectrometry study of tidally heated worlds was accomplished by Cassini (Waite et al., 2009) and is planned for Europa Clipper (Waite et al., 2015) and JUICE (Meyer et al., 2017; Wurz et al., 2018).

The mass resolution required is driven by the compounds expected to be present. At Europa, distinguishing between C_5H_{12} and $^{13}CC_4H_{11}$ requires a mass resolution (Delta M/M full width half maximum; FWHM) of 34,000; at Io, to distinguish between $^{34}S^{16}O_2$ and $^{34}S^{18}O^{16}O$ would require a resolution of 8,000 (FWHM). Such resolutions are readily achievable with present-day multi-bounce time-of-flight mass spectrometers. However, several challenges remain that require careful engineering to overcome. First, reactive species (including many S compounds) require an open source approach, which through careful design must maximize the sensitivity through increased collecting area. Second, an open source also avoids the fragmentation from high velocity

flybys that can result in a loss of information about high-mass species. And third, spacecraft contamination is a potential concern, especially for organic molecules.

2.5.3 Theoretical Advancements Needed

Escape from Io occurs predominantly from the atmosphere via collisions between Jovian magnetospheric plasma and the atmospheric neutrals at the exobase, which is composed primarily of SO_2 and its dissociation products. The dense Jovian magnetospheric plasma within which Io orbits strongly influences its atmospheric structure (cf. Strobel et al., 1994; Figure 2.5). Depending on assumptions about surface pressure and heat sources, the atmospheric temperature at the exobase can vary by as much as two orders of magnitude, based on 1-D calculations. The surface pressure is known to vary strongly with latitude and longitude (Feaga et al., 2009; Jessup et al., 2004). Therefore an accurate understanding of escape processes from Io would be significantly improved by development of 3-D, as opposed to the current 1-D (Moses et al., 2002; Summers and Strobel, 1996), calculations of atmospheric structure.

In the short term, the most critical need is to develop a “box model” of sources, sinks, and reservoirs for volatile species at Io. The atmosphere’s isotopic composition will evolve over time as a result of escape, photochemistry, condensation, sublimation, and the introduction of fresh material by volcanic outgassing. The rates for each of these processes are poorly understood under current conditions and even less is known about the recent and distant past. The first step

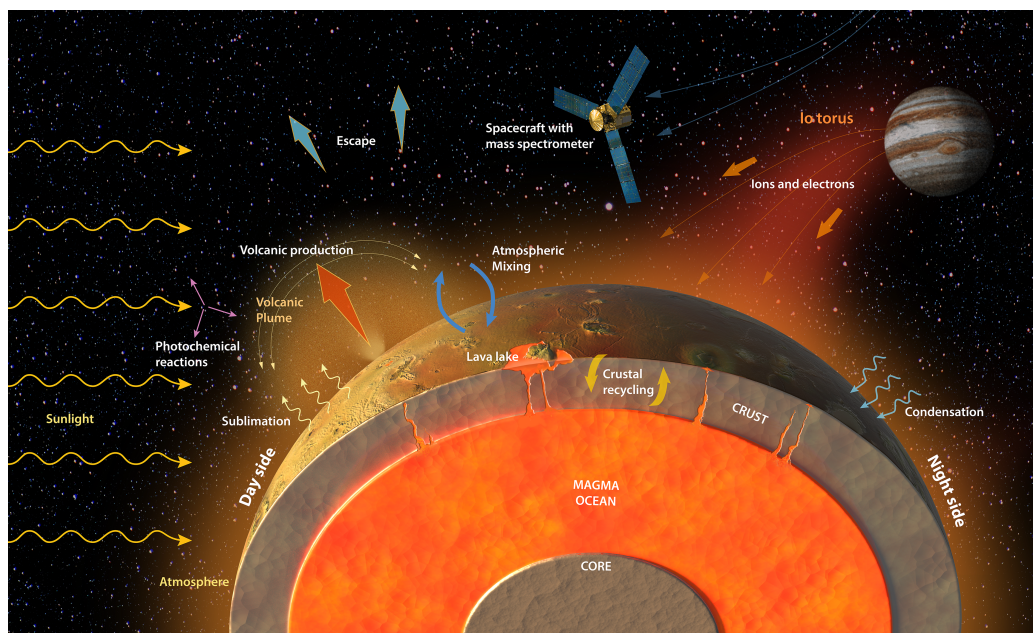


Figure 2.10: Schematic illustration of the sources, sinks, and transport processes controlling the chemical and isotopic species in/on/around Io.

for addressing this will be to develop a basic “box model” (Figure 2.10) that is constrained by what data is available. Requirements for future observations can be determined based on what limitations there are for constraining the model. Furthermore, this model will provide a basis for understanding measurements made by future missions to the Jupiter system.

2.5.4. Summary

Isotopic ratios on tidally heated satellites are measurable with currently available or in-development instrumentation (with some caveats) and have the potential to inform us about the mass-loss and long-term geological histories of these worlds. Currently, limitations in our understanding of these bodies’ atmospheric structures, and of the sources, sinks, and reservoirs for specific species, will lead to significant degeneracies in interpretation of measured isotopic ratios. However, with some theoretical advancements in these areas, isotopic ratios have the potential to be a powerful tool for understanding the long-term evolution of tidally-heated worlds.



3. Technical Development Possibilities

3.1 Improvements in Design for Jupiter's Radiation Environment

3.1.1 Impact of the Radiation Environment on Future Missions

High-energy particles trapped in the Jovian magnetosphere make the inner Jupiter environment especially challenging for space exploration (Adams et al., 2012). Megarad-level total doses behind typical spacecraft shielding can be reached in about one week near Io or about two months near Europa. It is necessary to have valid models of the space environment as well as accurate analysis tools to be able to predict the radiation levels expected for a particular mission. Radiation shielding is a significant percentage of overall spacecraft mass for missions to the Jovian moons and determines how much time the spacecraft can spend in the Jovian radiation belts. Degradation of materials and how this relates to solar cell power production also continues to be an engineering challenge for future missions.

3.1.2 Updates to Jupiter Radiation Environment Models

Divine–Garrett (DG) was the original model of the system developed in the 1980s (Divine and Garrett, 1983). It was based on Pioneer and Voyager flyby data as well as ground-based observations. This dataset had limited spatial and temporal ranges. The DG model was used to design the Galileo mission. The Galileo spacecraft far exceeded the radiation dose for which it was designed, but there were a number of system failures attributable to radiation effects, mainly total dose (Fieseler et al., 2002).

The Galileo Interim Radiation Electron (GIRE) model was an update to the DG model made in the 1990s based on data from the Galileo Energetic Particle Detector (EPD) instrument. This update incorporated significant data from the Jovian equatorial plane, between 8–16 R_J . Future model updates in 2016 and 2017 (GIRE2 and GIRE3) expanded the model to include data from higher energy ranges using additional data from EPD. This has improved the fidelity of the environment model and is especially applicable to the Europa Clipper and future Jovian moon exploration missions. GIRE2 added high-energy electrons out to 50 R_J and inside 8 R_J . GIRE2 is described in detail by de Soria-Santacruz et al. (2016). The focus of the GIRE3 update as detailed in Garrett et al. (2017) was to add higher-energy protons to the model, which is especially applicable to solar powered missions and the degradation of solar cells.

3.1.3 Transport Analysis Tool Updates

There are various methods for performing transport analysis currently in use to estimate the effect of radiation shielding on radiation dose internal to structures. Ray tracing is more efficient and faster than other models because it uses a pre-computed dose-depth curve. The forward Monte Carlo method is the most accurate ray tracing method, but it is highly inefficient for method or transport analysis. The reverse Monte Carlo method is the most commonly used for modeling and simulation for NASA and ESA missions. Both ray tracing and reverse Monte Carlo analysis are supported by multiple software tools. Ray tracing is used to get rough estimates quickly and to compare options, whereas the reverse Monte Carlo radiation transport analysis is used to provide a detailed design and provides validation of preliminary results.

The NOVICE 2015 tool was recently found to be over-predicting total dose. NOVICE 2017 was an update to correct for this, and is currently being used for Europa Clipper vault calculations for wall thickness. Comparison runs of NOVICE 2015 versus NOVICE 2017 for the same vault configuration yielded reduction of 15–20% in total dose estimates. Secondary electrons were being double counted and this has been corrected.

Comparisons have been performed in recent years between ray tracing and forward and reverse Monte Carlo analysis in support of the Europa Clipper and JUICE missions (Cherng et al., 2007). Good correlation has been demonstrated across techniques and tools. The result is that improvements in tools and analysis models have enabled lower-mass solutions for radiation protection.

3.1.4 Design Improvements for Radiation Environment

ESA internal studies in support of the JUICE mission demonstrated that for equivalent shielding mass, a reduction factor of two is possible in total ionizing dose when tantalum or lead layers are used as compared to aluminum alone. Based on simulations using the GRAS/GEANT4 model

the high atomic number (Z) material layer inside provides most benefit for energies >10 MeV. The results of the ESA studies were presented at the ESTEC RADECS conference in September 2016 (Vuolo et al., 2016).

3.1.4.1 Mini Vault for Europa Clipper

The electronic components planned for the Europa Clipper mission include parts that are radiation tolerant to 100 krad total dose. Rather than redesign these relatively small components, the design includes radiation shielding to protect them from the Jupiter environment. The initial design presented at the Mission Design Review in 2017 included an all-aluminum radiation housing with 0.88-inch-thick walls for a total mass estimate of 52 kg. After careful modeling using both FASTRAD and NOVICE for confirmation of equivalent shielding results, the preliminary design presented at a review in March 2018 uses only 0.125-inch Al walls with a 0.08-inch layer of Tantalum bonded to the inside of the Al structure with a total mass estimate of 36 kg. This is a significant mass savings of 30% based on a layered low Z /high Z shielding assembly to maintain the same internal total dose radiation environment of 50 krad. This allows use of 100-krad parts with a radiation design factor (RDF) of two for margin on the predicted radiation environment estimate.

3.1.4.2 Solar Arrays

Solar-powered missions to the outer planets are becoming more commonplace. Advancements in solar cell technologies for use in low temperature, low intensity (LILT) environments provide improved efficiency in solar panels for spacecraft. Design solutions include protection from the radiation and charging environment, such as coverglass of varying thickness, and the use of indium tin oxide coating that is grounded to the spacecraft structure to bleed off charge. Solar cell development of triple junction cells provides a higher efficiency across a wider spectrum of light to improve performance far from the Sun. NASA commissioned a detailed report in 2017 that summarizes much of this work, "Solar Power Technologies for Future Planetary Science Missions" published in December 2017 (NASA, 2017).

3.1.4.3 Measurements from Juno

Recent measurements performed by the Juno spacecraft radiation monitoring sensors indicate that the high-energy electron radiation >5 MeV is lower than the models predicted prior to launch. The observations were made at high latitudes and inside Io's orbit, and the discrepancies are most significant for spacecraft locations below $1.3 R_J$. See Becker et al. (2017) for details. Additional data from Juno should be incorporated into the radiation model to improve predictions for future missions.

3.1.4.4 Radiation-Hard Science Instrumentation

Substantial progress has been made in the development of radiation-hard science instruments, motivated by the BepiColombo, Europa Clipper, and JUICE missions and funded by a set of technology development programs in the United States and Europe (Furano et al., 2013). These include electronics needed for many instruments and other spacecraft systems (Cressler and Mantooth, 2017). Rad-hard instrument development includes cameras (Centurelli et al., 2018; Janesick et al., 2014; McEwen et al., 2012, 2014; Michaelis et al., 2017; Turtle et al., 2016), thermal imagers (Dartois et al., 2017; Gaalema et al., 2010; Hiesinger et al., 2010), laser altimeters (Althaus et al., 2016), and neutral mass spectrometers (Tulej et al., 2016). Instruments such as magnetometers (Raymond et al., 2015) and faraday cups (Westlake et al., 2016) are inherently radiation tolerant.

3.1.4.5 Summary

Recent NASA and ESA missions to Jupiter have brought new focus to radiation analysis tools and models. Environment models have been updated using additional data from the Galileo mission that had not previously been included. Furthermore, transport analysis tools have been updated and analysis methods compared and validated. Investment in design and simulation of advanced shielding designs with layered materials allows for more realistic estimates of the mass needed to shield sensitive spacecraft and instrument electronics. Shielding mass estimates can be reduced by 30–50% from previous concept studies for missions to the Jupiter system. Future missions to the Jupiter system will benefit from these improvements.

3.2 New Measurements and Technologies that Address Key Scientific Questions

3.2.1 Need for More Efficient Power Sources in Outer Solar System

There are sophisticated remote sensing and in situ techniques used to study Earth that have not been applied to the outer solar system because meeting their mass and power requirements would be prohibitively expensive (Sherwood et al., 2018). Active ice-penetrating radar is in development for Europa Clipper (Blankenship et al., 2018) and for JUICE (Bruzzone et al., 2015), and the JUICE mission carries a laser altimeter (Kimura et al., 2019), both on very large spacecraft with huge solar arrays. Use of solar arrays for power becomes increasingly difficult with range from the Sun. There have been many NASA and National Academies studies (e.g., National Research Council, 2012) calling for more efficient radioisotope power systems.

3.2.2 InSAR

Synthetic aperture radar (SAR) uses the motion of the spacecraft or aircraft to simulate having a large antenna to produce high-resolution images. Interferometric synthetic aperture radar (InSAR) uses two or more SAR images to generate maps of surface deformation or elevation, using differences in the phase of the waves returning to the satellite or aircraft (Bürgmann et al., 2000; Hanssen, 2001). The technique can measure cm-scale changes in deformation over spans of days to years. InSAR has been revolutionary in monitoring Earth's surface for land subsidence or uplift due to earthquakes, volcanic or magmatic activity, landslides, and other processes.

Use of InSAR in the outer solar system would be extremely challenging. At least three passes are required, two for topography and the third to measure changes. This will not work if the topography changes between the first two passes, so it is best to use tandem antennae or spacecraft to get both topography passes at once. Furthermore, each spacecraft pass must be within 300 m to 20 km of each other (tighter tolerance for shorter wavelengths) (Sandwell et al., 2004). But the biggest obstacles in the outer solar system are the need for 2–10 kW of power and the accommodation of >1000 kg of mass, at least for systems used at Earth. These requirements are more than ten times greater than the largest instruments sent to deep space. Clearly InSAR will not be brought to the outer solar system until power systems and launch capacity are greatly improved and/or SAR instruments with low mass and power have been developed.

3.2.3 Small Satellite Constellations

InSAR at X-band or C-band on small satellites flying in tandem could conceivably make high-precision topographic observations of planetary surfaces to identify the location and magnitude of change (Martin et al., 2001), as discussed in Section 3.2.2. Satellite-to-satellite (STS) ranging is a powerful technique for measuring the gravity field. STS ranging measures the relative speed (or distance) between two (or more) satellites at radio or optical frequencies. The recorded data can be used to recover both the static and temporal gravity fields of a target body. The main advantages of STS ranging are twofold: 1) high signal-to-noise ratio (i.e., high accuracy) due to close relative distance between satellites; and 2) flexible observation geometry (e.g., a station on Earth does not have to be in the loop). STS ranging has been successfully demonstrated by the Gravity Recovery and Climate Experiment (GRACE), Gravity Recovery and Interior Laboratory (GRAIL), and GRACE Follow-On missions.

A constellation of relatively cheap and expendable cubesats could conceivably be sent into the distal reaches of the Jovian system, where the radiation dose is low, to monitor Io and Europa for activity.

3.2.4 Radar Sounding

Today, active radar sounding is a well-established and powerful geophysical tool. Active sounding radars have been used on the Moon aboard Apollo 17, with the Apollo Lunar Sounder Experiment (Phillips et al., 1973), and on Mars with the radar sounders Mars Advanced Radar for Subsurface and Ionosphere Sounding (MARSIS) onboard the Mars Express spacecraft (Picardi et al., 2003) and Shallow Radar (SHARAD) on the Mars Reconnaissance Orbiter (MRO) (Seu et al., 2007). Active radar sounders are also key to the future exploration of icy satellites in the outer solar system with Radar for Icy Moons Exploration (RIME) on JUICE and Radar for Europa Assessment and Sounding: Ocean to Near-surface (REASON) on board the Europa Clipper aiming to characterize the icy shells and search for sub-surface water reservoirs. However, active radar systems are heavy, power-consuming, and susceptible to external radio noise sources like Jupiter. Therefore, in the context of future icy moon exploration, the concept of passive sounding has been studied (Hartogh and Ilyushin, 2016; Romero-Wolf et al., 2015; Schroeder et al., 2016). This principle makes use of radio sources and auto-correlates the noise with the reflected returns. Since such a system does not require an active transmitter, it is less power-consuming and less massive than active radars. These properties make passive radar especially attractive for the Jovian system, since Jupiter is the second strongest radio source in our solar system (after the Sun) and given the low availability of solar energy for power. However, to penetrate deep into terrestrial bodies like Io, long wavelengths are needed, requiring complicated antennas currently having a low Technology Readiness Level (TRL) (Steinbrügge et al., 2018). Further, the passive radar technology has not yet been used in space. Therefore, additional technological development is recommended to make radar investigations accessible for smaller missions and challenging environments like Io.

3.2.5 High Dynamic Range Thermal Imagers

High dynamic range imaging is desirable for observing the very hottest areas of Io's volcanic eruptions (>1400 K) to obtain unsaturated data needed to constrain lava eruption temperature (Davies et al., 2016). Hotspot intensities can vary by many orders of magnitude, depending on the temperatures and sizes of the hottest sources (often smaller than the pixel scale). Problems that must be overcome to obtain usable data are: (1) the rapid cooling of the lava between data acquisitions at different wavelengths; (2) the unknown magnitude of thermal emission, which has often led to detector saturation; and (3) thermal emission changing on a shorter timescale than the observation integration time. These problems can be addressed by using a detector with an advanced digital readout circuit (D-ROIC) to achieve a wide dynamic range sufficient to image lava on Io without saturating. A short-wavelength infrared instrument on an Io flyby mission can achieve simultaneity of observations by splitting the incoming signal for all relevant eruption processes and still obtain data fast enough to remove uncertainties in the accurate determination of the highest lava surface temperatures.

3.2.6 Advanced Pointing Imaging Camera

The Advanced Pointing Imaging Camera (APIC) is a high-resolution imaging system that simultaneously takes images of targets and star fields with two-axis control capability, allowing rapid target imaging and image motion compensation (IMC) with extremely precise pointing knowledge (Park et al., 2016). Such imaging data can accurately measure the geophysical properties and high-resolution topography of target objects. APIC is capable of measuring tidal flexing (e.g., h_2) and rotational parameters (i.e., libration, nutation, and precession) of natural satellites and asteroids with high accuracy.

3.2.7 Orbital Seismology Through Laser Vibrometry

Seismology will be a powerful tool for addressing the key questions outlined in this report. However, the operational complexity of delivering and deploying seismometers via landed spacecraft, especially deep in the gravity well of giant planets, is not trivial. Furthermore, they must survive very high radiation levels to be sufficiently long-lived on the surface of Io or Europa. The technique of laser Doppler vibrometry (LDV) shows promise for extending the tool of seismology to orbiting and flyby spacecraft (Sava and Asphaug, 2019a,b). LDV provides a non-contact tool for measuring surface vibrations through laser sensing at a distance. A vibrometer uses a laser interferometer to measure the phase difference between a reference beam and a measurement beam (Donges and Noll, 2015; Lutzmann et al., 2016). The amplitude and frequency of the ground vibration can be determined from the Doppler shift of the reflected laser beam frequency relative to the reference beam frequency.

LDV is an appealing solution for obtaining remotely-sensed seismic measurements, especially for planetary targets that can be lased at close-range. LDVs are mobile and eliminate the need to land, an advantageous property for satellites deep in the gravity well of Jupiter. Significant technical maturation is needed to maintain lasing capabilities at larger ranges-to-surface, such as those encountered by multi-flyby missions. To achieve this, the trade space between laser intensity and the size of the vibrometer's optical stack will need to be further explored as a function of ranging requirements; higher intensity lasers facilitate sensing at larger distances, but require larger cooling systems and heavier payloads. Furthermore, detecting ground vibrations by LDV requires that the spacecraft platform be free of vibration.

Modern LDV systems are extensively used in engineering applications and measure vibration radially along the laser boresight, which would enable single-component seismology from a space-borne payload. Such measurements are expected to capture frequencies from 0.1–100 Hz and resolve displacements as small as 10 μm (Sava and Asphaug, 2019a,b). The mission concept of operations (CONOPS) for using LDV to perform orbital seismology could be complex and should be optimized to acquire these data. Measuring long-period signals may require the laser to

be precisely sighted on a surface location (e.g., a large rock) for multiple seconds while in inertial, vibration-free flight. Improvements in spacecraft attitude control, and the possibility of jitter reduction in post-processing, may provide more flexibility in operations. Ground motion measured along the direction of the laser beam during an orbital mission can be sufficient to satisfy its specific science question. To observe multi-component ground motion, three simultaneous observations are required, which could be achieved with coordinated orbiting spacecraft, introducing another level of complexity.

Despite these challenges, achieving space-borne seismology with LDVs shows promise, and could revolutionize the way in which we infer the interior properties of planetary objects from flyby and orbital missions. Orbital seismology could provide data at multiple locations distributed around the studied body, thus enabling 3-D high-resolution imaging of its interior with techniques resembling medical computed tomography.

3.2.8 Landers and Penetrators

Large landers (and rovers) provide significant capability, including experiments like Gas Chromatography/Mass Spectroscopy (GCMS), and have been used extensively at Mars. Europa Lander concepts have also been described in detail (Hand et al., 2017; Pappalardo et al., 2013). Titan may get a quadcopter via Dragonfly (Lorenz et al., 2018). However, soft landing of significant mass deep within the gravity well of Jupiter (Io and Europa) is very challenging. The 2016 concept for Europa Lander could only be launched by NASA's Space Launch System, which is still in development. Below we consider concepts that may prove more affordable.

Penetrators have yet to be successfully used for planetary exploration. However, they have the potential to provide a number of key in situ geophysical measurements at lower cost than a classic soft lander like that used by the InSight mission. There are a number of concepts for penetrators able to carry out seismology, heat flow, and geochemical studies (e.g., Gowen et al., 2011; Wurz et al., 2018; Yamada et al., 2015). Penetrators that can melt through ice are of particular interest for icy worlds (Kömlé et al., 2018; Romero-Wolf et al., 2015). One of the challenges for tidally heated worlds is that we do not have good constraints on the mechanical properties of the upper few meters of these bodies.

Either laser or radio surface tracking can be used to accurately measure the time-varying three-dimensional rotations of the body, which are sensitive to its internal structure. Putting a laser retroreflector or a radio transponder on the surface of a tidally heated world is an excellent way to study its rotation and tidal deformation. A retroreflector can also facilitate LDV (Section 3.2.7). The retroreflectors left on the Moon by the Apollo and Luna missions have been used to study the internal structure of the moon (Dickey et al., 1994; Williams et al., 2006). The Rotation and Interior Structure Experiment (RISE) on-board the InSight mission will use the lander's X-band radio system in combination with tracking stations of the NASA Deep Space Network (DSN) to

determine the rotation of Mars (Folkner et al., 2018). The mean direction of Io's rotation axis is expected to precess with the orbital plane if the body is rigid. The laser or radio tracking can be used to detect if the true spin axis is displaced from the expected direction due to dissipation in Io's interior. A great advantage of a passive corner reflector is that it does not have electronics with limited lifetime in a high radiation environment.

The degree-2 tidal deformations parameterized by the Love numbers h_2 for radial and l_2 for tangential displacements are sensitive to the presence of liquid layers within the body. High values of h_2 and l_2 are indicative of a magma ocean that mechanically decouples the lid (Section 2.3.4). These tidal deformations can be directly measured by surface laser or radio ranging. In addition, the rotation is sensitive to the gravitational potential Love number k_2 .

Measurements of precession through surface laser or radio ranging can provide a constraint on the moment of inertia of the body. The moment of inertia derived from observing precession, unlike the one inferred from the gravity coefficients, does not require a hydrostatic equilibrium assumption and, thus, more directly constrains the differentiation state of the body. Moreover, observations of nutation provide insight into the interior of the body through the potential amplification of the nutation amplitude near the resonance with free nutation frequencies of the internal layers (e.g., Dehant and Mathews, 2015).



4. Conclusions and Future Directions

4.1 Spacecraft Mission Opportunities

Figure 4.1 shows planned and candidate exploration of the Galilean satellites.

4.1.1 Europa Clipper and JUICE

Both Europa Clipper and JUICE are currently in development and expected to arrive at Jupiter in the late 2020s or early 2030s. Both projects place emphasis on the study of habitability (Pappalardo et al., 2017; Witasse, 2018) and have significant potential to further our understanding of tidal heating. One of the most important measurements will be precision ranging during close flybys to measure changes in the orbits of Europa, Ganymede, and Callisto (see Section 2.4), a key constraint on equilibrium in the system along with comparable measurements of Io (Dirkx et al., 2016, 2017). Furthermore, gravity science will measure the tidal Love number k_2 and the altimeters will measure h_2 of Europa and Ganymede. It is expected that NASA will have future announcements of opportunity for a gravity science team and for participating scientists on Europa Clipper. The JUICE mission plans to be the first orbiter of an outer planet satellite, specifically Ganymede, reaching a circular orbit of 500 km altitude. This presents an opportunity for more detailed gravity and topography mapping (see Section 2.3.5) and magnetometry (Section 2.3.3), especially if a 200-km circular orbit is achieved in a potential extended mission.

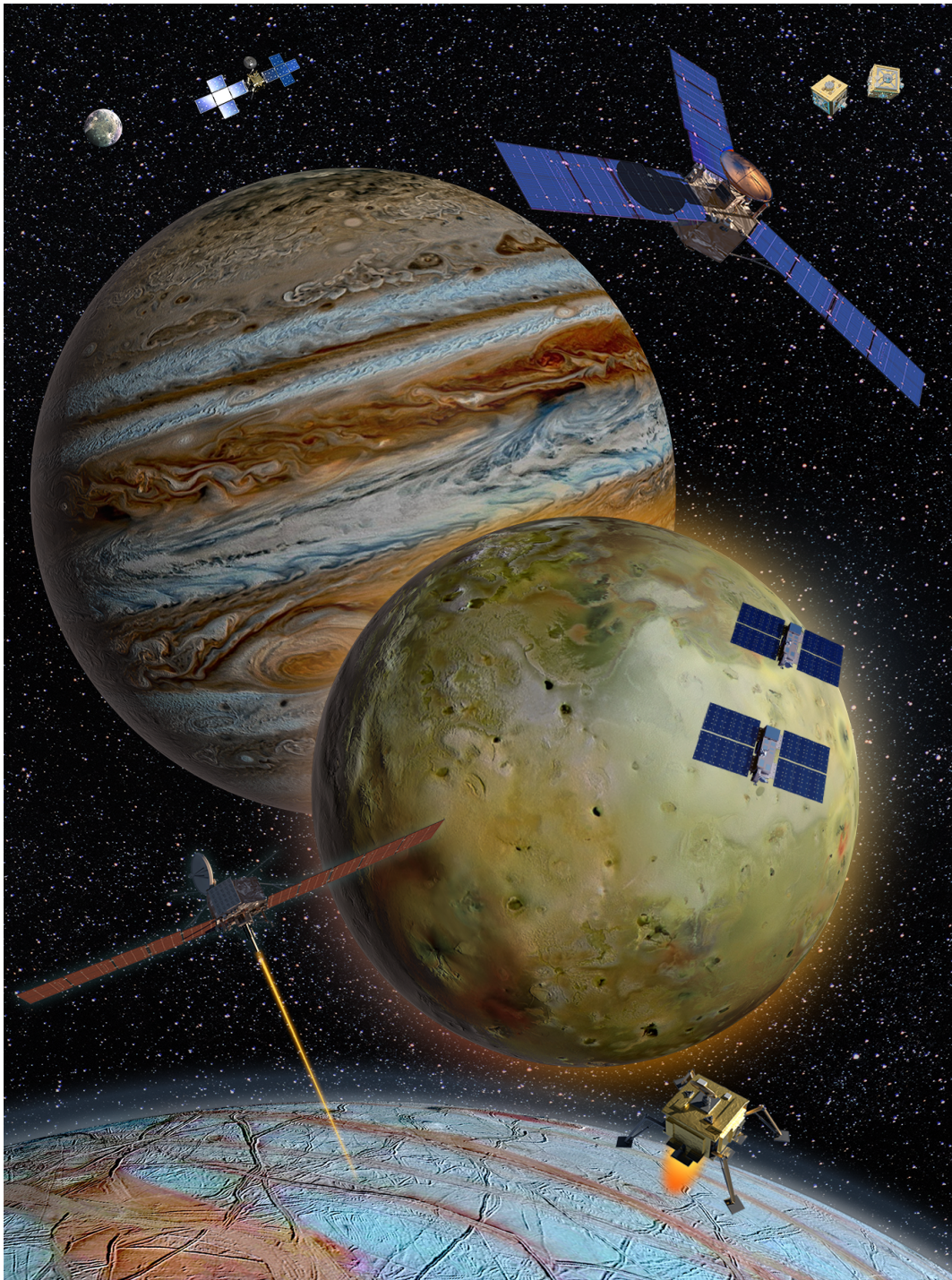


Figure 4.1: The Jupiter system provides exciting destinations for groundbreaking new science, enabled by a variety of different spacecraft architectures, instruments, observations, and experiments.

4.1.2 Discovery and New Frontiers

To date, relatively low-cost, competed missions have been proposed to focus on tidally heated moons of the outer solar system, including Io and Enceladus, but none has been selected for flight. However, the Dragonfly mission to Titan is one of two finalists for New Frontiers 4. Dragonfly is a rotorcraft mission emphasizing composition of surface materials, but also includes a seismometer experiment that may be the first of its kind to visit an outer planet satellite (Lorenz et al., 2018). In addition, electrodes on the landing skids are used to sense electric fields that may probe the depth of Titan's interior liquid water ocean. Based on this KISS study, we strongly support a future mission to Io (Section 4.4).

4.1.3 Europa or Enceladus Landers

The Europa Lander science definition team study (Hand et al., 2017) emphasizes the search for life, but also recommends a small seismometer or geophone inside the lander. Seismic energy sources will likely include cracking in the ice shell and turbulent motion in the oceans (Panning et al., 2018). NASA recently selected technology development grants for the Instrument Concepts for Europa Exploration 2 (ICEE-2), intended for a Europa lander but also useful for potential landers on other worlds. Penetrators represent a lower-cost alternative to consider for some science objectives (Section 2.3.4).

4.1.4 Satellite Orbiters

JUICE will orbit Ganymede, as mentioned above, and a Europa orbiter has been extensively studied (Clark et al., 2011). Although Europa Clipper will accomplish much of what was envisioned for a large Europa orbiter, much-improved gravity, topography, magnetic induction, and mass spectrometry could be achieved with a small orbiter (e.g., Hussmann et al., 2016; Postberg et al., 2011). Even an Io orbiter limited to a lifetime of ~8 days (Section 3.1.1) could return fundamental new results.

4.1.5 Ice Giants Flagship

The ice giants Uranus and Neptune are the most neglected planetary systems in our solar system, visited only by Voyager 2. Although a Uranus orbiter was recommended for a new start before 2023 in the Decadal Survey Vision and Voyages, a recent NASA study¹ recommends launch dates near 2030. The Uranus system contains six medium-sized moons and may provide another test of the resonance locking hypothesis (Section 2.4.2). However, the active moon Triton, a strong

¹http://www.lpi.usra.edu/icegiants/mission_study/

candidate for an ocean world, orbits Neptune, and was favored for exploration by the Roadmap to Ocean Worlds (Hendrix et al., 2019).

4.2 Telescopic Observations

The next generation of Earth-based telescopes will represent a major step toward higher sensitivity, spatial resolution, and spectral coverage on the satellites of the gas giants. The James Webb Space Telescope (JWST), currently scheduled to launch in 2021, will have unprecedented sensitivity at infrared wavelengths inaccessible from the ground, spanning about 1–50 μm in wavelength. These wavelengths cover, for example, atmospheric lines from Io and the icy satellites; signatures of organics at 5–8 μm ; and thermal emission at longer infrared wavelengths. Satellites at Saturn and beyond can be studied at these thermal wavelengths, but the Jupiter system will saturate even at the shortest JWST exposure times beyond $\sim 12 \mu\text{m}$ (and even shorter for Io due to volcanic emission). The extremely large telescopes currently under planning/construction (Giant Magellan Telescope, Thirty Meter Telescope, European Extremely Large Telescope) will have several times the sensitivity and a factor of ~ 3 higher spatial resolution than current 8–10-m-class telescopes. The higher sensitivity means that fainter atmospheric lines will be detectable on satellites, while the sensitivity and spatial resolution combined will lead to higher-resolution mapping of surface and atmospheric species, and the potential to characterize Io's small volcano population from Earth. Ongoing upgrades to the ALMA interferometer are continually increasing the sensitivity and spatial resolution of this instrument, and satellite thermal emission can now be mapped in the radio wavelengths at the same spatial resolution as reflected sunlight in the optical/infrared, providing a powerful multi-wavelength dataset for understanding surfaces. ALMA's sensitivity to molecular species in tenuous atmospheres is now allowing for the detection of new trace species and the mapping (and isotopic characterization) of more abundant molecules. Ongoing programs are even searching for radio signatures of plume-related species on both Europa and Enceladus.

4.3 Programs for Lab experiments

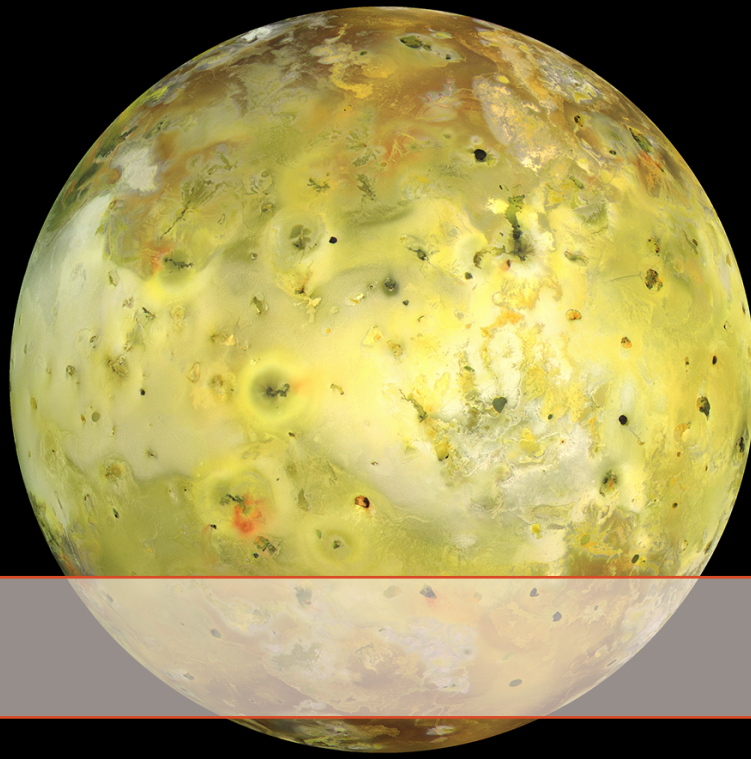
Funding opportunities for laboratory studies investigating tidal heating in planetary bodies may be available among NASA solicitations that welcome experimental research (e.g., Astrodynamics in Support of Icy Worlds Missions, Solar System Workings, Emerging Worlds). Both experimental proposals and multi-disciplinary proposals including an experimental section should be considered. The development of new high-pressure experimental techniques in order to investigate tidal heating processes in the lab (such as partial melting in deformation contexts) could also benefit geoscience studies. Such experimental projects that promote the development of new technologies for mineral physics research could be eligible for support from the NSF-funded Consortium for Materials Properties Research in Earth Sciences (COMPRES) program.

4.4 Summary Recommendation: Spacecraft Mission to Io

We have made many recommendations throughout this report for future spacecraft exploration, laboratory experiments, telescopic observations, modeling, and technology development to advance our understanding of tidal heating. However, we consider the best (most feasible) major next step to be a mission to explore Io (e.g., Esper et al., 2003; Keane et al., 2017; McEwen et al., 2014; McEwen, 2019; Suer et al., 2017; Williams et al., 2009). A relatively low-cost, competed mission in Discovery or New Frontiers that orbits Jupiter and makes multiple close flybys of Io does not require any new technologies. Such a mission could have a substantially lower total ionizing dose than Galileo or Juno, or anticipated for Europa Clipper or JUICE.

An Io mission in Discovery would be more limited than New Frontiers concepts, for example using a fixed high-gain antenna (HGA) rather than a gimbaled HGA. However, the astrometry and gravity science can still be accomplished with a fixed HGA sometimes tracking Earth near Io plus strategically placed fan beam antennae, as planned for Europa Clipper (Park et al., 2015; Verma and Margot, 2018).

A Discovery-class Io mission (McEwen, 2019) can at least partially address all five key questions identified in this study. The mission would provide extensive visible and infrared imaging to address Question 1: What do volcanic eruptions tell us about the interior of tidally heated bodies? It can make much-improved measurements of magnetic induction and measure tidal k_2 and libration amplitude to sufficient precision to answer Question 3: Does Io has a magma ocean? (Table 2.1). Radio tracking with precision radiometric ranging can produce a greatly improved measure of Io's tidal migration timescale, which along with comparable measurements of Europa and Ganymede and improved measure of Io's global heat flow (Section 2.1.7) will address Question 4: Is the Laplace resonance in equilibrium? A contributed neutral mass spectrometer can begin to address Question 5: Can stable isotopes inform long-term evolution? Finally, Question 2 (How is dissipation partitioned between solid and fluid layers?) will be partially addressed by answering Question 3 to understand Io's interior structure, but also requires new laboratory and theoretical work. An approved mission to Io would motivate funding such ground-based efforts and enable the best interpretation of spacecraft observations. An Io mission would also motivate support for Earth-based telescopic observations of Io.



Bibliography

- Adams, E. et al. (2012). "Io Volcano Observer's (IVO) integrated approach to optimizing system design for radiation challenges". In: *2012 IEEE Aerospace Conference*. IEEE, pp. 1–13.
- Althaus, C. et al. (2016). "The Ganymede Laser Altimeter–Instrument design overview with radiation hard transmitter". In: *3rd International Workshop on Instrumentation for Planetary Mission*. LPI Contribution No. 1980, ID 4015.
- Anderson, J. D. et al. (1998). "Europa's differentiated internal structure: Inferences from four Galileo encounters". In: *Science* 281.5385, pp. 2019–2022.
- Anderson, J. D. et al. (2001). "Io's gravity field and interior structure". In: *Journal of Geophysical Research: Planets* 106.E12, pp. 32963–32969.
- Arlot, J.-E. et al. (2014). "The PHEMU09 catalogue and astrometric results of the observations of the mutual occultations and eclipses of the Galilean satellites of Jupiter made in 2009". In: *Astronomy & Astrophysics* 572, A120.
- Bai, Q., Z.-M. Jin, and H. W. Green (1997). "Experimental investigation of the rheology of partially molten peridotite at upper mantle pressures and temperatures". In: *Mineralogical Society Series* 8, pp. 40–61.
- Baland, R.-M. and T. Van Hoolst (2010). "Librations of the Galilean satellites: The influence of global internal liquid layers". In: *Icarus* 209.2, pp. 651–664.
- Barr, A. C., V. Dobos, and L. L. Kiss (2018). "Interior structures and tidal heating in the TRAPPIST-1 planets". In: *Astronomy & Astrophysics* 613, A37.

- Becker, H. N. et al. (2017). "Observations of MeV electrons in Jupiter's innermost radiation belts and polar regions by the Juno radiation monitoring investigation: Perijoves 1 and 3". In: *Geophysical Research Letters* 44.10, pp. 4481–4488.
- Becker, T and PE Geissler (2005). "Galileo global color mosaics of Io". In: *36th Annual Lunar and Planetary Science Conference*. Abstract No. 1862.
- Beuthe, M. (2013). "Spatial patterns of tidal heating". In: *Icarus* 223.1, pp. 308–329.
- (2016). "Crustal control of dissipative ocean tides in Enceladus and other icy moons". In: *Icarus* 280, pp. 278–299.
- Bierson, C. J. and F. Nimmo (2016). "A test for Io's magma ocean: Modeling tidal dissipation with a partially molten mantle". In: *Journal of Geophysical Research: Planets* 121.11, pp. 2211–2224.
- Bland, M. T. et al. (2012). "Enceladus' extreme heat flux as revealed by its relaxed craters". In: *Geophysical Research Letters* 39.17.
- Blankenship, D. et al. (2018). "REASON for Europa". In: *42nd COSPAR Scientific Assembly*. Abstract ID B5.3-55-18.
- Blöcker, A. et al. (2018). "MHD Modeling of the Plasma Interaction With Io's Asymmetric Atmosphere". In: *Journal of Geophysical Research: Space Physics* 123.11, pp. 9286–9311.
- Böse, M. et al. (2017). "A probabilistic framework for single-station location of seismicity on Earth and Mars". In: *Physics of the Earth and Planetary Interiors* 262, pp. 48–65.
- Brown, R. H. et al. (2006). "Composition and physical properties of Enceladus' surface". In: *Science* 311.5766, pp. 1425–1428.
- Bruzzone, L. et al. (2015). "The Radar for Icy Moon Exploration (RIME) on the JUICE Mission". In: *AGU Fall Meeting Abstracts*. Abstract ID P53G-01.
- Bürgmann, R., P. A. Rosen, and E. J. Fielding (2000). "Synthetic aperture radar interferometry to measure Earth's surface topography and its deformation". In: *Annual Review of Earth and Planetary Sciences* 28.1, pp. 169–209.
- Burns, J. A., M. S. Matthews, et al. (1986). *Satellites*. 77. University of Arizona Press.
- Cantrall, C. et al. (2018). "Variability and geologic associations of volcanic activity on Io in 2001–2016". In: *Icarus* 312, pp. 267–294.
- Caricchi, L. et al. (2011). "Experimental determination of electrical conductivity during deformation of melt-bearing olivine aggregates: Implications for electrical anisotropy in the oceanic low velocity zone". In: *Earth and Planetary Science Letters* 302.1-2, pp. 81–94.

- Carr, M. H. et al. (1998). "Mountains and calderas on Io: Possible implications for lithosphere structure and magma generation". In: *Icarus* 135.1, pp. 146–165.
- Carter, S. P. et al. (2009). "Using radar-sounding data to identify the distribution and sources of subglacial water: application to Dome C, East Antarctica". In: *Journal of Glaciology* 55.194, pp. 1025–1040.
- Centurelli, J. L. et al. (2018). "Europa imaging system wide angle camera: the effect of gamma radiation on the refractive index and transmission of radiation resistant glasses". In: *Space Telescopes and Instrumentation 2018: Optical, Infrared, and Millimeter Wave*. Vol. 10698. International Society for Optics and Photonics, p. 106984D.
- Chen, E. M. A. and F. Nimmo (2016). "Tidal dissipation in the lunar magma ocean and its effect on the early evolution of the Earth–Moon system". In: *Icarus* 275, pp. 132–142.
- Chen, E. M. A., F. Nimmo, and G. A. Glatzmaier (2014). "Tidal heating in icy satellite oceans". In: *Icarus* 229, pp. 11–30.
- Cherng, M., I. Jun, and T. Jordan (2007). "Optimum shielding in Jovian radiation environment". In: *Nuclear Instruments and Methods in Physics Research Section A: Accelerators, Spectrometers, Detectors and Associated Equipment* 580.1, pp. 633–636.
- Civet, F. et al. (2015). "Electrical conductivity of the Earth's mantle from the first Swarm magnetic field measurements". In: *Geophysical Research Letters* 42.9, pp. 3338–3346.
- Clark, K. et al. (2011). "Return to Europa: Overview of the Jupiter Europa orbiter mission". In: *Advances in Space Research* 48.4, pp. 629–650.
- Clark, R. N. et al. (2013). "Observed ices in the solar system". In: *The science of solar system ices*. Springer, pp. 3–46.
- Clark, R. N. et al. (2019). "Isotopic ratios of Saturn's rings and satellites: Implications for the origin of water and Phoebe". In: *Icarus* 321, pp. 791–802.
- Comstock, R. L. and B. G. Bills (2003). "A solar system survey of forced librations in longitude". In: *Journal of Geophysical Research: Planets* 108.E9.
- Connolly, J. A. D. (2005). "Computation of phase equilibria by linear programming: a tool for geodynamic modeling and its application to subduction zone decarbonation". In: *Earth and Planetary Science Letters* 236.1-2, pp. 524–541.
- Constable, S. and C. Constable (2004). "Observing geomagnetic induction in magnetic satellite measurements and associated implications for mantle conductivity". In: *Geochemistry, Geophysics, Geosystems* 5.1.

- Cressler, J. D. and H. A. Mantooth (2017). *Extreme Environment Electronics*. 1st Edition. ISBN: 9781138074224. CRC Press.
- Ćuk, M., L. Dones, and D. Nesvorný (2013). "Titan-Hyperion Resonance and the Tidal Q of Saturn". In: *arXiv preprint arXiv:1311.6780*.
- (2016). "Dynamical evidence for a late formation of Saturn's moons". In: *The Astrophysical Journal* 820.2, p. 97.
- Ćuk, M. et al. (2018). "Secular resonance between Iapetus and the giant planets". In: *Monthly Notices of the Royal Astronomical Society* 481.4, pp. 5411–5421.
- Dartois, T. et al. (2017). "Environmental evaluation of the ULIS PICO1024 microbolometer". In: *Sensors, Systems, and Next-Generation Satellites XXI*. Vol. 10423. International Society for Optics and Photonics, p. 104231L.
- Das, M. K., P. P. Mukherjee, and K. Muralidhar (2018). *Modeling Transport Phenomena in Porous Media with Applications*. Springer. 241 pp.
- Davies, A. G. (2003). "Volcanism on Io: Estimation of eruption parameters from Galileo NIMS data". In: *Journal of Geophysical Research: Planets* 108.E9.
- Davies, A. G. (2007). *Volcanism on Io: A Comparison with Earth*. Cambridge University Press. 372 pp.
- Davies, A. G. and M. E. Ennis (2011). "The variability of volcanic activity at Zamama, Culann, and Tupan Patera on Io as seen by the Galileo Near Infrared Mapping Spectrometer". In: *Icarus* 215.1, pp. 401–416.
- Davies, A. G., L. P. Keszthelyi, and A. J. L. Harris (2010). "The thermal signature of volcanic eruptions on Io and Earth". In: *Journal of Volcanology and Geothermal Research* 194.4, pp. 75–99.
- Davies, A. G., L. P. Keszthelyi, and A. S. McEwen (2016). "Determination of eruption temperature of Io's lavas using lava tube skylights". In: *Icarus* 278, pp. 266–278.
- Davies, A. G. et al. (2001). "Thermal signature, eruption style, and eruption evolution at Pele and Pillan on Io". In: *Journal of Geophysical Research: Planets* 106.E12, pp. 33079–33103.
- Davies, A. G. et al. (2015). "Map of Io's volcanic heat flow". In: *Icarus* 262, pp. 67–78.
- Davies, A. G. et al. (2018). "Discovery of a Powerful, Transient, Explosive Thermal Event at Marduk Fluctus, Io, in Galileo NIMS Data". In: *Geophysical Research Letters* 45.7, pp. 2926–2933.

- De Kleer, K. and I. de Pater (2016a). "Spatial distribution of Io's volcanic activity from near-IR adaptive optics observations on 100 nights in 2013–2015". In: *Icarus* 280, pp. 405–414.
- (2016b). "Time variability of Io's volcanic activity from near-IR adaptive optics observations on 100 nights in 2013–2015". In: *Icarus* 280, pp. 378–404.
- De Kleer, K. et al. (2014). "Near-infrared monitoring of Io and detection of a violent outburst on 29 August 2013". In: *Icarus* 242, pp. 352–364.
- De Pater, I. et al. (2014). "Global near-IR maps from Gemini-N and Keck in 2010, with a special focus on Janus Patera and Kanehekili Fluctus". In: *Icarus* 242, pp. 379–395.
- De Soria-Santacruz, M. et al. (2016). "An empirical model of the high-energy electron environment at Jupiter". In: *Journal of Geophysical Research: Space Physics* 121.10, pp. 9732–9743.
- Dehant, V. and P. M. Mathews (2015). *Precession, nutation and wobble of the Earth*. Cambridge University Press. 554 pp.
- Dermott, S. F., R. Malhotra, and C. D. Murray (1988). "Dynamics of the Uranian and Saturnian satellite systems: A chaotic route to melting Miranda?" In: *Icarus* 76.2, pp. 295–334.
- Dickey, J. O. et al. (1994). "Lunar laser ranging: A continuing legacy of the Apollo program". In: *Science* 265.5171, pp. 482–490.
- Dirkx, D. et al. (2016). "Dynamical modelling of the Galilean moons for the JUICE mission". In: *Planetary and Space Science* 134, pp. 82–95.
- Dirkx, D. et al. (2017). "On the contribution of PRIDE-JUICE to Jovian system ephemerides". In: *Planetary and Space Science* 147, pp. 14–27.
- Divine, N. and H. B. Garrett (1983). "Charged particle distributions in Jupiter's magnetosphere". In: *Journal of Geophysical Research: Space Physics* 88.A9, pp. 6889–6903.
- Dobos, V. and E. L. Turner (2015). "Viscoelastic models of tidally heated exomoons". In: *The Astrophysical Journal* 804.1, p. 41.
- Donges, A. and R. Noll (2015). *Laser Measurement Technology*. Vol. 188. ISBN: 9783662436349. Springer Series in Optical Sciences. 422 pp.
- Egbert, G. D. and R. D. Ray (2000). "Significant dissipation of tidal energy in the deep ocean inferred from satellite altimeter data". In: *Nature* 405.6788, pp. 775–778.
- (2001). "Estimates of M2 tidal energy dissipation from TOPEX/Poseidon altimeter data". In: *Journal of Geophysical Research: Oceans* 106.C10, pp. 22475–22502.

- Elkins Tanton, L. T. et al. (2002). "Re-examination of the lunar magma ocean cumulate overturn hypothesis: melting or mixing is required". In: *Earth and Planetary Science Letters* 196.3-4, pp. 239–249.
- Esper, J. et al. (2003). "VOLCAN: a mission to explore Jupiter's volcanic moon Io". In: *Acta Astronautica* 52.2-6, pp. 245–251.
- Faul, U. H., J. D. Fitz Gerald, and I. Jackson (2004). "Shear wave attenuation and dispersion in melt-bearing olivine polycrystals: 2. Microstructural interpretation and seismological implications". In: *Journal of Geophysical Research: Solid Earth* 109.B6.
- Faul, U. H. and I. Jackson (2015). "Transient creep and strain energy dissipation: An experimental perspective". In: *Annual Review of Earth and Planetary Sciences* 43, pp. 541–569.
- Feaga, L. M., M. McGrath, and P. D. Feldman (2009). "Io's dayside SO₂ atmosphere". In: *Icarus* 201.2, pp. 570–584.
- Fieseler, P. D., S. M. Ardanan, and A. R. Frederickson (2002). "The radiation effects on Galileo spacecraft systems at Jupiter". In: *IEEE Transactions on Nuclear Science* 49.6, pp. 2739–2758.
- Folkner, W. M. et al. (2018). "The rotation and interior structure experiment on the InSight mission to Mars". In: *Space Science Reviews* 214 (5). Article ID 100.
- Fu, R. R. et al. (2017). "The interior structure of Ceres as revealed by surface topography". In: *Earth and Planetary Science Letters* 476, pp. 153–164.
- Fuller, J., J. Luan, and E. Quataert (2016). "Resonance locking as the source of rapid tidal migration in the Jupiter and Saturn moon systems". In: *Monthly Notices of the Royal Astronomical Society* 458.4, pp. 3867–3879.
- Furano, G., R. Jansen, and A. Menicucci (2013). "Review of radiation hard electronics activities at European Space Agency". In: *Journal of Instrumentation* 8.02, p. C02007.
- Gaalema, S. et al. (2010). "Thermopile detector radiation hard readout". In: *Detectors and Imaging Devices: Infrared, Focal Plane, Single Photon*. Vol. 7780. International Society for Optics and Photonics, p. 778002.
- Garrett, H. et al. (2017). "The latest Jovian-trapped proton and heavy ion models". In: *IEEE Transactions on Nuclear Science* 64.11, pp. 2802–2813.
- Ghiorso, M. S. et al. (2002). "The pMELTS: A revision of MELTS for improved calculation of phase relations and major element partitioning related to partial melting of the mantle to 3 GPa". In: *Geochemistry, Geophysics, Geosystems* 3.5, pp. 1–35.
- Gillon, M. et al. (2017). "Seven temperate terrestrial planets around the nearby ultracool dwarf star TRAPPIST-1". In: *Nature* 542.7642, p. 456.

- Gleason, G. C., V. Bruce, and H. W. Green (1999). "Experimental investigation of melt topology in partially molten quartzo-feldspathic aggregates under hydrostatic and non-hydrostatic stress". In: *Journal of metamorphic Geology* 17.6, pp. 705–722.
- Goldreich, P. and S. Soter (1966). "Q in the Solar System". In: *Icarus* 5.1-6, pp. 375–389.
- Gowen, R. A. et al. (2011). "Penetrators for in situ subsurface investigations of Europa". In: *Advances in Space Research* 48.4, pp. 725–742.
- Green, J. A. M. and J. Nycander (2013). "A comparison of tidal conversion parameterizations for tidal models". In: *Journal of Physical Oceanography* 43.1, pp. 104–119.
- Greenhagen, B. T. et al. (2010). "Global silicate mineralogy of the Moon from the Diviner Lunar Radiometer". In: *Science* 329.5998, pp. 1507–1509.
- Grotzinger, J. P. et al. (2012). "Mars Science Laboratory mission and science investigation". In: *Space Science Reviews* 170 (1-4), pp. 5–56.
- Hamilton, C. W. et al. (2013). "Spatial distribution of volcanoes on Io: Implications for tidal heating and magma ascent". In: *Earth and Planetary Science Letters* 361, pp. 272–286.
- Hamilton, C. W. et al. (2018). "The Io Volcano Observer (IVO): A NASA Discovery mission concept to investigate tidal heating". In: *130th Annual Meeting of the Geological Society of America*. Abstract No. 67-14.
- Hand, K. P. et al. (2017). "Europa Lander study 2016 report, europa lander mission". In: *NASA Jet Propulsion Laboratory, La Cañada Flintridge, CA, USA, Technical Report JPL D-97667*.
- Hansen, C. J. et al. (2006). "Enceladus' water vapor plume". In: *Science* 311.5766, pp. 1422–1425.
- Hanssen, R. F. (2001). *Radar interferometry: data interpretation and error analysis*. Vol. 2. Springer Science & Business Media.
- Hartogh, P. and Y. A. Ilyushin (2016). "A passive low frequency instrument for radio wave sounding the subsurface oceans of the Jovian icy moons: An instrument concept". In: *Planetary and Space Science* 130, pp. 30–39.
- Hay, H. C. F. C. and I. Matsuyama (2017). "Numerically modelling tidal dissipation with bottom drag in the oceans of Titan and Enceladus". In: *Icarus* 281, pp. 342–356.
- (2019). "Nonlinear tidal dissipation in the subsurface oceans of Enceladus and other icy satellites". In: *Icarus* 319, pp. 68–85.
- Hedman, M. M. et al. (2013). "An observed correlation between plume activity and tidal stresses on Enceladus". In: *Nature* 500.7461, pp. 182–184.

- Helbert, J. et al. (2013). "Olivine thermal emissivity under extreme temperature ranges: Implication for Mercury surface". In: *Earth and Planetary Science Letters* 371, pp. 252–257.
- Hendrix, A. R. et al. (2019). "The NASA Roadmap to Ocean Worlds". In: *Astrobiology* 19.1, pp. 1–27.
- Henning, W. G. et al. (2018). *Highly volcanic exoplanets, lava worlds, and magma ocean worlds: An emerging class of dynamic exoplanets of significant scientific priority*.
- Hiesinger, H., J. Helbert, and the MERTIS Co-I Team (2010). "The Mercury radiometer and thermal infrared spectrometer (MERTIS) for the BepiColombo mission". In: *Planetary and Space Science* 58.1-2, pp. 144–165.
- Hirth, G. and D. L. Kohlstedt (2015). "The stress dependence of olivine creep rate: Implications for extrapolation of lab data and interpretation of recrystallized grain size". In: *Earth and Planetary Science Letters* 418, pp. 20–26.
- Hood, L. L., F. Herbert, and C. P. Sonett (1982). "The deep lunar electrical conductivity profile: Structural and thermal inferences". In: *Journal of Geophysical Research: Solid Earth* 87.B7, pp. 5311–5326.
- Howell, R. R. et al. (1989). "High-resolution infrared spectroscopy of Io and possible surface materials". In: *Icarus* 78.1, pp. 27–37.
- Howett, C. J. A. et al. (2011). "High heat flow from Enceladus' south polar region measured using 10–600 cm⁻¹ Cassini/CIRS data". In: *Journal of Geophysical Research: Planets* 116.E3.
- Hurford, T. A. et al. (2018). "Tidally-driven seismicity: An application to Europa". In: *49th Lunar and Planetary Science Conference*. Abstract 2414.
- Hussmann, H. and T. Spohn (2004). "Thermal-orbital evolution of Io and Europa". In: *Icarus* 171.2, pp. 391–410.
- Hussmann, H. et al. (2016). "Constraints on dissipation in the deep interiors of Ganymede and Europa from tidal phase-lags". In: *Celestial Mechanics and Dynamical Astronomy* 126.1-3, pp. 131–144.
- less, L. et al. (2012). "The tides of Titan". In: *Science* 337.6093, pp. 457–459.
- less, L. et al. (2018). "Measurement of Jupiter's asymmetric gravity field". In: *Nature* 555.7695, pp. 220–222.
- Jaeger, W. L. et al. (2003). "Orogenic tectonism on Io". In: *Journal of Geophysical Research - Planets* 108.8.

- Janesick, J. et al. (2014). "Mk x Nk gated CMOS imager". In: *Target Diagnostics Physics and Engineering for Inertial Confinement Fusion III*. Vol. 9211. Proceedings of the SPIE. DOI: 10.1117/12.2063524, p. 921106.
- Jayne, S. R. and L. C. St. Laurent (2001). "Parameterizing tidal dissipation over rough topography". In: *Geophysical Research Letters* 28.5, pp. 811–814.
- Jessup, K. L. et al. (2004). "The atmospheric signature of Io's Prometheus plume and anti-jovian hemisphere: evidence for a sublimation atmosphere". In: *Icarus* 169.1, pp. 197–215.
- Jia, X. et al. (2018). "Evidence of a plume on Europa from Galileo magnetic and plasma wave signatures". In: *Nature Astronomy* 2 (6), pp. 459–464.
- Jin, Z. M., Q. Bai, and D. L. Kohlstedt (1994). "High-temperature creep of olivine crystals from four localities". In: *Physics of the Earth and Planetary Interiors* 82.1, pp. 55–64.
- Johnson, C. L. et al. (2016). "MESSENGER observations of induced magnetic fields in Mercury's core". In: *Geophysical Research Letters* 43.6, pp. 2436–2444.
- Kankanamge, D. G. J. and W. B. Moore (2019). "A Parameterization for Volcanic Heat Flux in Heat Pipe Planets". In: *Journal of Geophysical Research: Planets* 124 (1), pp. 114–127.
- Kargel, J. S. (1995). "Cryovolcanism on the icy satellites". In: *Comparative Planetology with an Earth Perspective*. Springer, pp. 101–113.
- Kargel, J. et al. (2003). "Extreme volcanism on Io: Latest insights at the end of Galileo era". In: *Eos, Transactions American Geophysical Union* 84.33, pp. 313–318.
- Keane, J. T. et al. (2017). "Io: The Volcanic World That Will Tell Us How Ocean Worlds Work (and a Mission Concept to Get Us There)". In: *Planetary Science Vision 2050 Workshop*. Vol. 1989.
- Keszthelyi, L. and A. S. McEwen (1997). "Magmatic differentiation of Io". In: *Icarus* 130.2, pp. 437–448.
- Keszthelyi, L., A. S. McEwen, and G. J. Taylor (1999). "Revisiting the hypothesis of a mushy global magma ocean in Io". In: *Icarus* 141.2, pp. 415–419.
- Keszthelyi, L. et al. (2001). "Imaging of volcanic activity on Jupiter's moon Io by Galileo during the Galileo Europa Mission and the Galileo Millennium Mission". In: *Journal of Geophysical Research: Planets* 106.E12, pp. 33025–33052.
- Keszthelyi, L. et al. (2007). "New estimates for Io eruption temperatures: Implications for the interior". In: *Icarus* 192.2, pp. 491–502.

- Khan, A. et al. (2006). "Constraining the composition and thermal state of the moon from an inversion of electromagnetic lunar day-side transfer functions". In: *Earth and Planetary Science Letters* 248.3-4, pp. 579–598.
- Khan, A. et al. (2014). "Geophysical evidence for melt in the deep lunar interior and implications for lunar evolution". In: *Journal of Geophysical Research: Planets* 119.10, pp. 2197–2221.
- Khurana, K. K. et al. (1998). "Induced magnetic fields as evidence for subsurface oceans in Europa and Callisto". In: *Nature* 395.6704, pp. 777–780.
- Khurana, K. K. et al. (2009). "Electromagnetic induction from Europa's ocean and the deep interior". In: *Europa*. Ed. by W. B. McKinnon R. T. Pappalardo and K. K. Khurana. Tucson: University of Arizona Press, pp. 572–586.
- Khurana, K. K. et al. (2011). "Evidence of a global magma ocean in Io's interior". In: *Science* 332.6034, pp. 1186–1189.
- Kimura, J. et al. (2019). "Science Objectives of the Ganymede Laser Altimeter (GALA) for the JUICE Mission". In: *Transactions of the Japan Society for Aeronautical and Space Sciences, Aerospace Technology Japan*, pp. 17–234.
- King, D. S. H., M. E. Zimmerman, and D. L. Kohlstedt (2010). "Stress-driven Melt Segregation in Partially Molten Olivine-rich Rocks Deformed in Torsion". In: *Journal of Petrology* 51.1-2, pp. 21–42.
- Kirchoff, M. R., W. B. McKinnon, and P. M. Schenk (2011). "Global distribution of volcanic centers and mountains on Io: Control by asthenospheric heating and implications for mountain formation". In: *Earth and Planetary Science Letters* 301.1-2, pp. 22–30.
- Kivelson, M. G., K. K. Khurana, and M. Volwerk (2002). "The permanent and inductive magnetic moments of Ganymede". In: *Icarus* 157.2, pp. 507–522.
- Kivelson, M. G. et al. (2000). "Galileo magnetometer measurements: A stronger case for a subsurface ocean at Europa". In: *Science* 289.5483, pp. 1340–1343.
- Koch, C., U. Christensen, and R. Kallenbach (2008). "Simultaneous determination of global topography, tidal Love number and libration amplitude of Mercury by laser altimetry". In: *Planetary and Space Science* 56.9, pp. 1226–1237.
- Koch, C., R. Kallenbach, and U. Christensen (2010). "Mercury's global topography and tidal signal from laser altimetry by using a rectangular grid". In: *Planetary and Space Science* 58.14-15, pp. 2022–2030.

- Kohlstedt, D. L. and B. K. Holtzman (2009). "Shearing melt out of the Earth: An experimentalist's perspective on the influence of deformation on melt extraction". In: *Annual Review of Earth and Planetary Sciences* 37, pp. 561–593.
- Kömler, N. I. et al. (2018). "Melting probes revisited—Ice penetration experiments under Mars surface pressure conditions". In: *Icarus* 308, pp. 117–127.
- Konôpková, Z. et al. (2016). "Direct measurement of thermal conductivity in solid iron at planetary core conditions". In: *Nature* 534.7605, pp. 99–101.
- Kovach, R. L. and C. F. Chyba (2001). "Seismic detectability of a subsurface ocean on Europa". In: *Icarus* 150.2, pp. 279–287.
- Lainey, V. et al. (2009). "Strong tidal dissipation in Io and Jupiter from astrometric observations". In: *Nature* 459.7249, pp. 957–959.
- Lainey, V. et al. (2012). "Strong Tidal Dissipation in Saturn and Constraints on Enceladus' Thermal State from Astrometry". In: *The Astrophysical Journal* 752 (14).
- Lainey, V. et al. (2017). "New constraints on Saturn's interior from Cassini astrometric data". In: *Icarus* 281, pp. 286–296.
- Le Roux, V., A. Tommasi, and A. Vauchez (2008). "Feedback between melt percolation and deformation in an exhumed lithosphere–asthenosphere boundary". In: *Earth and Planetary Science Letters* 274.3–4, pp. 401–413.
- Lee, R. and M. S. Ramsey (2016). "What Is the emissivity of active basaltic lava flows?" In: *AGU Fall Meeting*. Abstract MR51A-2690.
- Li, L. and D. J. Weidner (2013). "Effect of dynamic melting on acoustic velocities in a partially molten peridotite". In: *Physics of the Earth and Planetary Interiors* 222, pp. 1–7.
- Liang, M.-C. et al. (2007). "Source of nitrogen isotope anomaly in HCN in the atmosphere of Titan". In: *The Astrophysical Journal Letters* 664.2, p. L115.
- Liebske, C. et al. (2005). "Viscosity of peridotite liquid up to 13 GPa: Implications for magma ocean viscosities". In: *Earth and Planetary Science Letters* 240.3–4, pp. 589–604.
- Limare, A. et al. (2015). "Microwave-heating laboratory experiments for planetary mantle convection". In: *Journal of Fluid Mechanics* 777, pp. 50–67.
- Logan, L. M. et al. (1973). "Compositional implications of Christiansen frequency maximums for infrared remote sensing applications". In: *Journal of Geophysical Research* 78.23, pp. 4983–5003.
- Lopes-Gautier, R. et al. (1999). "Active volcanism on Io: Global distribution and variations in activity". In: *Icarus* 140.2, pp. 243–264.

- Lorenz, R. D. et al. (2018). "Dragonfly: A rotorcraft lander concept for scientific exploration at titan". In: *Johns Hopkins APL Technical Digest (Applied Physics Laboratory)* 34.3. <http://www.jhuapl.edu/techdigest>, pp. 374–387.
- Luger, R. et al. (2017). "A seven-planet resonant chain in TRAPPIST-1". In: *Nature Astronomy* 1.6, p. 0129.
- Lutzmann, P. et al. (2016). "Laser vibration sensing at Fraunhofer IOSB: review and applications". In: *Optical Engineering* 56.3, p. 031215.
- Mahaffy, P. (1999). "Mass Spectrometers Developed for Planetary Missions". In: *Astrophysics and Space Research*. Springer, pp. 355–376.
- Mandt, K. E. et al. (2009). "Isotopic evolution of the major constituents of Titan's atmosphere based on Cassini data". In: *Planetary and Space Science* 57.14–15, pp. 1917–1930.
- Mandt, K. E. et al. (2012a). "Ion densities and composition of Titan's upper atmosphere derived from the Cassini Ion Neutral Mass Spectrometer: Analysis methods and comparison of measured ion densities to photochemical model simulations". In: *Journal of Geophysical Research: Planets* 117.E10.
- Mandt, K. E. et al. (2012b). "The $^{12}\text{C}/^{13}\text{C}$ ratio on Titan from Cassini INMS measurements and implications for the evolution of methane". In: *The Astrophysical Journal* 749.2 (160).
- Mandt, K. E. et al. (2014). "Protosolar ammonia as the unique source of Titan's nitrogen". In: *The Astrophysical Journal Letters* 788.2 (L24).
- Mandt, K. E. et al. (2017). "Photochemistry on Pluto: Part II HCN and nitrogen isotope fractionation". In: *Monthly Notices of the Royal Astronomical Society* 472.1, pp. 118–128.
- Martin, M., S. Kilberg, and J. Winter (2001). "TechSat 21 and revolutionizing space missions using microsattellites". In: *Proc. 15th AIAA/USU Conference on Small Satellites, Logan, Utah*. Vol. 7.
- Matsuyama, I. (2014). "Tidal dissipation in the oceans of icy satellites". In: *Icarus* 242, pp. 11–18.
- Matsuyama, I. et al. (2018). "Ocean tidal heating in icy satellites with solid shells". In: *Icarus* 312, pp. 208–230.
- Maturilli, A. et al. (2014). "Komatiites as Mercury surface analogues: spectral measurements at PEL". In: *Earth and Planetary Science Letters* 398, pp. 58–65.
- Maumus, J., N. Bagdassarov, and H. Schmeling (2005). "Electrical conductivity and partial melting of mafic rocks under pressure". In: *Geochimica et Cosmochimica Acta* 69.19, pp. 4703–4718.

- Mazarico, E. et al. (2014). "Detection of the lunar body tide by the Lunar Orbiter Laser Altimeter". In: *Geophysical Research Letters* 41.7, pp. 2282–2288.
- McCarthy, C. and R. F. Cooper (2016). "Tidal dissipation in creeping ice and the thermal evolution of Europa". In: *Earth and Planetary Science Letters* 443, pp. 185–194.
- McCarthy, C. et al. (2011). "Transient and steady state creep response of ice I and magnesium sulfate hydrate eutectic aggregates". In: *Journal of Geophysical Research: Planets* 116.E4.
- McEwen, A. S. et al. (1998). "High-temperature silicate volcanism on Jupiter's moon Io". In: *Science* 281.5373, pp. 87–90.
- McEwen, A. S. et al. (2000). "Galileo at Io: Results from high-resolution imaging". In: *Science* 288.5469, pp. 1193–1198.
- McEwen, A. S. et al. (2004). "The lithosphere and surface of Io". In: *Jupiter. The planet, satellites and magnetosphere*. Ed. by F Bagenal, TE Dowling, and WB McKinnon. Vol. 1. ISBN: 0521818087. Cambridge, UK: Cambridge University Press, pp. 307–328.
- McEwen, A. S. et al. (2012). "Radiation-Hard Camera for Jupiter System Science". In: *International Workshop on Instrumentation for Planetary Missions*. Vol. 1683.
- McEwen, A. S. et al. (2014). "Io volcano observer (IVO): Budget travel to the outer solar system". In: *Acta Astronautica* 93, pp. 539–544.
- McEwen, AS et al. (2019). "Io Volcano Observer (IVO): Follow the Heat!" In: *50th Lunar and Planetary Science Conference*. Abstract 1316.
- Meyer, J. and J. Wisdom (2007). "Tidal heating in Enceladus". In: *Icarus* 188.2, pp. 535–539.
- Meyer, S., M. Tulej, and P. Wurz (2017). "Mass spectrometry of planetary exospheres at high relative velocity: direct comparison of open-and closed source measurements". In: *Geoscientific Instrumentation, Methods and Data Systems* 6.1, pp. 1–8.
- Michaelis, H. et al. (2017). "Planetary exploration with optical imaging systems review: what is the best sensor for future missions". In: *International Conference on Space Optics—ICSO 2014*. Vol. 10563. International Society for Optics and Photonics, p. 1056322.
- Moore, W. B. (2001). "The thermal state of Io". In: *Icarus* 154.2, pp. 548–550.
- (2003). "Tidal heating and convection in Io". In: *Journal of Geophysical Research: Planets* 108.E8.
- Moore, W. B. et al. (2007). "The interior of Io". In: *Io After Galileo*. Ed. by JR Lopes and JR Spencer. Chichester, UK: Praxis, pp. 89–108.

- Moses, J. I., M. Y. Zolotov, and B. Fegley Jr. (2002). "Alkali and chlorine photochemistry in a volcanically driven atmosphere on Io". In: *Icarus* 156.1, pp. 107–135.
- Moulet, A. et al. (2013). "Exploring Io's atmospheric composition with APEX: First measurement of 34SO₂ and tentative detection of KCl". In: *The Astrophysical Journal* 776.1, p. 32.
- Murakami, M. et al. (2014). "High-pressure radiative conductivity of dense silicate glasses with potential implications for dark magmas". In: *Nature communications* 5, p. 5428.
- Murray, C. D. and S. F. Dermott (1999). *Solar system dynamics*. Cambridge university press.
- NASA (2017). *Solar Power Technologies for Future Planetary Science Missions*. JPL D-101316.
- National Research Council et al. (2012). *Vision and voyages for planetary science in the decade 2013–2022*. National Academies Press. 398 pp.
- Neumann, G., ed. (1968). *Ocean currents*. Vol. 4. Elsevier. 352 pp.
- Ni, H., H. Keppler, and H. Behrens (2011). "Electrical conductivity of hydrous basaltic melts: implications for partial melting in the upper mantle". In: *Contributions to Mineralogy and Petrology* 162.3, pp. 637–650.
- Nikurashin, M. and R. Ferrari (2013). "Overturning circulation driven by breaking internal waves in the deep ocean". In: *Geophysical Research Letters* 40.12, pp. 3133–3137.
- Nimmo, F. and R. T. Pappalardo (2016). "Ocean worlds in the outer solar system". In: *Journal of Geophysical Research: Planets* 121.8, pp. 1378–1399.
- Nimmo, F. and J.R. Spencer (2015). "Powering Triton's recent geological activity by obliquity tides: Implications for Pluto geology". In: *Icarus* 246, pp. 2–10.
- Nimmo, F. et al. (2018). "The thermal and orbital evolution of Enceladus: observational constraints and models". In: *Enceladus and the Icy Moons of Saturn*. Ed. by P. M. Schenk et al. University of Arizona Press, pp. 79–94.
- Nixon, C. A. et al. (2012). "Isotopic ratios in Titan's methane: measurements and modeling". In: *The Astrophysical Journal* 749.2 (159).
- Nover, G. (2005). "Electrical properties of crustal and mantle rocks—a review of laboratory measurements and their explanation". In: *Surveys in Geophysics* 26.5, pp. 593–651.
- Nycander, J. (2005). "Generation of internal waves in the deep ocean by tides". In: *Journal of Geophysical Research: Oceans* 110.C10.
- Oberst, J. and P. Schuster (2004). "Vertical control point network and global shape of Io". In: *Journal of Geophysical Research: Planets* 109.E4.

- Ojakangas, G. W. and D. J. Stevenson (1989). "Thermal state of an ice shell on Europa". In: *Icarus* 81.2, pp. 220–241.
- Ojakangas, Gregory Wayne and DJ Stevenson (1986). "Episodic volcanism of tidally heated satellites with application to Io". In: *Icarus* 66.2, pp. 341–358.
- O'Reilly, T. C. and G. F. Davies (1981). "Magma transport of heat on Io: A mechanism allowing a thick lithosphere". In: *Geophysical Research Letters* 8.4, pp. 313–316.
- Palmer, P. T. and T. F. Limero (2001). "Mass spectrometry in the US space program: past, present, and future". In: *Journal of the American Society for Mass Spectrometry* 12.6, pp. 656–675.
- Panning, M. P. et al. (2015). "Verifying single-station seismic approaches using Earth-based data: Preparation for data return from the InSight mission to Mars". In: *Icarus* 248, pp. 230–242.
- Panning, M. P. et al. (2018). "Expected seismicity and the seismic noise environment of Europa". In: *Journal of Geophysical Research: Planets* 123.1, pp. 163–179.
- Panning, M. et al. (2006). "Long-period seismology on Europa: 2. Predicted seismic response". In: *Journal of Geophysical Research: Planets* 111.E12.
- Pappalardo, R. T. et al. (2013). "Science potential from a Europa lander". In: *Astrobiology* 13.8, pp. 740–773.
- Pappalardo, R. T. et al. (2017). "The Planned Europa Clipper Mission: Exploring Europa to Investigate its Habitability". In: *AAS/Division for Planetary Sciences Meeting Abstracts*. Vol. 49. Abstract ID 214.09.
- Park, R. S. et al. (2011). "Detecting tides and gravity at Europa from multiple close flybys". In: *Geophysical Research Letters* 38.24.
- Park, R. S. et al. (2015). "Improved detection of tides at Europa with radiometric and optical tracking during flybys". In: *Planetary and Space Science* 112, pp. 10–14.
- Park, R. S. et al. (2016). "Advanced pointing imaging camera (APIC) concept". In: *3rd International Workshop on Instrumentation for Planetary Mission*. Vol. 1980. Abstract ID 4018.
- Peale, S. J. (1999). "Origin and evolution of the natural satellites". In: *Annual Review of Astronomy and Astrophysics* 37.1, pp. 533–602.
- Peale, S. J., P. Cassen, and R. T. Reynolds (1979). "Melting of Io by tidal dissipation". In: *Science* 203.4383, pp. 892–894.
- Pearl, J. et al. (1979). "Identification of gaseous SO₂ and new upper limits for other gases on Io". In: *Nature* 280, pp. 755–758.

- Phillips, R. J. et al. (1973). "The Apollo 17 lunar sounder". In: *Proceedings of the 4th Lunar Science Conference*, pp. 2821–2831.
- Picardi, G. et al. (2003). "Mars advanced radar for subsurface and ionosphere sounding (MARSIS): Subsurface performances evaluation". In: *2003 Proceedings of the International Conference on Radar (IEEE Cat. No. 03EX695)*. IEEE, pp. 515–521.
- Plainaki, C. et al. (2018). "Towards a global unified model of Europa's tenuous atmosphere". In: *Space Science Reviews* 214.1 (40).
- Platzman, G. W. (1984). "Planetary energy balance for tidal dissipation". In: *Reviews of Geophysics* 22.1, pp. 73–84.
- Pommier, A. (2014). "Interpretation of magnetotelluric results using laboratory measurements". In: *Surveys in Geophysics* 35.1, pp. 41–84.
- Pommier, A. et al. (2008). "Laboratory measurements of electrical conductivities of hydrous and dry Mount Vesuvius melts under pressure". In: *Journal of Geophysical Research: Solid Earth* 113.B5.
- Pommier, A. et al. (2015). "Experimental constraints on the electrical anisotropy of the lithosphere–asthenosphere system". In: *Nature* 522.7555, pp. 202–206.
- Pommier, A. et al. (2018). "Melting phase relations in the Fe-S and Fe-SO systems at core conditions in small terrestrial bodies". In: *Icarus* 306, pp. 150–162.
- Porco, C. C. et al. (2006). "Cassini observes the active south pole of Enceladus". In: *science* 311.5766, pp. 1393–1401.
- Postberg, F. et al. (2011). "Compositional mapping of planetary moons by mass spectrometry of dust ejecta". In: *Planetary and Space Science* 59.14, pp. 1815–1825.
- Qi, C. and D. L. Kohlstedt (2018). "Influence of compaction length on radial melt segregation in torsionally deformed partially molten rocks". In: *Geochemistry, Geophysics, Geosystems* 19.11, pp. 4400–4419.
- Radebaugh, J. et al. (2001). "Paterae on Io: A new type of volcanic caldera?" In: *Journal of Geophysical Research: Planets* 106.E12, pp. 33005–33020.
- Radebaugh, J. et al. (2004). "Observations and temperatures of Io's Pele Patera from Cassini and Galileo spacecraft images". In: *Icarus* 169.1, pp. 65–79.
- Rathbun, J. A., R. M. C. Lopes, and J. R. Spencer (2018). "The global distribution of active Ionian Volcanoes and implications for tidal heating models". In: *The Astronomical Journal* 156.5. Article 207.

- Rathbun, J. A. et al. (2004). "Mapping of Io's thermal radiation by the Galileo photopolarimeter-radiometer (PPR) instrument". In: *Icarus* 169.1, pp. 127–139.
- Rathbun, J. A. et al. (2014). "Io's active volcanoes during the New Horizons era: Insights from New Horizons imaging". In: *Icarus* 231, pp. 261–272.
- Raymond, C. A. et al. (2015). "Interior Characterization of Europa using Magnetometry (ICEMAG): probing the European ocean and exosphere". In: *AGU Fall Meeting Abstracts*.
- Renaud, J. P. and W. G. Henning (2018). "Increased tidal dissipation using advanced rheological models: Implications for Io and tidally active Exoplanets". In: *The Astrophysical Journal* 857.2. Article 98.
- Romero-Wolf, A. et al. (2015). "A passive probe for subsurface oceans and liquid water in Jupiter's icy moons". In: *Icarus* 248, pp. 463–477.
- Roth, L. et al. (2014). "Transient water vapor at Europa's south pole". In: *Science* 343.6167, pp. 171–174.
- Roth, L. et al. (2017). "Constraints on Io's interior from auroral spot oscillations". In: *Journal of Geophysical Research: Space Physics* 122.2, pp. 1903–1927.
- Salisbury, J. W. and L. S. Walter (1989). "Thermal infrared (2.5–13.5 μm) spectroscopic remote sensing of igneous rock types on particulate planetary surfaces". In: *Journal of Geophysical Research: Solid Earth* 94.B7, pp. 9192–9202.
- Sandwell, D. et al. (2004). "Radar interferometry for measuring tidal strains across cracks on Europa". In: *Journal of Geophysical Research: Planets* 109.E11.
- Saquet, E. et al. (2018). "The PHEMU15 catalogue and astrometric results of the Jupiter's Galilean satellite mutual occultation and eclipse observations made in 2014–2015". In: *MNRAS* 474, pp. 4730–4739.
- Sava, P. C. and E. Asphaug (2019a). "Orbital seismology by laser Doppler vibrometry". In: *50th Lunar and Planetary Science Conference*. Abstract 1709.
- (2019b). "Seismology on small planetary bodies by orbital Laser Doppler Vibrometry". In: *Advances in Space Research*.
- Schenk, P. et al. (2001). "The mountains of Io: Global and geological perspectives from Voyager and Galileo". In: *Journal of Geophysical Research: Planets* 106.E12, pp. 33201–33222.
- Schilling, F. R. et al. (1997). "Partial melting below the magmatic arc in the central Andes deduced from geoelectromagnetic field experiments and laboratory data". In: *Physics of the Earth and Planetary Interiors* 103.1-2, pp. 17–31.

- Schroeder, D. M. et al. (2016). "Assessing the potential for passive radio sounding of Europa and Ganymede with RIME and REASON". In: *Planetary and Space Science* 134, pp. 52–60.
- Segatz, M. et al. (1988). "Tidal dissipation, surface heat flow, and figure of viscoelastic models of Io". In: *Icarus* 75.2, pp. 187–206.
- Seu, R. et al. (2007). "SHARAD sounding radar on the Mars Reconnaissance Orbiter". In: *Journal of Geophysical Research: Planets* 112.E5.
- Sherwood, B. et al. (2018). "Program options to explore ocean worlds". In: *Acta Astronautica* 143, pp. 285–296.
- Shoji, D. and H. Hussmann (2016). "A stochastic basis to the spatially uniform distribution of randomly generated Ionian paterae". In: *Journal of Geophysical Research: Planets* 121.10, pp. 2055–2062.
- Shoji, D. et al. (2014). "Non-steady state tidal heating of Enceladus". In: *Icarus* 235, pp. 75–85.
- Sifré, D. et al. (2014). "Electrical conductivity during incipient melting in the oceanic low-velocity zone". In: *Nature* 509.7498, p. 81.
- Simonelli, D. P., C. Dodd, and J. Veverka (2001). "Regolith variations on Io: Implications for bolometric albedos". In: *Journal of Geophysical Research: Planets* 106.E12, pp. 33241–33252.
- Smith, B. A. et al. (1979a). "The Galilean satellites and Jupiter: Voyager 2 imaging science results". In: *Science* 206.4421, pp. 927–950.
- Smith, B. A. et al. (1979b). "The Jupiter system through the eyes of Voyager 1". In: *Science* 204.4396, pp. 951–972.
- Soderblom, L. A. et al. (1990). "Triton's geyser-like plumes: Discovery and basic characterization". In: *Science* 250.4979, pp. 410–415.
- Soderlund, K. M. et al. (2014). "Ocean-driven heating of Europa's icy shell at low latitudes". In: *Nature Geoscience* 7.1.
- Sparks, W. B. et al. (2016). "Probing for evidence of plumes on Europa with HST/STIS". In: *The Astrophysical Journal* 829.2, p. 121.
- Spencer, J. R. et al. (2002). "A new determination of Io's heat flow using diurnal heat balance constraints". In: *33rd Lunar and Planetary Science Conference*. Abstract 1831.
- Spencer, J. R. et al. (2006). "Cassini encounters Enceladus: Background and the discovery of a south polar hot spot". In: *Science* 311.5766, pp. 1401–1405.

- Stähler, S. C. et al. (2018). "Seismic wave propagation in icy ocean worlds". In: *Journal of Geophysical Research: Planets* 123.1, pp. 206–232.
- Steinbrügge, G. et al. (2015). "Measuring tidal deformations by laser altimetry. A performance model for the Ganymede Laser Altimeter". In: *Planetary and Space Science* 117, pp. 184–191.
- Steinbrügge, G. et al. (2018). "Assessing the potential for measuring Europa's tidal Love number h_2 using radar sounder and topographic imager data". In: *Earth and Planetary Science Letters* 482, pp. 334–341.
- Stevenson, D. J. (1989). "Spontaneous small-scale melt segregation in partial melts undergoing deformation". In: *Geophysical Research Letters* 16.9, pp. 1067–1070.
- Stevenson, D. J. and S. C. McNamara (1988). "Background heatflow on hotspot planets: Io and Venus". In: *Geophysical Research Letters* 15.13, pp. 1455–1458.
- Strobel, D. F., X. Zhu, and M. E. Summers (1994). "On the vertical thermal structure of Io's atmosphere". In: *Icarus* 111.1, pp. 18–30.
- Suer, T.-A. et al. (2017). "FIRE-Flyby of Io with Repeat Encounters: A conceptual design for a New Frontiers mission to Io". In: *Advances in Space Research* 60.5, pp. 1080–1100.
- Summers, M. E. and D. F. Strobel (1996). "Photochemistry and vertical transport in Io's atmosphere and ionosphere". In: *Icarus* 120.2, pp. 290–316.
- Tackley, P. J. et al. (2001). "Three-dimensional simulations of mantle convection in Io". In: *Icarus* 149.1, pp. 79–93.
- Takei, Y. and R. F. Katz (2013). "Consequences of viscous anisotropy in a deforming, two-phase aggregate. Part 1. Governing equations and linearized analysis". In: *Journal of Fluid Mechanics* 734, pp. 424–455.
- Tarcea, N. et al. (2008). "Raman spectroscopy—A powerful tool for in situ planetary science". In: *Strategies of Life Detection*. Springer, pp. 281–292.
- Thomas, P. C. et al. (2016). "Enceladus's measured physical libration requires a global subsurface ocean". In: *Icarus* 264, pp. 37–47.
- Tinker, D. et al. (2004). "High-pressure viscometry of polymerized silicate melts and limitations of the Eyring equation". In: *American Mineralogist* 89.11-12, pp. 1701–1708.
- Tobie, G., A. Mocquet, and C. Sotin (2005). "Tidal dissipation within large icy satellites: Applications to Europa and Titan". In: *Icarus* 177.2, pp. 534–549.
- Tulej, M. et al. (2016). "Experimental investigation of the radiation shielding efficiency of a MCP detector in the radiation environment near Jupiter's moon Europa". In: *Nuclear Instruments*

- and Methods in Physics Research Section B: Beam Interactions with Materials and Atoms* 383, pp. 21–37.
- Turcotte, D. and G. Schubert (2002). *Geodynamics*. ISBN: 9780521666244. Cambridge University Press.
- Turtle, E. P. et al. (2016). “The Europa Imaging System (EIS), a Camera Suite to investigate Europa’s Geology, Ice Shell, and Potential for Current Activity”. In: *3rd International Workshop on Instrumentation for Planetary Mission*. Abstract 1980.
- Tyler, R. (2011). “Tidal dynamical considerations constrain the state of an ocean on Enceladus”. In: *Icarus* 211.1, pp. 770–779.
- Tyler, R. H., W. G. Henning, and C. W. Hamilton (2015). “Tidal heating in a magma ocean within Jupiter’s moon Io”. In: *The Astrophysical Journal Supplement Series* 218.2.
- Van Hoolst, T., R.-M. Baland, and F. Nimmo (2018). “The Rotation of Io”. In: *Fall AGU Meeting*. Abstract P51E-2929.
- Van Hoolst, T., R.-M. Baland, and A. Trinh (2013). “On the librations and tides of large icy satellites”. In: *Icarus* 226.1, pp. 299–315.
- (2016). “The diurnal libration and interior structure of Enceladus”. In: *Icarus* 277, pp. 311–318.
- Vance, S. D. et al. (2018). “Geophysical investigations of habitability in ice-covered ocean worlds”. In: *Journal of Geophysical Research: Planets* 123.1, pp. 180–205.
- Veeder, G. J. et al. (1994). “Io’s heat flow from infrared radiometry: 1983–1993”. In: *Journal of Geophysical Research: Planets* 99.E8, pp. 17095–17162.
- Veeder, G. J. et al. (2009). “Io: Heat flow from dark volcanic fields”. In: *Icarus* 204.1, pp. 239–253.
- Veeder, G. J. et al. (2011). “Io: Heat flow from dark paterae”. In: *Icarus* 212.1, pp. 236–261.
- Veeder, G. J. et al. (2012). “Io: Volcanic thermal sources and global heat flow”. In: *Icarus* 219.2, pp. 701–722.
- (2015). “Io: Heat flow from small volcanic features”. In: *Icarus* 245, pp. 379–410.
- Verhoeven, O. et al. (2009). “Constraints on thermal state and composition of the Earth’s lower mantle from electromagnetic impedances and seismic data”. In: *Journal of Geophysical Research: Solid Earth* 114.B3.
- Verma, A. K. and J.-L. Margot (2018). “Expected precision of Europa Clipper gravity measurements”. In: *Icarus* 314, pp. 35–49.

- Vuolo, M. et al. (2016). "Shielding strategies for JUICE: Material options". In: *Topical Day for RADECS Conference, B*. Vol. 16. Bremen, Germany.
- Wahr, J. M. et al. (2006). "Tides on Europa, and the thickness of Europa's icy shell". In: *Journal of Geophysical Research: Planets* 111.E12.
- Waite Jr., J. H. et al. (2009). "Liquid water on Enceladus from observations of ammonia and ^{40}Ar in the plume". In: *Nature* 460, pp. 487–490.
- Waite Jr., J. H. et al. (2015). "Maspex Europa". In: *AGU Fall Meeting*. Abstract P13E-06.
- Walker, A. C. et al. (2012). "A parametric study of Io's thermophysical surface properties and subsequent numerical atmospheric simulations based on the best fit parameters". In: *Icarus* 220.1, pp. 225–253.
- Wark, D. A. and E. B. Watson (2000). "Effect of grain size on the distribution and transport of deep-seated fluids and melts". In: *Geophysical Research Letters* 27.14, pp. 2029–2032.
- Watts, A. B. (2001). *Isostasy and Flexure of the Lithosphere*. Cambridge University Press. 458 pp.
- Webb, E. K. and D. J. Stevenson (1987). "Subsidence of topography on Io". In: *Icarus* 70.2, pp. 348–353.
- Westlake, J. H. et al. (2016). "The Plasma Instrument for Magnetic Sounding (PIMS) for the Europa Clipper mission". In: *3rd International Workshop on Instrumentation for Planetary Missions*. Vol. 1980. LPI Contributions, p. 4037.
- Williams, D. A. et al. (2009). "Future Io exploration for 2013-2022 and beyond: A white Paper submitted for the 2011 Planetary Science Decadal Survey". In: *AGU Fall Meeting*. Abstract P43D-1469.
- Williams, J. G. et al. (2006). "Lunar laser ranging science: gravitational physics and lunar interior and geodesy". In: *Advances in Space Research* 37.1, pp. 67–71.
- Williams, Q. and E. J. Garnero (1996). "Seismic evidence for partial melt at the base of Earth's mantle". In: *Science* 273.5281, pp. 1528–1530.
- Wilson, L. and J. W. Head III (1981). "Ascent and eruption of basaltic magma on the Earth and Moon". In: *Journal of Geophysical Research: Solid Earth* 86.B4, pp. 2971–3001.
- Witasse, O. (2018). "JUICE: A European mission to explore the emergence of habitable worlds around gas giants". In: *European Planetary Science Congress*. Vol. 12.
- Witte, M. G. and G. J. Savonije (1999). "Tidal evolution of eccentric orbits in massive binary systems. A study of resonance locking". In: *Astronomy & Astrophysics* 350, pp. 129–147. eprint: astro-ph/9909073.

- Witteborn, F. C., J. D. Bregman, and J. B. Pollack (1979). "Io: An intense brightening near 5 micrometers". In: *Science* 203.4381, pp. 643–646.
- Wu, X. et al. (2001). "Probing Europa's hidden ocean from tidal effects on orbital dynamics". In: *Geophysical Research Letters* 28.11, pp. 2245–2248.
- Wurz, P. et al. (2018). "The Neutral Gas and Ion Mass spectrometer of the PEP experiment on the JUICE mission". In: *EGU General Assembly Conference*. Vol. 20. Abstract 10091.
- Yamada, R. et al. (2015). "Frequency band enlargement of the penetrator seismometer and its application to moonquake observation". In: *Advances in Space Research* 56.2, pp. 341–354.
- Zhai, X., H. L. Johnson, and D. P. Marshall (2010). "Significant sink of ocean-eddy energy near western boundaries". In: *Nature Geoscience* 3, pp. 608–612.
- Zhang, B. et al. (2014). "Electrical conductivity anisotropy in partially molten peridotite under shear deformation". In: *Earth and Planetary Science Letters* 405, pp. 98–109.
- Zhang, Z. and A. Pommier (2017). "Electrical investigation of metal-olivine systems and application to the deep interior of Mercury". In: *Journal of Geophysical Research: Planets* 122.12, pp. 2702–2718.
- Zimmer, C., K. K. Khurana, and M. G. Kivelson (2000). "Subsurface oceans on Europa and Callisto: Constraints from Galileo magnetometer observations". In: *Icarus* 147.2, pp. 329–347.
- Zschau, J. (1978). "Tidal friction in the solid Earth: Loading tides versus body tides". In: *Tidal Friction and the Earth's Rotation*. Springer, pp. 62–94.